UNIMORE
UNIVERSITÀ DEGLI STUDI DI
MODENA E REGGIO EMILIA

UNIVERSITÀ DEGLI STUDI DI MODENA E REGGIO EMILIA

Dottorato di ricerca in

Physics and nano sciences

Ciclo XXXVIII

Tailoring graphene oxide-polysulfone membranes for advanced water treatment technologies

Candidata: Angela Pintus

Relatore: Dr. Manuela Melucci

Correlatore (Tutor): Prof. Marco Affronte

Secondo Correlatore: Dr. Letizia Bocchi

Coordinatore del Corso di Dottorato: Prof. Marco Affronte

Summary

List of Acronyms

AA – Amino Acid

AsA – Ascorbic Acid

ATR-FTIR – Attenuated Total Reflection Fourier Transform Infrared Spectroscopy

BE – Binding Energy

BET – Brunauer-Emmett-Teller (surface area analysis)

BIO – Biodegradation (control condition)

BOD – Biological Oxygen Demand

BP3 – Benzophenone-3

BP4 – Benzophenone-4

BPA – Bisphenol A

CA – Contact Angle

CAE – Constant Analyzer Energy (XPS mode)

CAF – Caffeine

CBZ – Carbamazepine

C_{IN} –Initial Concentration

CNR – National Research Council of Italy

CO_2 – Carbon Dioxide

DCF – Diclofenac

DMF – N,N-Dimethylformamide

EA – Elemental Analysis

ECs – Emerging Contaminants

EF – Electro-Fenton

FWHM – Full Width at Half Maximum

GAC – Granular Activated Carbon

GLY – Glyphosate

GO – Graphene Oxide

GO-AA – Amino Acid-Functionalized Graphene Oxide

GO-Lys – Lysine-Functionalized Graphene Oxide

GO-Met – Methionine-Functionalized Graphene Oxide

GO-Glu – Glutamate-Functionalized Graphene Oxide

GO-Arg – Arginine-Functionalized Graphene Oxide

HF – Hollow Fiber

HPLC – High-Performance Liquid Chromatography

HTA – 2-Hydroxyterephthalic Acid

IOD – Iopamidol

ISO – International Organization for Standardization

ISOF – Institute for Organic Synthesis and Photoreactivity (CNR)

MF – Microfiltration

NMP – N-Methyl-2-pyrrolidone

NMR – Nuclear Magnetic Resonance

OFLOX – Ofloxacin

•OH – Hydroxyl Radical

PCM – Paracetamol

PE – Polyethylene

PES – Polyethersulfone

PES-GO – Polyethersulfone-Graphene Oxide coated Membrane

PES-GOLys – Polyethersulfone-Lysine-functionalized Graphene Oxide coated Membrane

PES-rGO – Polyethersulfone-Reduced Graphene Oxide coated Membrane

PFAS – Per- and Polyfluoroalkyl Substances

PSU – Polysulfone

PSU-GO – Polysulfone-Graphene Oxide Composite Granules

PSU-GO-A / PSU-GO-B – Polysulfone-Graphene Oxide composite A/B series

PSU-GOLys – Polysulfone-Graphene Oxide composite functionalized with Lysine
rGO – Reduced Graphene Oxide
RhB – Rhodamine B
SD – Standard Deviation
SEM – Scanning Electron Microscopy
TA – Terephthalic Acid
UF – Ultra filtration
UV-Vis – Ultraviolet-Visible Spectroscopy
XPS – X-ray Photoelectron Spectroscopy

Tesi di dottorato finanziata dall'Unione europea- Next Generation EU, Missione 4, componente 2 "Dalla Ricerca all'Impresa" - Investimento 3.3 "Introduzione di dottorati innovativi che rispondono ai fabbisogni di innovazione delle imprese e promuovono l'assunzione dei ricercatori dalle imprese".

Abstract

This doctoral research, conducted within an industrial PhD framework, aimed to develop functionalized polysulfone (PSU) and polyethersulfone (PES) hollow fiber membranes for advanced water treatment technologies. The core objective was to move beyond the chemical inertness of the base polymers by exploiting the intrinsic reactivity of integrated graphene oxide (GO) as a tunable platform for post-synthetic functionalization. This approach establishes GO not merely as a passive filler but as an active, chemically addressable component. The investigation first established the chemical foundation using GO nanosheets in dispersion, focusing on covalent modification through selective epoxide ring opening by amino acids (e.g., Lysine, Methionine, Arginine) under mild aqueous conditions. These derivatives showed markedly enhanced adsorption affinity toward emerging contaminants (ECs) like carbamazepine (CBZ) and bisphenol A (BPA). This methodology was successfully translated to polymer-integrated systems in two complementary routes: PSU-GO composite granules, obtained by upcycling manufacturing scraps, were chemically modified in situ with Lysine (Lys). This functionalization resulted in an estimated Lys loading of about 6% and yielded a four-fold increase in CBZ adsorption capacity (up to ~260 μg g^{-1}) compared to unmodified PSU-GO, transforming manufacturing residues into high-value sorbent materials consistent with circular-economy principles. PES hollow fiber membranes coated with GO films were also functionalized with Lysine for enhanced CBZ affinity or chemically reduced with L-ascorbic acid to form PES-rGO membranes. The PES-rGO membranes displayed significantly reduced resistivity and were successfully investigated as electroactive cathodes in electro-Fenton processes. This configuration promoted the oxidation and enhanced microbial biodegradation of polyethylene waste, extending the role of GO-modified membranes to reactive interfaces. Overall, this research establishes that graphene oxide, embedded or coated within commercial PSU and PES membranes, remains chemically addressable post-fabrication. These findings bridge fundamental GO chemistry with large-scale membrane manufacturing, enabling the development of adaptive, multifunctional membranes tailored for targeted adsorption or catalytic properties and supporting sustainable resource management.

Premise

Membrane separation processes have emerged as a central focus of research and industrial innovation worldwide, owing to their significant impact on human health, environmental protection, and sustainable resource management.[1] Their ability to provide high selectivity, operational efficiency, and reduced energy consumption compared to conventional separation methods has made them indispensable in applications ranging from water purification and wastewater treatment to biomedical filtration and gas separation.

Within the broad spectrum of membrane technologies, hollow fiber membranes fabricated from polysulfone hold a distinctive position due to their mechanical robustness, chemical stability, and versatility in addressing diverse application requirements. These properties have enabled their use in both biomedical devices, such as hemodialyzers and plasma filters, as well as in industrial processes requiring advanced separation capabilities.

Medica S.p.A. (Medolla, MO, Italy) is a leading manufacturer of hollow fiber membranes for biomedical applications and has, over the past decade, engaged in a productive collaboration with the Institute for Organic Synthesis and Photoreactivity of the National Research Council of Italy (CNR-ISOF). This thesis, conceived within the framework of this long-standing partnership and further supported by the expertise of the University of Modena and Reggio Emilia (UniMoRe), focuses on the engineering of polysulfone-based hollow fiber membranes and their granular derivatives, with the aim of enabling selective recognition and advanced filtration processes.

1 Introduction

1.1 Polysulfone hollow fiber membranes

Hollow fiber (HF) membranes represent one of the most widely adopted configurations in membrane technology, particularly in processes such as water and wastewater treatment, biomedical applications (e.g., hemodialysis), and gas separation.[2, 3] They offer significant advantages over traditional flat-sheet or tubular membranes, especially in processes requiring high throughput and compact filtration units.[4-7] Polymeric materials are the predominant choice for HF membrane fabrication due to their tunable processability, mechanical robustness, and cost-effectiveness.[8-10] Polymeric HF membranes consist of thin, capillary-like fibers with an internal lumen, arranged in bundles within a module. Each fiber is an asymmetric membrane, with a dense polymer layer supported by a porous structure. Their small diameter (typically 200-800 μm) allows the assembly of thousands of fibers into compact modules, yielding a very high surface area-to-volume ratio. This high packing density, combined with the ability to operate in both inside-out and outside-in flow configurations, makes HF membranes ideal for applications requiring high throughput in a minimal footprint.[11] The separation principle of HF

membranes is based on physical sieving, where a high density of small pores on the inner and/or outer surface retains particles, colloids, and macromolecules larger than the pores diameter, while smaller species permeate under the influence of a transmembrane pressure gradient.[12, 13]

The average pore size and molecular weight cut-off determines the size-exclusion selectivity of the membrane, classifying their performance into micro- and ultra-filtration (Fig. 1.1).

- Microfiltration (MF): characterized by pore sizes ranging from 0.1-1 µm, is designed to retain larger particles such as suspended solids, bacteria, and other colloidal particles. It is commonly applied in drinking water and sewage treatment, food and beverage filtration.[14]
- Ultrafiltration (UF): characterized by pore sizes typically between 1-100 nm, is designed to retain macromolecules such as proteins, viruses, and high-molecular-weight organic compounds. It is commonly used for biomedical separations, pharmaceutical processing, and advanced water treatment.[15, 16]

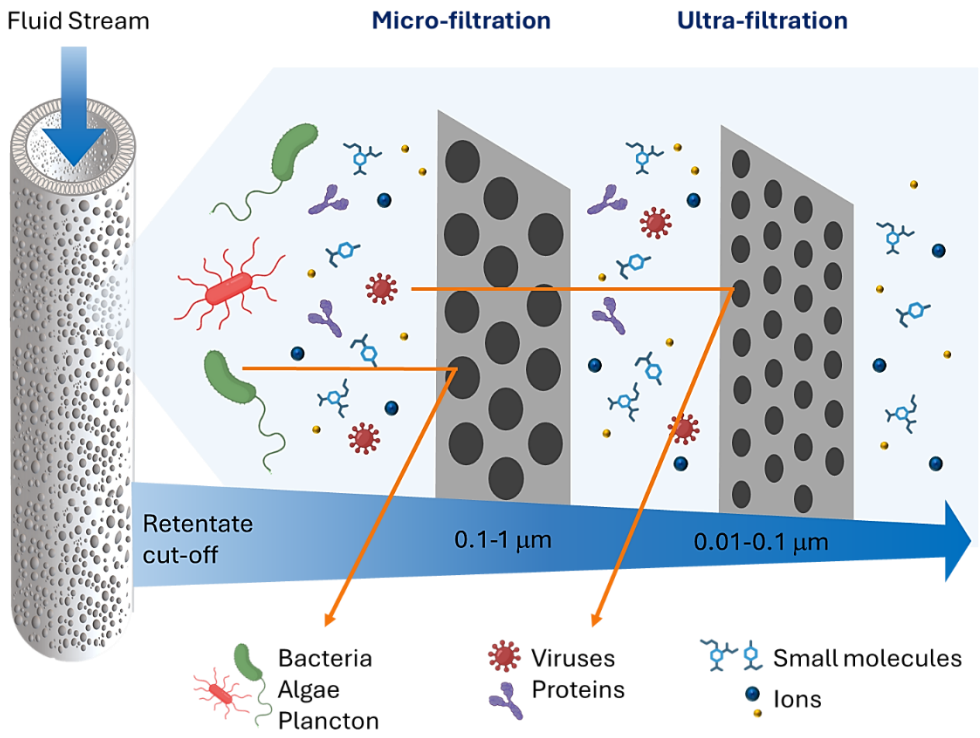

Figure 1.1 *Size-exclusion effect in micro- and ultra-filtration hollow fiber membranes based on pores dimension.*

The pore size and distribution of HF membranes depend on several interrelated factors, including fabrication method, processing conditions, and the intrinsic chemistry of the base polymer.[17-21] A variety of polymers are employed for HFs, including polyvinylidene fluoride (PVDF), polytetrafluoroethylene (PTFE), polyamide (PA), polysulfone (PSU) and polyethersulfone (PES), each offering distinct balances of thermal stability, chemical resistance, and mechanical strength.[22] Among these, PSU and PES have become leading materials due to their outstanding robustness and versatility.

Both PSU and PES are thermoplastic polymers belonging to the family of aromatic sulfone-based materials. Their chemical structures, characterized by rigid aromatic rings and sulfone (-SO_2-) linkages (Fig. 1.2), impart outstanding thermal stability, mechanical robustness, and resistance to chemical degradation, making them ideal candidates for advanced membrane fabrication. These materials exhibit high glass transition temperatures (around 190°C for PSU and 230°C for PES), excellent dimensional stability due to the aromatic backbone, and good solubility in polar aprotic solvents such as N-methyl-2-pyrrolidone (NMP) and dimethylformamide (DMF), facilitating membrane fabrication via phase inversion techniques.[23-26]

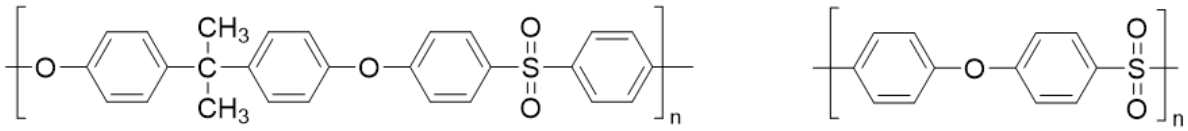

Figure 1.2 *Chemical structures of Polysulfone and Polyetheresulfone polymers.*

1.1.1 Industrial context: Medica S.p.A.

Medica S.p.A. (Medolla, MO, Italy) is an Italian industrial leader in the development and commercialization of polysulfone- and polyethersulfone- based hollow fiber membrane technologies, with a long-standing focus on both biomedical and environmental applications. The company's expertise covers the entire membrane manufacturing chain, from polymer selection and formulation to large-scale fiber spinning, bundle assembly, and device integration, ensuring tight control over quality and performance. Its product portfolio includes a range of membrane modules, each engineered with distinct pore size cut-off, internal morphologies, and mechanical properties to meet the demands of their respective sectors.[27] MediSulfone® membranes are manufactured from PSU and are designed for ultrafiltration applications. These membranes are applied in critical biomedical devices such as hemofilters and dialyzers, as well as in environmental water disinfection systems, where their robustness ensures long operational lifetimes and resistance to harsh cleaning protocols. Their structure offers precise removal of bacteria, viruses, and endotoxins, while maintaining high permeability for efficient processing. Versatile-PES® membranes (Fig. 1.3) are fabricated from PES and are optimized for microfiltration and plasma separation applications. In biomedical contexts, they are widely used in applications such as plasma exchange and therapeutic apheresis, as well as in industrial processes where high flux and precise particle retention are needed.

Today, Medica's membranes are deployed worldwide in high-performance filtration devices for renal replacement therapies, apheresis procedures, plasma fractionation, and blood purification, as well as point-of-use and point-of-entry systems for drinking water treatment. In these latter applications, the high packing density of hollow fibers allows the design of compact cartridges that can be directly

integrated into domestic and industrial purification units, ensuring continuous access to microbiologically safe water. Their broad adoption across biomedical and environmental fields underscores the versatility of PSU and PES hollow fibers and motivates ongoing efforts to expand their selectivity and applicability by integrating additional functionalities.

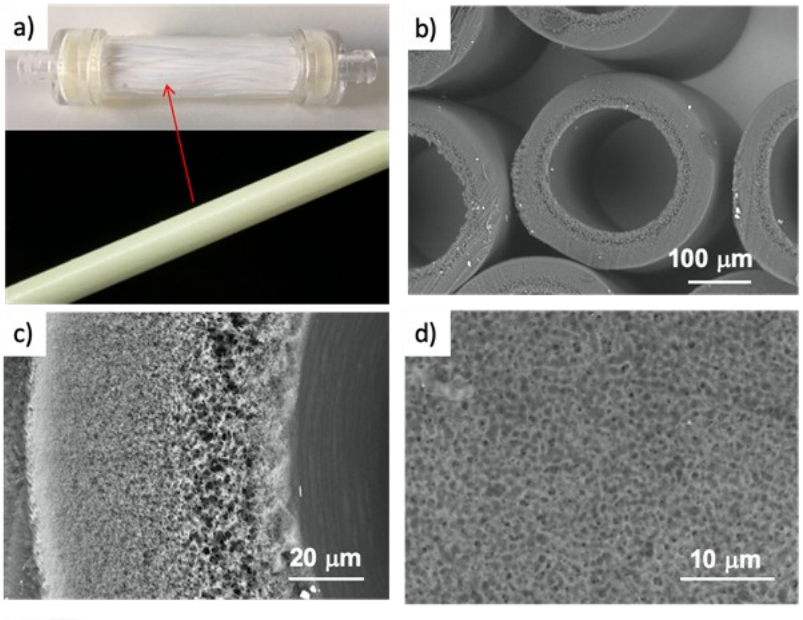

Figure 1.3 *a) Versatile PES® (Medica S.p.A.) hollow fiber filtration cartridge and single fiber, b) fibers, c) cross-section and d) detail of the outer wall pores. (Reprinted from Kovtun A. et al.,[28] with permission).*

1.1.2 Advanced polysulfone-based hollow fiber membranes

Over the past two decades, increasing analytical techniques have revealed the widespread presence of emerging contaminants (ECs) in natural waters, wastewater effluents, and even treated drinking water.[29-31] Pharmaceuticals, plastic additives, and personal care ingredients, including widely studied compounds such as and benzophenone derivatives (e.g., BP3, BP4), carbamazepine, bisphenol A, endocrine disruptors, heavy metals, and per- and polyfluoroalkyl substances (PFAS), are among the most frequently detected substances.[32, 33] These compounds are often found at trace concentrations and their chemical stability and resistance to biodegradation further limit removal by standard treatment processes, making the development of advanced purification technologies particularly relevant.[34-36] Their continuous input into aquatic systems and resistance to conventional treatment processes have raised concerns about long-term ecological and human health impacts.[37-40] From a separation science perspective, their critical feature is molecular size: most ECs are well below the nominal cut-off of ultrafiltration membranes, and thus readily permeate through pores designed to retain only macromolecular species.[41] Against this backdrop, PSU- and PES-based hollow fiber membranes, while highly reliable for removing particulates, bacteria, viruses, and macromolecules, remain intrinsically constrained by their passive sieving mechanism.

Pore dimensions define the molecular weight cut-off, but offer no control over smaller dissolved species, which permeate unaffected. This is compounded by the chemical inertness of PSU and PES surfaces: the aromatic sulfone-based backbones that confer their outstanding chemical and thermal stability, also results in negligible affinity for dissolved solutes, preventing adsorption or selective recognition at the membrane surface. As a result, these polymers do not readily engage in adsorption or specific interactions; such capabilities can instead be introduced by integrating additional functionalities that extend membrane performance beyond size exclusion.

These considerations have driven a paradigm shift toward adsorptive membranes, which combine filtration with the additional capacity to interact with dissolved species.[42, 43] Such systems transform the membrane from a passive barrier into a multifunctional platform, capable of capturing contaminants that would otherwise permeate. Adsorption is widely recognized as one of the most effective and operationally simple approaches for removing micropollutants from water, offering high removal efficiencies and the possibility of regenerating the sorbent material.[44] Granular activated carbon (GAC) represents the industrial benchmark for adsorption-based water treatment, but requires frequent regeneration,[45, 46] and often must be combined with other advanced oxidation or membrane filtration for complete contaminant removal.[47, 48] By contrast, integrating adsorption directly into hollow fiber membranes offers the possibility of combining high throughput, compact design, and selective contaminant removal within a single device.[43, 49-51]

Together, these factors define a central challenge: conventional polysulfone-based hollow fibers are robust filters, but cannot actively capture, adsorb, or transform dissolved contaminants. Meeting this challenge requires new approaches that go pore governed separation, introducing functionalities such as adsorption capacity, catalytic activity, or selective recognition. In this context, the incorporation of nanostructured additives into polymeric membranes has proven particularly effective in expanding their physicochemical functionality, enabling synergistic combinations of structural robustness and surface reactivity.[52, 53] It is within this framework that Medica S.p.A., in collaboration with the Institute for Organic Synthesis and Photoreactivity of the CNR (CNR-ISOF), initiated research on the integration of graphene oxide into polysulfone-based membranes.

1.2 Graphene oxide-modified hollow fiber membranes

Graphene oxide (GO) is a two-dimensional nanomaterial derived from the chemical oxidation of graphite. Its structure consists of single, or few-layer sheets of carbon atoms arranged in a hexagonal lattice, decorated with a heterogeneous distribution of oxygen-containing functional groups, including hydroxyl, epoxide, and carboxyl moieties (Fig. 1.4). This heterogeneous surface chemistry imparts GO with a dual character: hydrophilic domains, associated with oxidized regions, allow stable dispersion in water, while residual sp^2-hybridized carbon regions maintain π- conjugation. Together, these features allow GO to participate in a broad spectrum of non-covalent interactions with molecular species.

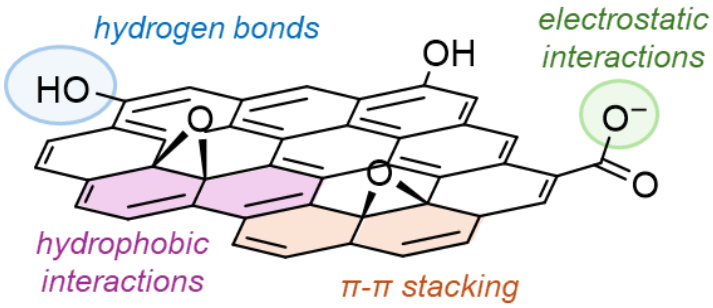

Figure 1.4 *Representation of the GO structure with highlighted interactions enabled by its surface chemistry.*

The coexistence of oxidized domains with residual graphitic domains gives GO an amphiphilic character and a distinctive combination of chemical and physical properties.[54-56] The oxygenated groups impart a strong hydrophilicity, allowing GO to form stable dispersions in water without the need for surfactants.[57] Electrostatic repulsion between negatively charged sheets, combined with hydrogen bonding interactions with water molecules, keeps the layers well-separated in dispersion. At the same time, the conjugated carbon regions enable π–π interactions with aromatic molecules, providing an additional non-covalent binding mode.[58] These properties translate into a high affinity toward various classes of contaminants, from metal ions to pharmaceuticals, dyes, and other emerging pollutants through a combination of polar interactions and aromatic surface affinity, rather than a single dominant mechanism.[59-61] The negative charge associated with carboxyl and hydroxide groups further promotes binding of cationic species.[62-64]

GO is commercially available at relatively low cost, owing to the abundance of graphite and the simplicity of the oxidation process, making it suitable for large-scale applications.[65] Even at low loadings, its ultrathin lamellar architecture and stiffness can significantly improve the tensile strength and modulus of polymer composites. Its layered structure also acts as a physical barrier to gas or liquid permeation, with interlayer spacing tunable through chemical modification or environmental conditions. The theoretical surface area of a monolayer GO sheet can reach 2630 $m^2 g^{-1}$, providing a high density of potential adsorption sites.[66, 67] While GO is electrically insulating due to disruption of the π-conjugated network, partial reduction to reduced graphene oxide (rGO) restores a degree of conductivity while retaining residual oxygenated functionalities, enabling applications where electroactivity is required.[68]

1.2.1 Composite membrane

The characteristics described above motivated Medica S.p.A. to explore the integration of GO into hollow fiber membranes, leveraging the expertise of CNR-ISOF. Throughout a ten-year collaboration, Medica expanded its research and development efforts with CNR-ISOF within the framework of the *Graphil* project,[69, 70] combining fundamental nanomaterial research with industrial membrane production to develop scalable graphene-based filtration systems for drinking water purification.

Two complementary strategies were pursued: (i) the coating of already commercially available Versatile-PES® membranes[28] and (ii) the development of a PSU-GO composite hollow fiber membrane, resulting in the product now marketed as Graphisulfone®.[43, 71, 72] Graphisulfone membranes are produced by embedding GO directly within the polysulfone polymeric matrix, through the phase inversion extrusion method. The process was designed for scalability and facilitated by an *ad hoc* developed industrial pilot line, capable of producing ~20 km of fibers per kg of material, with a production capacity of 200,000 km/year, in compliance with ISO 14644 cleanroom standards and EN ISO 10993 biocompatibility requirements.[71] The manufacturing process involved dissolving PSU in a suspension of GO in NMP to create a dope solution, which is then extruded to form the hollow fiber structure. The resulting membranes (PSU-GO) can be prepared with different GO loadings relative to PSU (Fig. 1.5) and their morphology resemble pristine PSU HF, exhibiting an average wall thickness of ~45 μm and an inner diameter of 220 μm. Raman mapping confirmed a homogeneous GO distribution throughout the fiber cross-section, with nanosheets exposed at the outer surface of the pores. This is due to the hydrophilic nature of GO, which tends to position itself at the interface between the solidifying polymer and the surrounding water during phase inversion. The resulting Graphisulfone membranes retain the ultrafiltration capabilities of pristine PSU, while acquiring the adsorptive capacity typical of GO. Adsorption capacity increased proportionally to GO content, with superior removal efficacy toward several classes of water contaminants, including antibiotics (e.g. ciprofloxacin), heavy metals (Pb, Cu, Cr), and PFAS, compared to pristine PSU and GAC which is the industrial standard for adsorption. Adsorption mechanisms involve a combination of electrostatic forces, hydrophobic interactions, and π-π stacking between GO and the contaminants.

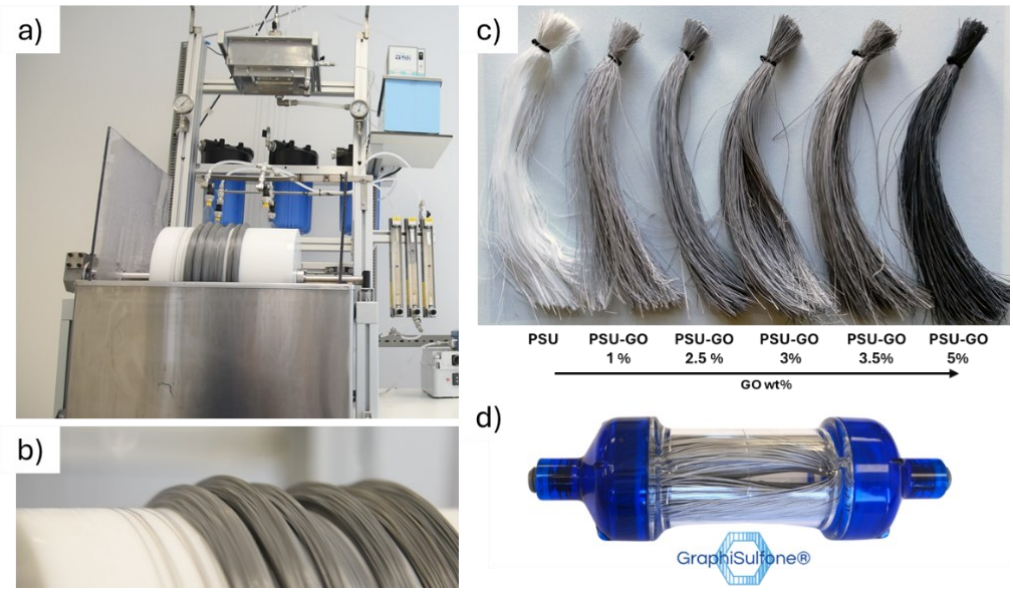

Figure 1.5 *a) Spinning plant pilot for hollow fiber fabrication. b) Collection wheel with hollow fibers bundle. c) PSU hollow fibers with increasing quantities of GO (wt%) (Adapted from ref. 43 with permission). d) Commercial filter of Graphil line made by Graphisulfone hollow fibers (Medica S.p.A.).*

Safety tests confirmed no GO release from the membranes during filtration (detection limit of 0.1 μg L^{-1}), underscoring their suitability for drinking water treatment. These membranes are particularly suitable for removing emerging contaminants as revised in the EU Drinking Water Directive (EU 2020/2184), making them ideal for point-of-use and portable water purification systems. More detailed information regarding the development and testing of PSU-GO HF membranes and the industrial journey that led Graphil filters can be found in the full articles (Zambianchi et al., Melucci et al.).[43, 72]

1.2.2 Composite granules

Building on the success of Graphisulfone®, Medica and CNR extended their collaboration under the European *Life Remembrance* project,[73] aimed at upcycling membrane production waste into valuable materials. The manufacturing of HF membranes, including Graphisulfone®, involves a hot-wire cutting process to shape the fiber bundles into the required cartridge sizes (Fig. 1.6). This process generates membrane scraps, which results in about 10% of the total mass produced, and are usually disposed of through incineration. Medica and CNR-ISOF had previously explored the conversion of membrane scraps from the production of blood filters into sorbents for water purification, by coating them with graphene oxide or polydopamine nanoparticles.[74-76] The case of Graphisulfone® scraps is particularly noteworthy, as they contain embedded active GO, which already imparts significant adsorptive properties, thus providing substantial high value to the material for recycling. The upcycling strategy consisted in the manual and mechanical grinding of membranes' cut-offs, converting them into PSU-GO composite granules, preserving both the polymer matrix structure and the active GO domains. These granules exhibit high removal efficiencies for lead (Pb), diclofenac (DCF), and perfluorooctanoic acid (PFOA), with ~98% regeneration efficiency after two adsorption-desorption cycles.[77] The scaling up of the grinding process enabled the production of larger amounts of material for testing in standard commercial cartridges. Pilot-scale tests demonstrated that PSU-GO granules outperformed GAC under realistic flow conditions in removing Pb and PFOA, confirming their potential as practical adsorbents for drinking water purification.

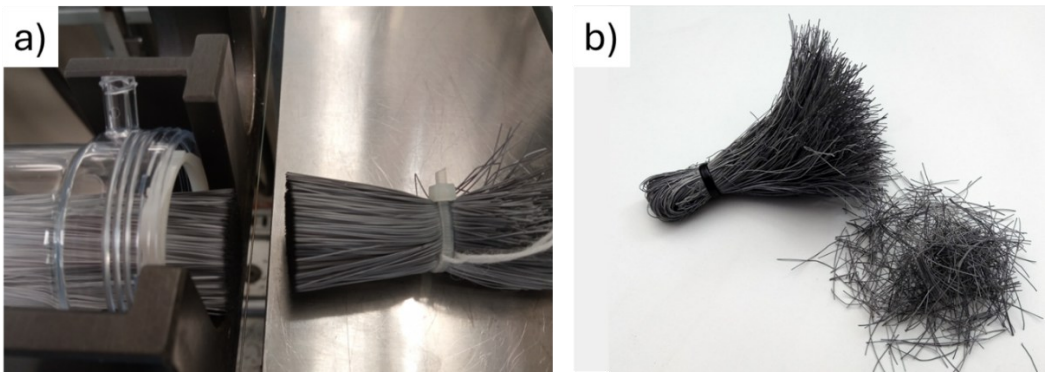

Figure 1.6 *a) Industrial hot-wire cutting of hollow fiber bundles, generating membrane scraps, b) PSU-GO hollow fiber scraps. From Medica S.p.A. production plant (SarMed Srl., IT). (Adapted from ref. 77 with permission).*

The recovery and reuse of Graphisulfone production waste thus reduces plastic disposal while enhancing water purification capacity. This approach aligns with Medica's and CNR commitment to sustainability and circular economy and is now undergoing real-world validation at the HERA potabilization plant (Ferrara, Italy).

Together, the PSU-GO composite hollow fibers and their upcycled granular derivatives represent scalable industrial solutions where GO plays an active role. Yet, their performance ultimately highlights a broader challenge. Because conventional HF membranes filtration rely solely on physical sieving, achieving true selectivity requires deliberate strategies to control morphology, surface chemistry, or integration of functional nanomaterials. These concepts are discussed in the following section.

1.3 Modification strategies for functionality tuning

Following these industrial advances, membrane science has increasingly focused on a wide range of modification strategies, designed to improve membrane's performance and functionality. Such approaches target enhanced resistance to fouling (*i.e.* the undesired accumulation of organic, inorganic, or biological matter on the membrane surface that compromises permeability),[78, 79] as well as improved selectivity toward dissolved molecules,[80-82] antimicrobial or catalytic activity, and adsorption capabilities for specific contaminants. These strategies include: (i) morphological control during fabrication, where processing conditions and additives are tuned to alter pore size, porosity, and internal architecture;[83-86] (ii) post-synthetic surface modifications, which introduce new chemical functionalities to tailor specific recognition or interaction behavior at the membrane surface;[87-90] (iii) incorporation of functional nanomaterials, where inorganic or carbon-based fillers impart properties such as adsorption, catalytic activity, or antimicrobial effects.[91-93]

Each of these approaches offers distinct opportunities but also presents limitations in terms of scalability, stability, and industrial applicability. As already illustrated with the development of Graphisulfone membranes and their granular derivatives, the incorporation of nanomaterials, particularly graphene oxide, offers a versatile pathway to extend the role of hollow fibers beyond passive sieving. GO's tunable chemistry, large surface area, and compatibility with polymer matrices make it an exemplary case of how advanced additives can be exploited to impart adsorption or catalytic functionalities to polymeric membranes. Its broader role as a platform for chemical tuning will be examined in section 1.3.3, after introducing the fundamental approaches for membrane's morphology control and surface modification.

1.3.1 Structural and morphological control during fabrication

The final morphology and performance of polymeric HF is primarily determined during fabrication. Small variations in parameters such as polymer concentration, solvent and non-solvent choice, temperature, or extrusion conditions can result in substantial differences in pore size distribution, porosity and internal architecture. HF production typically consists in spinning techniques involving

extrusion and phase inversion.[3, 25] In the case of thermoplastic polymers like PSU and PES, melt-spinning and phase inversion are predominantly employed.[26] During this process, a dope solution is prepared by dissolving the polymer in a solvent like NMP or DMF. The concentration of the polymer in the solution is critical in determining the final membrane's permeability, porosity, and mechanical properties. Once the dope solution is prepared, it is extruded through a spinneret, a device with a tube-in-orifice design, along with a bore fluid (often water), to form the hollow fiber structure. The subsequent phase inversion process occurs when the extruded polymer is immersed in a coagulation bath, typically water, causing a solvent-non solvent exchange that solidifies the polymer, forming a porous membrane structure. Several processing parameters, such as the rate of solvent-nonsolvent exchange, the temperature of the coagulation bath, and the air gap between the extruder and bath, are essential in controlling the morphology of the membrane.[94-97] By fine-tuning these parameters, it is possible to tailor characteristics such as pore size distribution, skin layer thickness, and porosity, for specific applications, including high selectivity for certain contaminants or enhanced fouling resistance.[98, 99] The choice of polymer or polymer blend is equally influential. Hybrid designs such as co-polymers and mixed matrix membranes are increasingly used to incorporate inorganic fillers (e.g. silica, metal oxides, or carbon nanomaterials) into the polymer matrix, combining the benefits of organic flexibility and inorganic functionality.[8, 100-103] Additionally, post-processing steps such as washing, drying, and chemical treatments further stabilize the membrane structure and improve properties like fouling resistance and adsorptive capacity. However, they remain limited in their ability to impart chemical selectivity: while fabrication tuning can optimize flux and mechanical stability, it cannot by itself enable the targeted retention or transformation of dissolved micropollutants. For this reason, morphology control is often combined with surface modification or nanomaterial incorporation, strategies that will be discussed in the following sections.

1.3.2 Surface modifications post-fabrication

While fabrication parameters largely determine the bulk morphology of PSU and PES membranes, their surface properties can be further enhanced post-production through a variety of modification techniques. Such approaches are particularly relevant when enhanced interfacial functionality is required, extending behaviors that cannot be introduced through morphology control alone. Plasma treatment is one such method, where the membrane surface is exposed to ionized gases, creating a variety of reactive groups such as hydroxyl, carboxyl, and amine functionalities.[104] These groups can enhance the membrane's hydrophilicity and fouling resistance, as well as improve its adsorption capacity for polar and charged species.[105] Another technique involves UV irradiation, which can induce polymerization or cross-linking on the membrane surface, leading to the formation of a more reactive surface with improved adsorption properties.[106] Surface coating offers a flexible approach to enhance membrane functionality, while preserving the bulk characteristics of the membrane.

By applying thin layers of materials such as nanoparticles, polymers, or metal oxides, membranes can acquire new properties, including improved fouling resistance, increased hydrophilicity, and enhanced selectivity.[107, 108] Chemical grafting is another widely studied post-production modification method, where reactive monomers or functional groups are covalently attached to the membrane surface via free-radical polymerization or condensation reactions.[109, 110] This allows for the precise tuning of surface chemistry to enhance the membrane's affinity for specific contaminants, such as heavy metals, organic molecules, or even biofouling agents.[111] Additionally, the introduction of hydrophilic or hydrophobic groups can also tailor the membrane's wettability and improve its performance in selective filtration applications.

Despite the demonstrated benefits of these strategies, one of the key limitations of traditional polymeric membranes like PSU and PES is their inherent lack of surface reactivity. While the chemical stability of these polymers is beneficial in many applications, it also makes them relatively inert in processes that require selective molecular recognition, catalytic activity, or targeted adsorption.[112, 113] This lack of reactivity presents a significant challenge when attempting to enhance membrane properties, as functionalizing these membranes often demands the use of reactive intermediates, catalysts, or harsh processing conditions.[114-116]

These requirements make the surface modification process more complex, limiting its feasibility for large-scale industrial applications. Furthermore, the difficulty in applying these types of surface modifications at an industrial scale is an additional challenge. Traditional methods often involve specialized equipment, long processing times, and specific reaction conditions, all of which can complicate integration into established production lines.[117, 118] This limits the scalability and cost-effectiveness of such modifications, which is particularly problematic for industries that require high throughput and efficiency in membrane production.

In this scenario, nanomaterial incorporation provides an effective route to endow membranes with additional functionalities, that are otherwise difficult to achieve through fabrication or surface chemistry alone, significantly enhancing membrane performance. These improvements may include increased adsorption capacity, selective molecular recognition, catalytic activity, and mechanical reinforcement.[119, 120] Graphene oxide is particularly appealing in this context due to its combination of dispersibility, mechanical strength, and surface chemical versatility. The following section examines the broader role of nanomaterials in membrane modification, with a specific focus on the use of GO as a functional additive.

1.3.3 Incorporation of functional nanomaterials

The use of nanomaterials for the functionalization of polymeric membranes has become an effective and scalable strategy to impart advanced properties beyond those of the base polymer.[121] From an industrial perspective, nanomaterials are particularly appealing because they can offer scalable, cost-effective

solutions with the potential to improve membrane efficiency and performance in various filtration applications.[53] Their incorporation modifies how the membrane interacts with its surrounding environment, influencing not only its capacity to bind or repel certain molecules but also water transport, fouling behavior, and mechanical resilience. Nanomaterials can enhance multiple aspects of membrane performance simultaneously. Their high surface-to-volume ratio and tunable surface chemistry allow for improved wettability and water flux, reduced fouling via hydration layer formation, and selective binding of target contaminants such as heavy metals, pharmaceuticals, or dyes.[53, 119, 122] Additional functionalities may arise depending on the additive: titanium dioxide enables photocatalytic degradation of organic pollutants,[123] while silver or zinc oxide nanoparticles confer antimicrobial properties and extend durability under harsh conditions.[124] Carbon-based nanomaterials represent another important class. Activated carbon enhances adsorption-driven separations, carbon nanotubes (CNTs) contribute to mechanical strength and selective transport through nanochannels, and porous or layered structures such as zeolites, metal organic frameworks (MOFs), MXenes, and graphene derivatives provide molecular sieving, barrier effects, or tunable ion rejection.[124-127]

Integration methods depend on the desired function. Bulk incorporation during membrane spinning ensures uniform distribution, affecting both surface and bulk properties, while post-fabrication methods (e.g., dip-coating, spray-coating, or filtration-assisted deposition) localize the nanomaterials at the membrane interface for direct interaction with the feed stream.

Among these candidates, GO stands out for its unique combination of high surface area, excellent compatibility with polymer matrices, and versatile surface chemistry, making it a model additive for next-generation membranes, with tunable chemical properties.

1.3.3.1 Graphene oxide as a chemically tunable platform

In PSU- and PES-based systems, the combination of GO's industrial compatibility, scalable processability, and chemical versatility makes it an exceptional platform for creating multifunctional membranes, referred to the deliberate and modular tunability of membrane properties through controlled chemical modification of the GO phase, enabling adaptive interactions with specific target species rather than relying solely on passive separation mechanisms. As discussed in section 1.2, GO is a chemically versatile nanomaterial, whose structure combines extended sp^2 domains with a heterogeneous distribution of oxygenated functional groups that can undergo several chemical transformations (Fig. 1.7) Epoxide groups on the basal plane are susceptible to nucleophilic ring-opening reactions with amines, thiols, or alcohols.[67, 128-130] Carboxyl groups can be activated for amide or ester formation,[76, 77] while hydroxyl groups can participate in condensation or etherification reactions.[129, 131]

This reactivity is particularly important in the context of PSU and PES membranes: while the base polymers are chemically inert, GO embedded within their matrix or deposited on their surface offers accessible reactive domains that can be exploited for post-fabrication functionalization under mild,

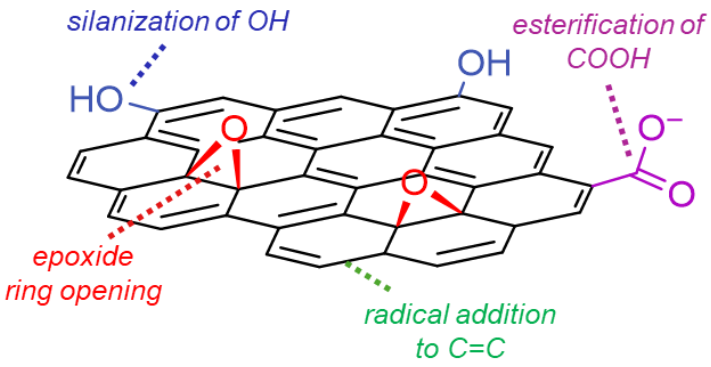

Figure 1.7 *Overview of possible chemical reactions that can occur through the oxygen groups present on GO surface.*

scalable conditions. Among oxygen functionalities, epoxide moieties are both abundant and highly reactive, making them privileged sites for covalent modification through nucleophilic ring-opening under mild, aqueous conditions.[132] By tailoring GO's surface chemistry at the molecular level, it is possible to modulate its polarity, charge, and specific interaction modes, thereby extending its performance far beyond that of pristine GO.[133-135] Covalent approaches are particularly attractive because they provide robust and permanent functionalization, compatible with harsh operating conditions and long-term use. Over recent years, the research group I joined at CNR-ISOF has developed a wide portfolio of covalently modified GO, consistently exploiting the epoxide ring-opening pathway to create materials optimized for specific contaminants or reactions. Examples include diamine-functionalized GO for enhanced adsorption of short- and medium-chain PFAS through combined electrostatic and hydrophobic interactions;[136] polyethyleneimine-grafted GO for selective Pb removal, leveraging the high density of chelating amines for selective metal binding;[137] and cyclodextrin-modified GO for the targeted capture of hydrophobic PFAS, such as perfluoro butanoic acid (PFBA), leveraging host-guest inclusion together with GO's π-interactions.[138] These cases illustrate how careful selection of the nucleophile enables the tailoring of GO's surface to match the structural and chemical features of the target molecule.[130] Other covalent strategies have also been explored to broaden GO's functional landscape, including visible-light-assisted arylation to introduce aromatic moieties,[139] amide coupling for integration into biosensor, and azide-microwave-assisted silylation for interface engineering.[129, 140] Collectively, these studies underline a key design principle in which the choice of covalent linker and functional group determines whether GO can be transformed from a generic adsorbent into a highly specialized material platform tailored to a specific application.

2 Aim of the thesis

This thesis was carried out within the framework of an industrial doctorate in collaboration between Medica S.p.A., the Institute of Organic Synthesis and Photoreactivity of the CNR in Bologna, and the University of Modena and Reggio Emilia. The project was also supported by the Italian National Recovery and Resilience Plan (PNRR), which emphasizes the development of sustainable technologies through strong connections between research institutions and industry. Within this setting, my research has been guided by the ambition to expand the role of polysulfone- and polyethersulfone-based hollow fiber membranes, moving beyond their traditional function as passive filters toward a new generation of active, adaptable materials for advanced water treatment.

The collaboration between Medica and CNR had already laid an important foundation by demonstrating that graphene oxide can be integrated into membrane technologies at industrial scale. Multilayer GO coatings on PES fibers were developed and validated,[28] a PSU-GO composite commercialized as Graphisulfone® (jointly owned registered trademark of Medica S.p.A. and CNR) was shown to couple adsorption with ultrafiltration,[43, 72] and production offcuts from membrane manufacturing were upcycled into granular sorbents retaining adsorptive activity.[74, 75, 77] These outcomes are evidenced by coordinated research programs - notably *Graphil* within the Graphene Flagship and *Life Remembrance* -[70, 73] by a consistent body of peer-reviewed publications, and by a consolidated patent portfolio covering GO treatment of polysulfone hollow fibers and related fabrication routes.[141-144] These achievements provided a unique starting point for the present work, which aims to further exploit the chemical versatility of graphene oxide once integrated into such industrially relevant systems. Rather than focusing on polymer chemistry or on the intrinsic properties of GO as an additive, the objective was to demonstrate that the reactive domains of GO can serve as a platform for post-synthetic functionalization, enabling deliberate tuning of sorption, selectivity, and reactivity in membrane-based devices.

In this perspective, this thesis investigates increasing levels of material complexity and two complementary modes of GO integration within polymeric membranes: (i) GO embedded within a PSU matrix, where the reactive domains are confined inside the bulk material and accessed through diffusion-driven processes, and (ii) GO deposited as a multilayer coating on PES hollow fibers, where the functional phase is directly exposed at the membrane–solution interface. These configurations allow evaluation of post-synthetic functionalization under structurally distinct constraints, while maintaining a common chemical platform based on GO reactivity.

The functionalization of free graphene oxide nanosheets was first revisited, not as an isolated exercise, but as a conceptual and methodological bridge to more complex systems. The knowledge gained in these model studies was then transferred to the upcycled polysulfone-graphene oxide granules, where the challenge was to validate whether covalent modification could be performed under scalable conditions while preserving the structural integrity of the polymer matrix. In parallel, functionalization of graphene oxide multilayer coatings on polyethersulfone hollow fibers was explored, focusing on tuning surface

chemistry in already validated membrane configurations, addressing both adsorption-driven processes and electrochemical activity.

Taken together, these research directions converge toward a common objective: to establish post-synthetic functionalization of graphene oxide as a transferable strategy across distinct membrane architectures based on polysulfone and polyethersulfone, thereby expanding the functional scope of hollow fiber technologies. The ambition is not limited to the adsorption of selected contaminants but to contribute to a broader paradigm of advanced water treatment in which membranes operate as chemically interactive interfaces capable of selective recognition, catalytic or electroactive behavior, and sustainable material valorization. Through this approach, the thesis connects molecular-level control of nanomaterial chemistry with membrane device engineering, promoting the integration of chemically tunable nanomaterials into scalable membrane technologies for sustainable water treatment.

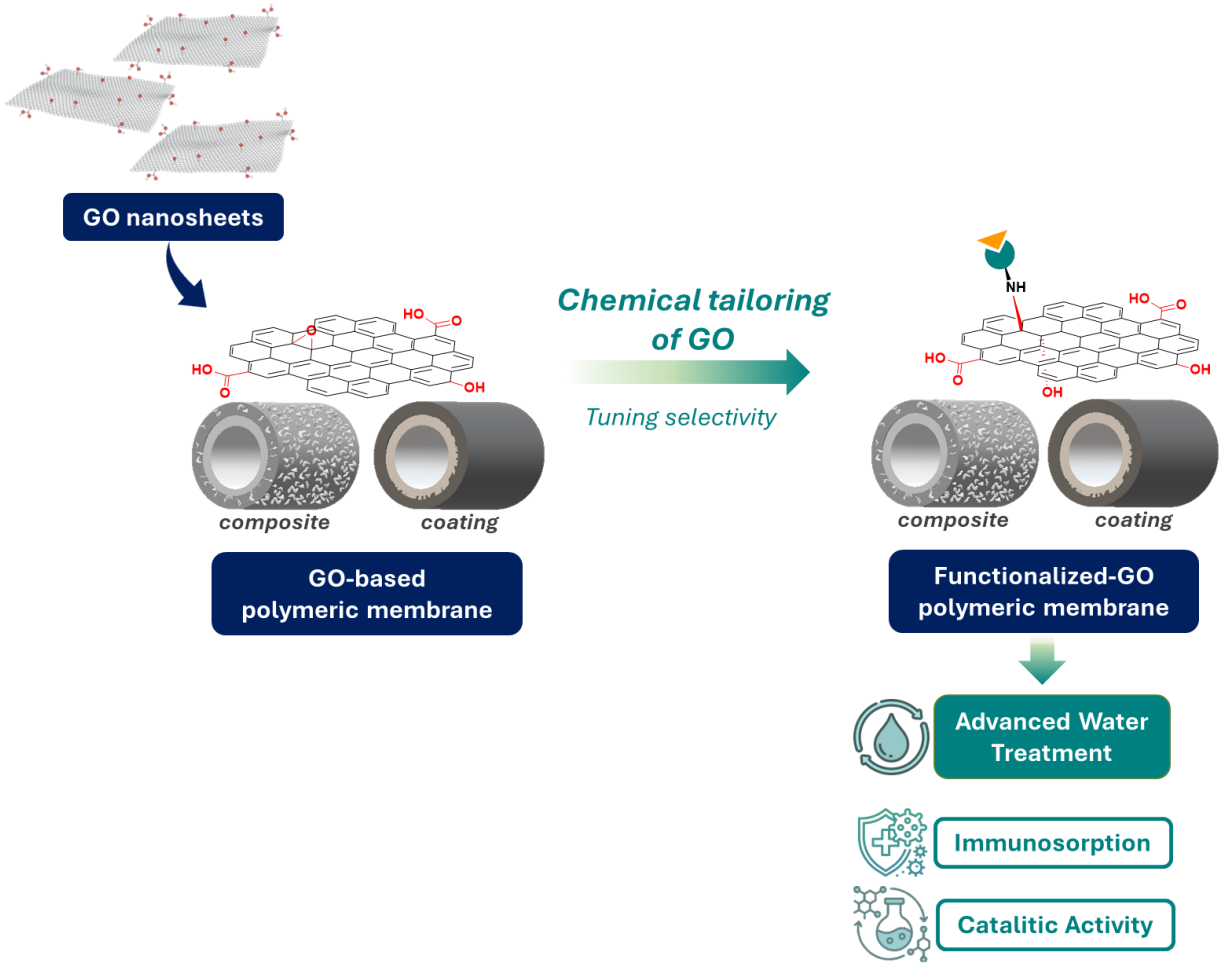

Figure 2.1 *Graphical abstract.*

3 Results

3.1 Covalent modification of graphene oxide nanosheets in solution phase

As outlined in Chapter 1, covalent modification of graphene oxide provides a powerful route to expand its surface chemistry and introduce functionalities capable of selective interactions with contaminants. Numerous examples have demonstrated how epoxide ring-opening, amide coupling or grafting strategies can transform GO from a general-purpose adsorbent into a task-specific material. By tailoring GO's surface chemistry at the molecular level, it is possible to modulate polarity, charge, and specific interaction modes, thereby extending its performance far beyond that of pristine GO.[133-135] Within this framework, different functionalization approaches have been explored in our research group, including GO-β-cyclodextrin (GO-βCD, Fig. 3.1), as an additional example of task-specific GO derivative for the selective adsorption of PFAS.[136, 138] Among these systems, amino acid–modified GO (GO-AA) was selected as the representative platform to be discussed in detail, since it exemplifies how epoxide ring-opening can be exploited under mild aqueous conditions to modulate surface chemistry and guide interactions with different classes of environmentally relevant compounds. The work presented in this chapter, adapted from previously published studies,[128, 145-148] played a fundamental role in shaping both the methodology and scientific direction of my PhD. During the initial phase of my research, I became directly involved in this line of investigation, building the methodological and conceptual foundations that underpin the central aim of this doctoral thesis: to translate the selective reactivity of functionalized GO nanosheets into *in situ* post-synthetic modification of industrially relevant GO-polymer composites. By examining GO-AA performance in multiple application domains, this chapter illustrates the versatility of epoxide ring-opening chemistry as a design strategy for tailoring GO-based materials,

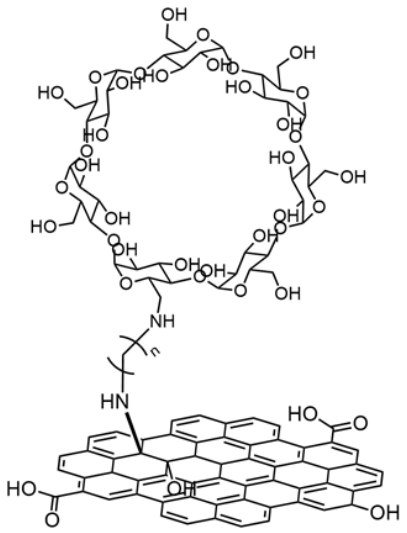

Figure 3.1 *Graphene oxide covalently functionalized via epoxide ring opening with amino terminated β-cyclodextrin (GO-βCD).*

while also providing the conceptual and experimental bridge to the composite systems explored in later chapters. Covalent functionalization of GO nanosheets with amino acids provides a simple and scalable strategy to tune GO's interfacial chemistry while preserving its high surface area, dispersibility and structural integrity. Among the oxygen functionalities decorating the GO surface, epoxide moieties are both abundant and highly reactive, making them privileged sites for nucleophilic ring-opening by amines under mild aqueous conditions.

Amino acids are particularly attractive modifiers for several reasons. They are biocompatible and widely available, making them suitable for scalable and environmentally responsible material functionalization. Depending on purity and grade, their costs range from laboratory-grade values on the order of 10^3 €·kg^{-1} to only tens of euros per Kg for technical and bulk-grade materials.[149] Their water solubility allows reactions to be conducted under mild aqueous conditions, while their structural diversity provides access to a wide range of side-chain chemistries, including amines, carboxylates, hydroxyl, guanidinium, and sulfur-containing thioethers. This diversity allows systematic variation of polarity, charge, hydrogen-bonding capacity, and metal-binding motifs. As such, amino acids serve as green modular covalent linkers that simultaneously act as molecular probes to establish structure-function relationships at the GO-sorbent interface. Several representative derivatives have been investigated within this framework (Fig. 3.2): (i) lysine, bearing two amine groups, to enhance hydrogen bonding and electrostatic interactions;[128, 150] (ii) methionine, with a thioether side chain, offering potential for hydrophobic and polar interactions;[151, 152] (iii) glutamic acid, with an additional carboxyl group, capable of introducing acidity and metal coordination sites;[153, 154] (iv) arginine, whose guanidinium group provides strong basicity and potential polar interaction modes.[155-157] This selection covers a representative range of chemical functionalities, illustrating of how small, modular, water-processable reagents can direct GO's interfacial behavior across different environmental contexts.

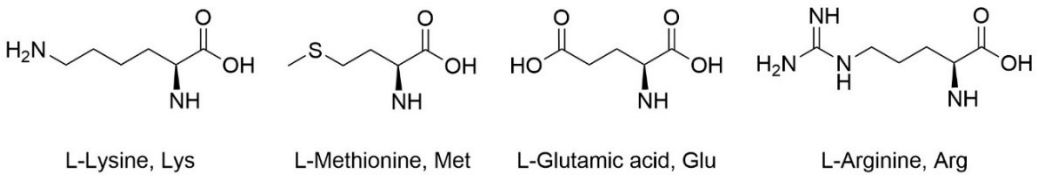

Figure 3.2 *Structures of the amino acids selected for GO functionalization.*

3.1.1 Functionalization methodology and materials characterization

Amino acids-modified graphene oxide derivatives were synthesized through a unified protocol based on the selective nucleophilic ring-opening of epoxide groups under basic aqueous conditions (Scheme 3.1).[133] This methodology enabled covalent modification without the need for organic solvents or harsh coupling agents, aligning with principles of simplicity, selectivity, and environmental compatibility.

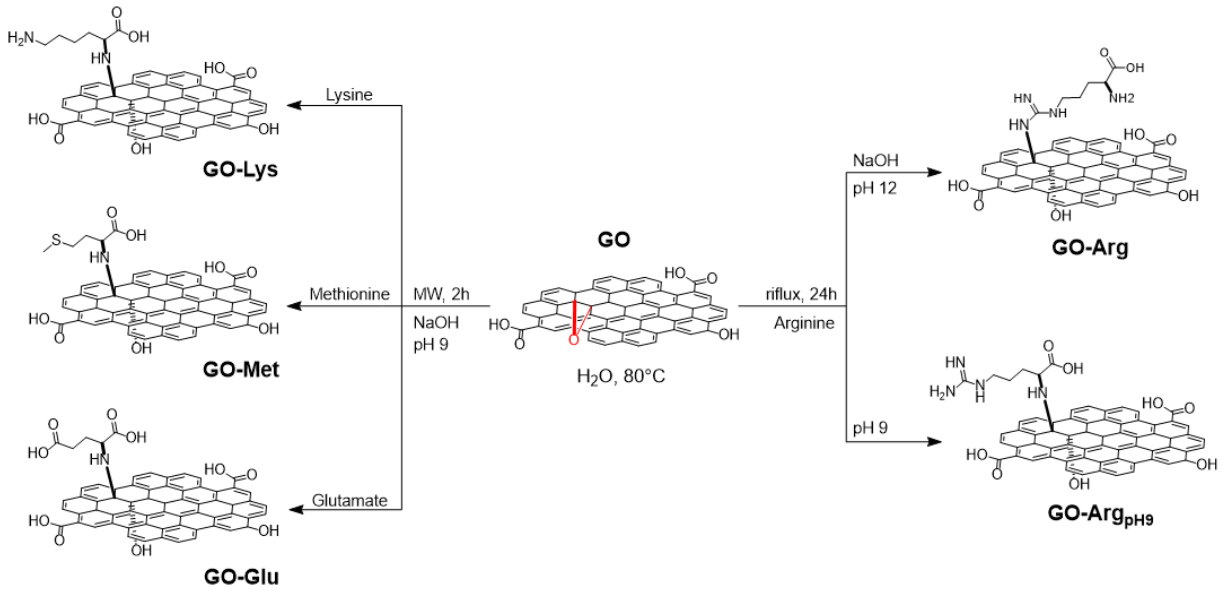

Scheme 3.1 *Synthetic pathway to amino acid-modified GO.*

Graphene oxide (Layer One, S-126/36, Norway) was used as received. L-lysine (Lys), L-methionine methyl ester (Met), L-glutamic acid monosodium salt monohydrate (Glu), and L-arginine (Arg), were obtained from Sigma-Aldrich and used without further purification. For Lys, Met and Glu derivatives (i.e. GO-Lys, GO-Met, and GO-Glu), a concentrated aqueous amino acid (AA) solution was prepared, maintaining a GO:AA weight ratio of 1:3. The pH was adjusted to ~9 by addition of NaOH to deprotonate the α-amino group and enhance its nucleophilicity. The solution was added to a GO suspension (5 mg mL^{-1}, previously sonicated for 2 h) and irradiated in a microwave reactor for 2 hours. Crude products were purified by microfiltration on Versatile™ PES hollow fiber modules, until the permeate reached neutral pH, ensuring the removal of unreacted reagents and byproducts (Scheme 3.2).[128] A control sample (GO-NaOH) was also prepared under identical reaction conditions without amino acid addition.

A modified protocol was adopted for the functionalization of GO with L-arginine (GO-Arg). In the standard procedure, a 1:3 GO:Arg weight ratio was used, and the pH was raised above ~12 by adding NaOH, to promote nucleophilic attack from the guanidinium group.[147] This route is hereafter referred to as GO-Arg. A milder variant was conducted without NaOH addition (pH ~9), favoring reaction via the α-amino group, leading to a distinct grafting outcome;[146, 158] this sample is denoted as $GO\text{-}Arg_{pH9}$. Both reactions proceeded by stirring at 80°C for 24 hours, followed by purification according to the microfiltration protocol described above, until neutral pH was reached in the permeate. For the GO-Arg system, additional synthesis at different GO:Arg weight ratios of 1:1 and 1:5 were also investigated to assess their influence on arginine loading.[148]

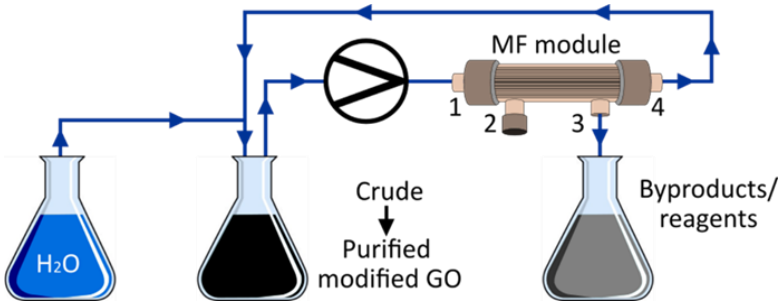

Scheme 3.2 *Sketch of purification set-up of GO-amino acid by microfiltration. (Reprinted from ref 122, with permission).*

The successful modification of GO with AA was confirmed through a combination of spectroscopic and morphological characterization techniques. The chemical structure and degree of functionalization were primarily assessed by X-ray photoelectron spectroscopy (XPS), revealing the incorporation of nitrogen- and sulfur-containing functionalities, depending on the amino acid. The atomic composition (Table 3.1, Fig. 5.1, Appendix A) showed nitrogen contents ranging from 1.3% to 5.9%, allowing for an estimation of AA loading on the GO surface based on the stoichiometric ratios of the grafted molecules.

Table 3.1 *XPS atomic composition of the amino acid modified graphene materials.*

Material	C%	O%	N%	S%	Ca%	AA Loading[a]
GO	70.4	27	0.7	2.0	-	-
GO-NaOH	70.4	25.6	0.2	-	-	-
GO-Lys	81.5	13.9	3.1	-	-	15%
GO-Met	81.2	15.6	0.9	0.8	-	5%
GO-Glu	77.1	19.7	0.7	-	2.3	6%
GO-Arg_{pH9}	74.8	20.3	4.8	-	<1	12%
GO-Arg (1:1)	84.3	14.4	1.6	-	<1	5%
GO-Arg (1:3)	73.7	19.6	4.5	-	<1	14%
GO-Arg (1:5)	73.1	21.1	5.9	-	1.5	18%

[a] Relative loading of amino acid in the materials obtained by considering the atomic ratios of: L-Lysine (C:N:O=6:2:2), L-Methionine (C:N:O:S=5:1:2:1), L-Glutamic acid (C:N:O=5:1:4) and L-Arginine (C:N:O=6:4:2).

For samples synthesized under basic conditions (GO-Lys, GO-Met, GO-Glu and GO-Arg), GO-NaOH was used as the reference material to account for the effect of alkaline treatment, whereas pristine GO was adopted as the reference for GO-Arg_{pH9}, synthesized without NaOH addition. XPS survey spectra also revealed minor residual sodium signals (from Auger Na KLL signal with kinetic energy ~994 eV) in samples synthesized in the presence of NaOH, attributable to the alkaline reaction environment.

Elemental analysis (EA) provided complementary bulk-averaged atomic compositions and confirmed the trends observed by XPS, particularly in the N/C ratios (Tables 5.1-3, Appendix A), indicating that amino acids were incorporated throughout the bulk of the material rather than only on the surface. Fourier Transform Infrared Spectroscopy (FTIR) further supported the presence of grafted arginine, with characteristic CH_2 and carboxyl bands appearing in the GO-Arg spectrum (Fig. 5.2, Appendix A), while scanning electron microscopy (SEM) imaging confirmed the preservation of GO's flake-like morphology (Fig. 3.3). Full characterization datasets, including instrumental parameters and spectral assignments, are reported in Appendix A together with the corresponding publications.[145, 147, 148]

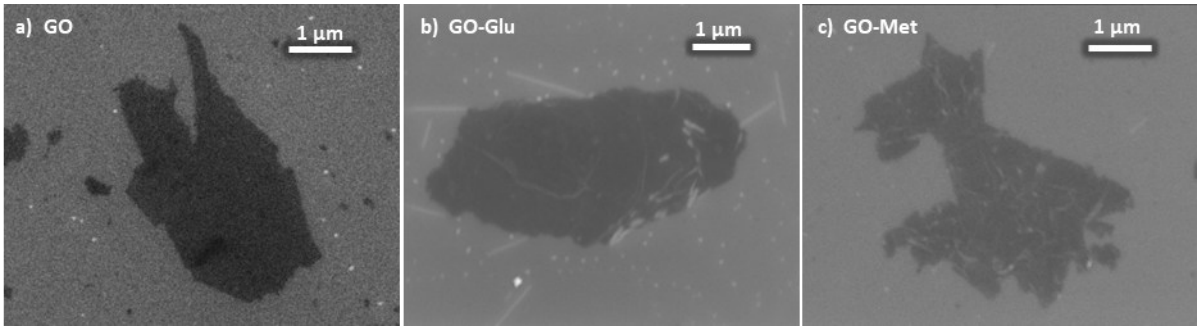

Figure 3.3 *Representative SEM images of a) GO, b) GO-Glu and c) GO-Met.*

3.1.2 Applications in adsorption of emerging contaminants in water

Amino acid-modified graphene oxide nanosheets were evaluated for their ability to adsorb emerging contaminants from water, with the aim of assessing how covalent functionalization enhances affinity and selectivity toward structurally diverse compounds. GO is a widely studied adsorbent owing to its extended π-conjugated domains, high surface area, and versatile oxygen functionalities, which enable π–π stacking and hydrogen-bonding with aromatic pollutants.[62, 159-161] However, pristine GO often displays limited efficiency due to the non-specific nature of its interactions and the heterogeneous distribution of surface groups.[162, 163] Introducing amino acids offers a route to overcome these limitations by providing polar, nucleophilic, and ionizable moieties that expand GO's interaction modes.

To prove this effect, GO-Lys, GO-Glu, and GO-Met were tested alongside pristine GO and a control (GO-NaOH) in a multicomponent adsorption experiment using eight model ECs, including caffeine, pharmaceuticals (carbamazepine, diclofenac, ofloxacin), personal care products (benzophenone derivatives), a plastic additives (bisphenol A) and a dyes (rhodamine B), which are widely detected in surface and groundwater, sediments, and even drinking water worldwide.[164-166] This selectivity screening (Fig. 3.4).revealed a consistent enhancement of adsorption capacity in the functionalized materials, particularly for neutral aromatic contaminants such as carbamazepine (CBZ), bisphenol A (BPA), and benzophenone-4 (BP4). improved uptake reflected the contribution of the grafted amino acid groups, which facilitated hydrogen bonding, dipolar interactions, and polar–π contacts, thereby complementing

the intrinsic π–π stacking capacity of the GO backbone. Among the tested derivatives, GO-Lys exhibited the most uniform improvement across the contaminant panel, highlighting the synergistic role of amine functionalities in promoting sorption and improving aqueous dispersibility.

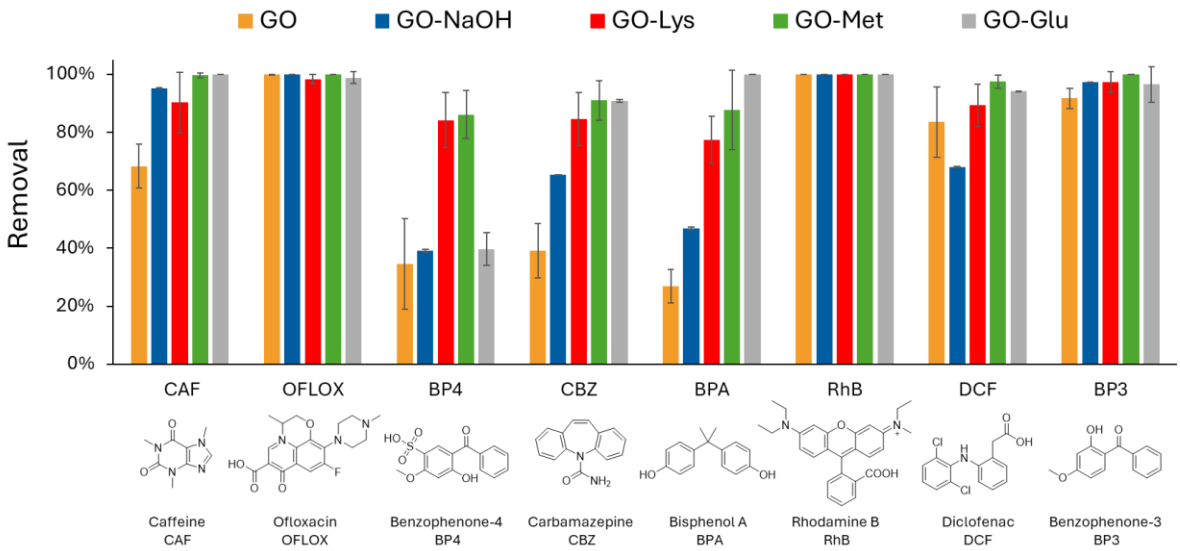

Figure 3.4 *Removal of the selected ECs mixture in tap water (contact time = 4 h, total volume = 10 mL, sorbent amount = 25 mg,* C_{IN} *= 5 mg* L^{-1} *of each contaminant) by GO (orange), GO-Glu (grey), GO-Lys (red) GO-Met (green) and GO-NaOH (dark blue).*

To quantify adsorption performance, equilibrium isotherms were obtained for CBZ, BPA, and BP4, chosen as representative contaminants with distinct functional groups, and the corresponding maximum adsorption capacities (Q_m) were extracted from model fitting using Langmuir and BET equations, which account for monolayer adsorption on homogeneous surfaces and multilayer adsorption on heterogeneous surfaces, respectively. Results are summarized in Table 3.2.

Table 3.2 *Maximum adsorption capacity (Qm, mg* g^{-1}*) of amino acid–functionalized GO toward selected contaminants. Best-fitting isotherm models indicated in parentheses (L = Langmuir, B = BET).*

	Qm (mg g^{-1})		
Material	**BP4**	**BPA**	**CBZ**
GO	11 ± 5 (B)	14 ± 5 (B)	7 ± 2 (L)
GO-NaOH	62 ± 12 (L)	48 ± 11 (L)	80 ± 15 (L)
GO-Lys	292 ± 30 (L)	295 ± 50 (L)	172 ± 20 (L)
GO-Met	205 ± 20 (L)	147 ± 30 (L)	128 ± 15 (L)
GO-Glu	77 ± 20 (B)	237 ± 40 (L)	121 ± 20 (L)

While pristine GO showed modest uptake (7-14 mg g^{-1}), GO-AA derivatives reached capacities one order of magnitude higher. GO-Lys achieved the highest adsorption values overall (172-295 mg g^{-1}), consistently outperforming both pristine and NaOH-treated GO. GO-Glu displayed excellent affinity for BPA (237 mg g^{-1}), consistent with carboxylate-mediated hydrogen bonding with phenolic and carbonyl groups, while GO-Met reached the highest uptake for BP4 (205 mg g^{-1}), likely due to thioether-driven dipolar or weak hydrophobic interactions. These experimental observations are consistent with the expected interaction modes between the contaminants and the functional groups introduced on the GO surface. While π–π stacking remains a dominant mechanism for aromatic systems, the addition of polar and ionizable groups creates complementary binding domains that facilitate cooperative interactions. In this way, amino acid modification enhances both the affinity and accessibility of the GO surface for target molecules. Molecular dynamics (MD) simulations provided further support for the experimental findings, revealing that pollutant adsorption induces local rearrangements in the GO-AA structure, increasing solvent-accessible surface area and stabilizing noncovalent interactions at the interface. In summary, amino acid grafting enables rational tuning of GO adsorption performance through the deliberate introduction of polar, ionizable, and electron-rich functionalities. The markedly improved capacities and selectivities observed for GO-Lys, GO-Glu, and GO-Met highlight how covalent functionalization provides a molecular-level handle to tailor sorbent performance. Detailed experimental procedures, including adsorption protocols, isotherm acquisition, and molecular dynamics methodologies and outputs, are reported in Appendix A.

3.1.3 Other Applications

3.1.3.1 Electrochemical Sensing

Covalent modification of GO with amino acids also enables selective sensing platforms for analytes that interact only weakly with pristine GO. Glyphosate (N-[phosphonomethyl]glycine, GLY), one of the most widely used herbicides worldwide, is frequently detected in water sources and has raised concerns due to its environmental persistence and potential health impacts.[167, 168] Its persistence in the environment, combined with concerns over potential ecotoxicological and human health impacts, has led to increasingly stringent regulatory limits and growing demand for rapid, sensitive detection methods.[169-172] By introducing amino acid functionalities, the GO surface acquires binding motifs capable of hydrogen bonding and electrostatic attraction with glyphosate's phosphonate group. This tailored chemistry improves target pre-concentration and orientation at the electrode interface, enhancing electron transfer during electrochemical detection.

Adsorption tests confirmed superior affinity of functionalized materials for glyphosate, with GO-Lys outperforming pristine GO and even granular activated carbon (Fig. 5.4, Appendix A). For sensing experiments, aqueous GO-AA dispersions were drop-cast onto conductive substrates to prepare working electrodes. Unlike pristine GO, which requires electrochemical reduction to rGO to restore

conductivity,[173, 174] GO-AA electrodes were used directly, as amino acid grafting already improved their electron-transfer properties. Differential pulse voltammetry revealed that GO-Lys electrodes delivered the highest and most stable current responses at both high (10 mg L^{-1}) and environmentally relevant (2 µg L^{-1}) concentrations, with a clear signal enhancement compared to rGO and the other GO-AA derivatives (Fig. 3.5). MD simulations carried out at near-neutral pH provide a quantitative description of the interaction trends. Under these conditions, glyphosate is predominantly in its anionic form and interacts with the amino acid side chains grafted on the basal plane of GO. The calculated binding energies increase progressively from rGO (−3.2 kcal mol^{-1}) to GO-Met (−4.7 kcal mol^{-1}), and further to the cationic derivatives GO-Arg_{pH9} (−8.6 kcal mol^{-1}) and GO-Lys (−26.5 kcal mol^{-1}), reflecting the growing contribution of electrostatic interactions upon introduction of positively charged residues. The higher stabilization observed for the lysine-functionalized surface is consistent with the more spatially localized protonated ε-amino group, which forms salt bridges and hydrogen bonds with the phosphonate moiety of glyphosate. Details on the adsorption tests, electrode preparation, and electrochemical protocols are reported in Appendix A. Here, the focus is placed on demonstrating how amino acid functionalization transforms GO from a general sorbent into a selective sensing interface, enabling efficient detection of targets otherwise inaccessible to its pristine form.

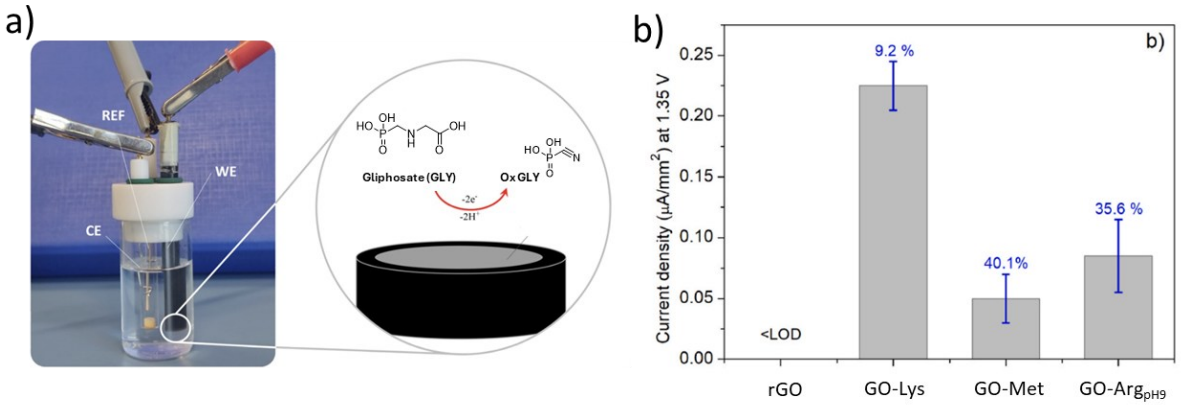

Figure 3.5 *(a) Electrochemical detection of Gliphosate previous oxidation at the interface of the working electrode. (b) Mean current values and standard deviations obtained from three independent analyses after 15 min immersion of different modified electrodes in a 2 µg L^{-1} GLY solution).*

3.1.3.2 CO_2 Capture and Conversion

In parallel to liquid-phase applications, the versatility of amino acid functionalization was investigated for environmental gas capture and transformation. Previous studies carried out in collaboration with the University of Bologna demonstrated that pristine graphene oxide can act as a carbocatalyst in a variety of reactions,[175, 176] but its affinity for CO_2 is modest. Grafting L-arginine introduces guanidinium groups able to stabilize CO_2 through acid–base and hydrogen-bonding interactions.[155-157] GO-Arg composites were prepared at GO:Arg weight ratios of 1:1, 1:3, and 1:5, yielding nitrogen contents of 1.6, 4.5, and 5.9 at% (corresponding to estimated loadings of 5%, 14%, and 18% Arg, respectively, Table 3.1).

Thermogravimetric analyses showed CO_2 uptake increasing with loading, from 16.3 ± 0.8 mg g^{-1} for GO-Arg (1:1) up to 39.3 ± 1.9 mg g^{-1} for GO-Arg (1:5), equivalent to ~1 mmol CO_2 g^{-1} (Table 3.3). Remarkably, the most functionalized sample also captured atmospheric CO_2 at room temperature, approaching its static capacity within four days. Beyond capture, these composites acted as efficient metal-free catalysts for the cycloaddition of CO_2 with epoxides to yield cyclic carbonates (Scheme 3.3, Fig. 5.5 Appendix A). In sequential "capture-conversion" experiments, GO-Arg (1:5) achieved 86% conversion efficiency, while GO-Arg (1:3) reached 83% under identical conditions (Table 3.3). This dual role exploits guanidinium groups for CO_2 activation and residual hydroxyl/carboxyl sites on GO for epoxide activation, enabling cooperative sorption–catalysis.

Table 3.3 *CO_2 uptake (TGA) and catalytic performance of GO-Arg composites in the cycloaddition of CO_2 to epoxides under metal-free conditions.*

GO:Arg ratio (w:w)	N content (at.%)	CO_2 uptake-Flow[a] ($mg_{CO2}/g_{adsorbent}$)	CO_2 uptake-Static[b] ($mg_{CO2}/g_{adsorbent}$)	Conversion[c] (%)
1:1	1.6	16.3 ± 0.8	20.1 ± 1.0	60
1:3	4.5	26.5 ± 1.3	26.5 ± 1.3	83
1:5	5.9	39.3 ± 1.9	39.3 ± 1.9	86

Uptake values determined by TGA: [a]under CO_2/N_2 mixture flow (1:1 % v/v); [b] after static CO_2 (99.995%) exposure for 2h. [c] Sequential capture/conversion workflow: (i) adsorption stage: 40 mg GO-Arg exposed to ~0.7 mmol CO_2 (99.9%) under dry conditions for 2 h at 100 °C (closed system); (ii) conversion stage: 0.1 mmol styrene oxide (0.1 M) in DMF, 48 h at 100 °C. Conversions determined by ^{1}H NMR with mesitylene as internal standard, assuming absorbed CO_2 as the limiting reagent.

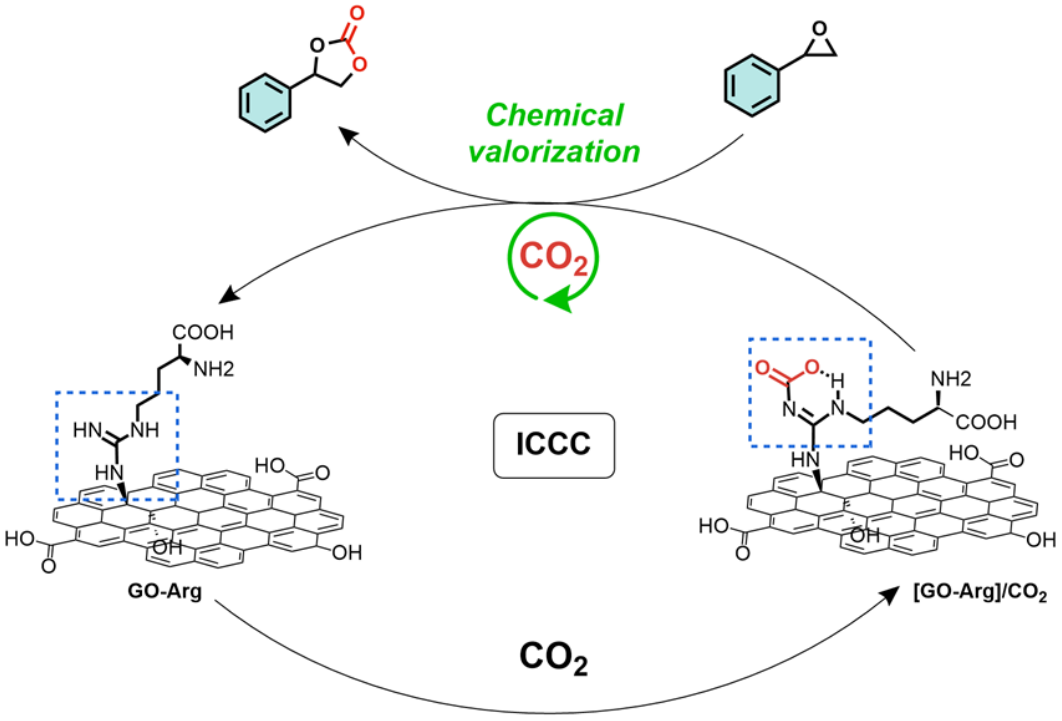

Scheme 3.3 *Schematic representation of the "integrated capture-CO_2-conversion" (ICCC) strategy, with the structural representation of chemically activated CO_2 by GO-Arg composite.*

Recyclability tests also demonstrated that the catalytic performance of GO-Arg was retained over at least five consecutive capture-conversion cycles, with >80% of the initial conversion efficiency preserved. This stability underscores the robustness of the covalently grafted guanidinium functionalities and confirms the potential of these composites as reusable, sustainable sorbent-catalyst systems.

The results presented in this section demonstrate how covalent grafting of small, inexpensive amino acids can impart distinct chemical identities to graphene oxide, turning it from a broadly reactive adsorbent into a set of task-specific materials. By comparing lysine, glutamic acid, methionine, and arginine derivatives, clear correlations emerged between side-chain functionality and material performance: amines enhanced affinity for neutral micropollutants, while guanidinium units enabled cooperative CO_2 binding and subsequent catalytic valorization. These examples highlight that even simple molecular modifications are sufficient to tune GO's polarity, charge distribution, and interaction landscape in a predictable way. Equally important, the synthetic approach employed (aqueous epoxide ring-opening under mild conditions) proved general, scalable, and compatible with downstream integration. This methodological robustness makes the findings relevant beyond dispersed nanosheets, providing the foundation for their transfer into more complex and industrially relevant systems.

In the broader logic of this thesis, the amino acid-GO hybrids thus represent a conceptual bridge: they translate the abstract idea of molecularly designed interfaces into a practical framework that can be applied to GO embedded in polymer matrices. The next section explores this translation, moving from nanoscale model systems to polysulfone-GO composites where the same chemistry is implemented in solid-state architectures.

3.2 In situ functionalization of graphene oxide-polysulfone composite granules

Building on the molecular-level insights gained from the functionalization of free-standing GO nanosheets, this section addresses the central aim of the thesis: translating selective GO reactivity into industrially relevant composite systems. We focus on polysulfone-graphene oxide composite granules, obtained by upcycling production scraps of Graphisulfone® membranes. Within these materials, embedded GO nanosheets offer reactive domains that can potentially be post-synthetically functionalized under mild aqueous conditions, thus overcoming the chemical inertness of the PSU matrix itself. The results presented in the following sections were published in *RSC Applied Interfaces* (DOI: 10.1039/D5LF00105F), and the work was selected for inclusion in the journal's collection on *Sustainable Development Goal 12: Responsible Production and Consumption*.

PSU-GO composite granules (Fig. 3.6), obtained by upcycling production scraps from Graphisulfone® hollow fiber membranes represent an industrially relevant platform.[43, 77] These granules retain the porous structure of the fibers and incorporate dispersed GO domains within the polysulfone matrix, already exhibiting intrinsic adsorptive properties for drinking water treatment. Their preparation from waste material also directly addresses circular economy goals, linking material development with sustainable production practices.

Among the various functionalization strategies applied to GO, amino acid modifications have proven particularly effective in tailoring surface chemistry toward organic micropollutants.[145] In particular, lysine-modified GO has shown remarkable adsorption performance for carbamazepine, an antiepileptic drug of increasing concern as emerging water contaminant.[177] Reported adsorption capacities reached values up to two orders of magnitude higher than those of pristine GO, underscoring the role of amine-bearing functionalities in driving hydrogen bonding and polar interactions with aromatic molecules.[128]

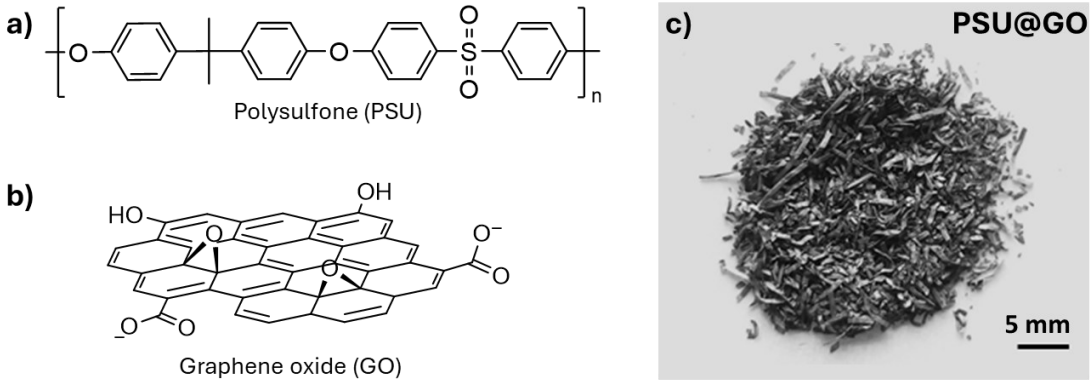

Figure 3.6 *Chemical structures of a) polysulfone and b) graphene oxide. c) granules of PSU-GO composite.*

These results have also been confirmed in composite systems: for example, alginate–GO-Lys hydrogels displayed enhanced removal of multiple organic contaminants, demonstrating that amino acid modification can be successfully translated into functional polymer-based materials.[178]

However, while embedding GO into polymers has become a consolidated strategy, the post-functionalization of GO domains already integrated within a composite remains comparatively unexplored. This limitation is particularly evident for engineering polymers such as polysulfone, whose high chemical stability generally requires harsh reagents or organic solvents for modification, thus limiting the feasibility of mild post-production tuning.[179-182] Only a few precedents suggest that embedded GO can still be chemically addressed: for instance, the covalent attachment of biomolecules within photosensitive acrylic resins has been reported to improve both mechanical performance and functional properties.[183] On this basis, the following section investigates whether mild aqueous-phase functionalization strategies, previously validated for free-standing GO nanosheets, can be extended to PSU-GO granules prepared from Graphisulfone® production scraps, with the aim of tailoring their adsorption performance without compromising material integrity.

3.2.1 Epoxide ring opening reaction on GO embedded nanosheets

To translate the amino acid functionalization approach from free-standing GO nanosheets to industrially relevant PSU-GO composites, an *in situ* recirculation strategy was developed. This method was designed to selectively modify GO domains embedded within the polymer matrix while preserving the structural integrity of the polysulfone backbone. A loop recirculation-based functionalization setup was employed, in which an aqueous solution of L-lysine was circulated through cartridges filled with PSU-GO granules using a peristaltic pump (Fig. 3.7). PSU-GO samples with different GO amounts (i.e. PSU-GO-A with 3.5% w/w and PSU-GO-B with 10% w/w GO/PSU ratios) were modified with lysine by an epoxide ring-opening reaction (Scheme 3.4).

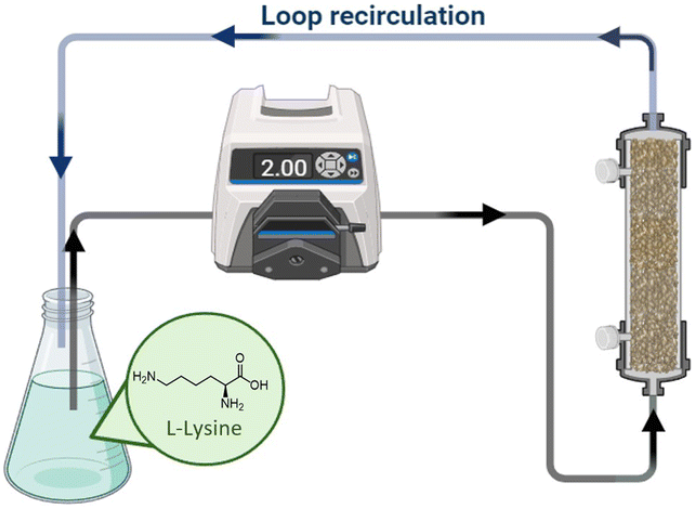

Figure 3.7 *Set up for in situ GO modification. The L-lysine solution is recirculated using a peristaltic pump through the PSU-GO cartridge.*

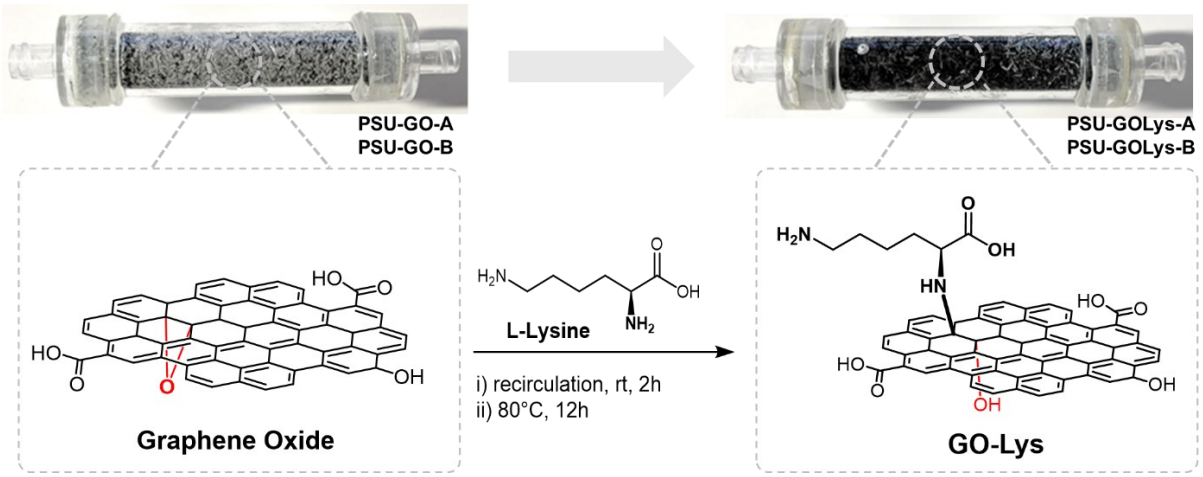

Scheme 3.4 *In situ lysine functionalization of GO embedded in PSU-GO granules with two different GO amounts (A: 3.5% w/w and B: 10% w/w PSU/GO).*

Basic conditions (pH 9.7) were maintained to ensure the deprotonation of the α-amino group of lysine, which acts as the nucleophile in the ring-opening of epoxide groups on the GO surface.[128, 184] The PSU backbone, characterized by its aromatic and sulfone-rich structure, does not contain reactive electrophilic sites under these conditions and thus remained chemically inert throughout the process.[185] The functionalization protocol avoided the use of organic solvents, coupling agents, or catalysts, ensuring compatibility with environmental applications and preserving the green character of the method. The recirculation step was introduced to address mass-transport limitations in the packed cartridge configuration and was carried out for 2 hours at a constant flow rate of 5 mL min^{-1}, ensuring homogeneous exposure of all GO-containing granules to the lysine solution and preventing preferential flow pathways. Subsequently, the cartridges were sealed and thermally treated at 80 °C overnight, providing the activation energy required to promote nucleophilic epoxide ring-opening and covalent bond formation between lysine and GO. After reaction, the system was washed with 2.5 L of ultrapure water to remove unreacted lysine, ensuring that only covalently bound species remained in the composite material (Fig. 5.6, Appendix B). The resulting materials, denoted as PSU-GOLys-A and PSU-GOLys-B, were then dried under ambient conditions prior to characterization and adsorption testing. The PSU-GOLys composites were characterized to confirm successful lysine modification and to assess any morphological or chemical changes induced by the process. SEM images provide insight into the morphology of the PSU-GO composites before and after functionalization (Fig. 5.7, Appendix B). Pristine PSU-GO granules display a hollow tubular structure with surface pores in the range of 5-10 µm (Fig. 3.8). After lysine treatment, no significant morphological changes were observed, indicating that the recirculation-based functionalization protocol preserved the structural integrity of the granules. ATR-FTIR was initially employed to compare the spectra of PSU, PSU-GO, and PSU-GOLys materials (Fig. 5.8, Appendix B). In all composites, the spectra were dominated by the sharp signals of the PSU matrix, which constitutes over 80% of the material and completely overlaps the broader features of GO.

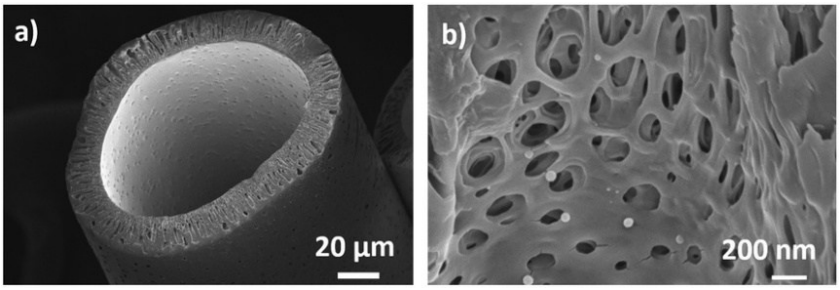

Figure 3.8 *SEM images of a) the cross section of a PSU-GO granule and b) the pores.*

As a result, and given the relatively low concentration of grafted lysine, no distinct vibrational bands attributable to lysine could be discerned. The only notable spectral variations were observed when comparing GO and GO-Lys, where a marked decrease of the C=O stretching band at 1720 cm^{-1} was accompanied by an increase and shift of the C=C stretching band at 1570 cm^{-1}.Thus, ATR-FTIR provided only limited information on the effective functionalization of PSU-GOLys A/B due to the spectral dominance of the PSU phase. XPS provided more definitive evidence of surface chemical changes following lysine functionalization. The survey spectra of PSU-GO and PSU-GOLys composites are shown in Figure 3.9, with the corresponding atomic compositions reported in Table 3.4. Lysine grafting was confirmed by the increase of the nitrogen (N 1s) signal, from 0.8% to 1.5% for PSU-GOLys-A (3.5% GO) and from 0.7% to 1.9% for PSU-GOLys-B (10% GO). These increments correspond to estimated lysine loadings of approximately 3.5% and 6%, respectively.

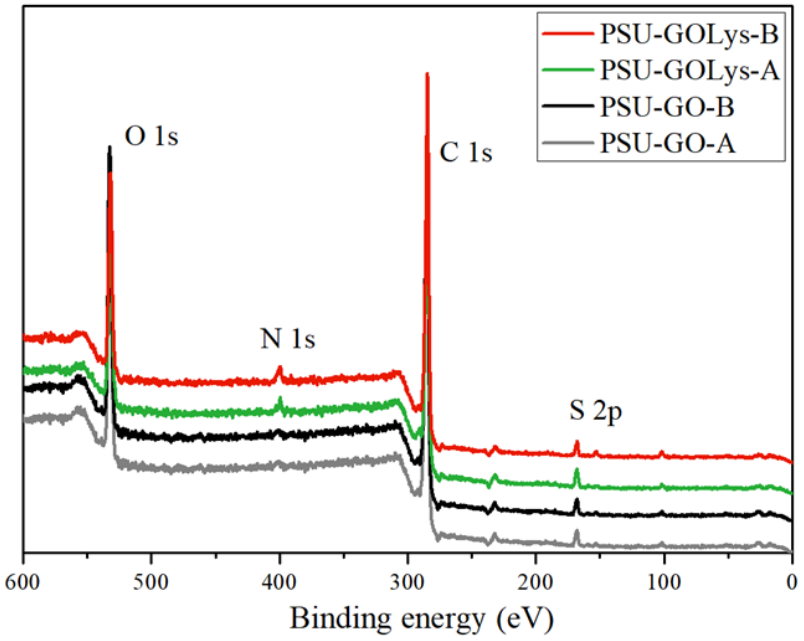

Figure 3.9 *XPS survey spectra of PSU-GO and PSU-GOLys composites.*

The C/O atomic ratio also increased after functionalization, from 4.2 to 4.5 for PSU-GO-A and from 3.6 to 4.3 for PSU-GO-B, indicating partial reduction of GO during the reaction, likely induced by the basic conditions and elevated temperature.[133] This interpretation is further supported by the visible darkening of PSU-GO granules after lysine functionalization (Scheme 3.4), in agreement with previous reports of mild GO reduction accompanying nucleophilic epoxide ring-opening.[186]

Table 3.4 *Atomic composition of PSU-GO and PSU-GOLys obtained by XPS.*

Composites	C%	O%	N%	S%	C/O	Lys Loading
PSU-GO-A	78.4	18.5	0.8	2.3	4.1	—
PSU-GO-B	76.5	21.2	0.7	1.6	3.6	—
PSU-GOLys-A	78.7	17.6	1.5	2.2	4.5	3.5%
PSU-GOLys-B	78.6	18.1	1.9	1.4	4.3	6%

High-resolution C 1s, O 1s, and N 1s spectra (Fig. 5.9, Appendix B) confirm the introduction of C–N functionalities and a relative decrease in oxygen content post-functionalization. The relatively low nitrogen content detected in pristine PSU-GO can be attributed to residual NMP (N 1s at 400 eV) from the hollow fiber fabrication process.[43, 187]

To more accurately determine the lysine content, the N contribution from pristine PSU-GO was subtracted from that of PSU-GOLys at 400 eV, and the remaining nitrogen was converted to lysine loading based on the atomic composition of lysine ((2N + 6C + 2O):2N), yielding the values reported in Table 3.4. GO and PSU show well-defined chemical states that can be reliably fitted, but PSU-GO and PSU-GOLys exhibit a higher variance in chemical states due to overlapping contributions from both components (e.g., C-O-C, C-OH, C=C, O-C=O, C=O, C-C, C-S in C 1s; C-O-C, S=O, C-OH, C=O in O 1s) and from lysine (C-N). To avoid overfitting, qualitative comparisons of line shapes were performed. For GO, the O 1s and C 1s fits (Fig. 5.9a-b, Appendix B) confirmed the presence of expected oxygen functionalities, with a C/O ratio of 2.6 and minor Cl and S contaminants. PSU spectra (Fig. 5.9e-f, Appendix B) matched literature values, with C:O and C:S ratios in close agreement with theoretical ones. In PSU-GO-B (Fig. 5.9g-l, Appendix B), O 1s and C 1s signals show combined PSU and GO features, while S 2p remains unchanged. For PSU-GOLys-B, only minor changes in C 1s (Fig. 5.9k, Appendix B) were observed compared to PSU-GO-B.

3.2.2 Lysine-driven enhanced ECs adsorption in water

The adsorption performance of PSU-GOLys composites was assessed using carbamazepine as a representative probe molecule for emerging organic contaminants. The choice of CBZ was informed by previous reports on its preferential interaction with amino acid-modified GO[128, 145] and by preliminary

selectivity tests carried out during this work on a selection of six emerging organic contaminants, including CBZ, iopamidol, paracetamol, caffeine, ofloxacin and bisphenol A (structures shown in Fig. 5.10, Appendix B). The selectivity screening involved both batch adsorption experiments on GO and GO-Lys powders and flow-through tests on PSU, PSU-GO, and PSU-GOLys composite cartridges. As expected, batch condition experiments showed a markedly improved CBZ removal with GO-Lys (65%) compared to unmodified GO (13%) after only 15 minutes of contact time (Fig. 5.11a, Appendix B).

Flow-through experiments on the contaminant mixture, using the same cartridge configuration adopted for functionalization (Fig. 3.10a), confirmed this trend. PSU-GOLys-A removed 58% of CBZ compared to 35% for PSU-GO-A, while PSU-GOLys-B reached 84% removal, versus 60% for PSU-GO-B (Fig. 5.11b-c, Appendix B). These findings supported the use of CBZ as a selective molecular probe to evaluate the effectiveness of lysine-based functionalization.

Subsequent adsorption tests were performed under continuous flow conditions using CBZ as the sole contaminant to quantify adsorption capacity and removal dynamics in more controlled conditions. The introduction of GO and subsequent lysine functionalization both contributed to significant increases in adsorption performance (Fig. 3.10b-c). PSU-GOLys-A (3.5% GO) exhibited an initial CBZ removal rate of 64%, compared to 41% for PSU-GO-A and 16% for unmodified PSU. After filtering 200 mL of CBZ-spiked solution, PSU-GOLys-A maintained a removal efficiency of 40%, while that of PSU-GO-A and PSU dropped to 12% and 5%, respectively. Complete breakthrough occurred after 600 mL of treated volume, with total CBZ uptakes of 107.2 $\mu g\ g^{-1}$ for PSU-GOLys-A, 27.5 $\mu g\ g^{-1}$ for PSU-GO-A, and 6.6 $\mu g\ g^{-1}$ for pristine PSU (Fig. 5.13a, Appendix B).

The enhancement associated with lysine modification was even more pronounced for PSU-GOLys-B, which contains a higher GO fraction (10% w/w). The lysine-modified granules reached an initial CBZ removal rate of 87%, maintaining over 60% removal within the first 500 mL of treated water. Complete breakthrough occurred after 1 L, corresponding to a final adsorption capacity of 259.5 $\mu g\ g^{-1}$, substantially higher than PSU–GO-B (66.5 $\mu g\ g^{-1}$) and pristine PSU (Fig. 5.13b, Appendix B). This trend is consistent with XPS analysis (Table 3.4), which shows higher lysine incorporation at increased GO loading, resulting in a greater density of adsorptive sites.

To validate that lysine functionalization involved covalent interactions with the GO surface rather than nonspecific physisorption, a control material (PSU@Lys) was synthesized by treating PSU-only granules under identical functionalization conditions. The resulting material showed CBZ removal performance comparable to pristine PSU, confirming that GO was essential for lysine anchoring and that enhanced adsorption was not attributable to polymer-based interactions (Fig. 5.12, Appendix B).

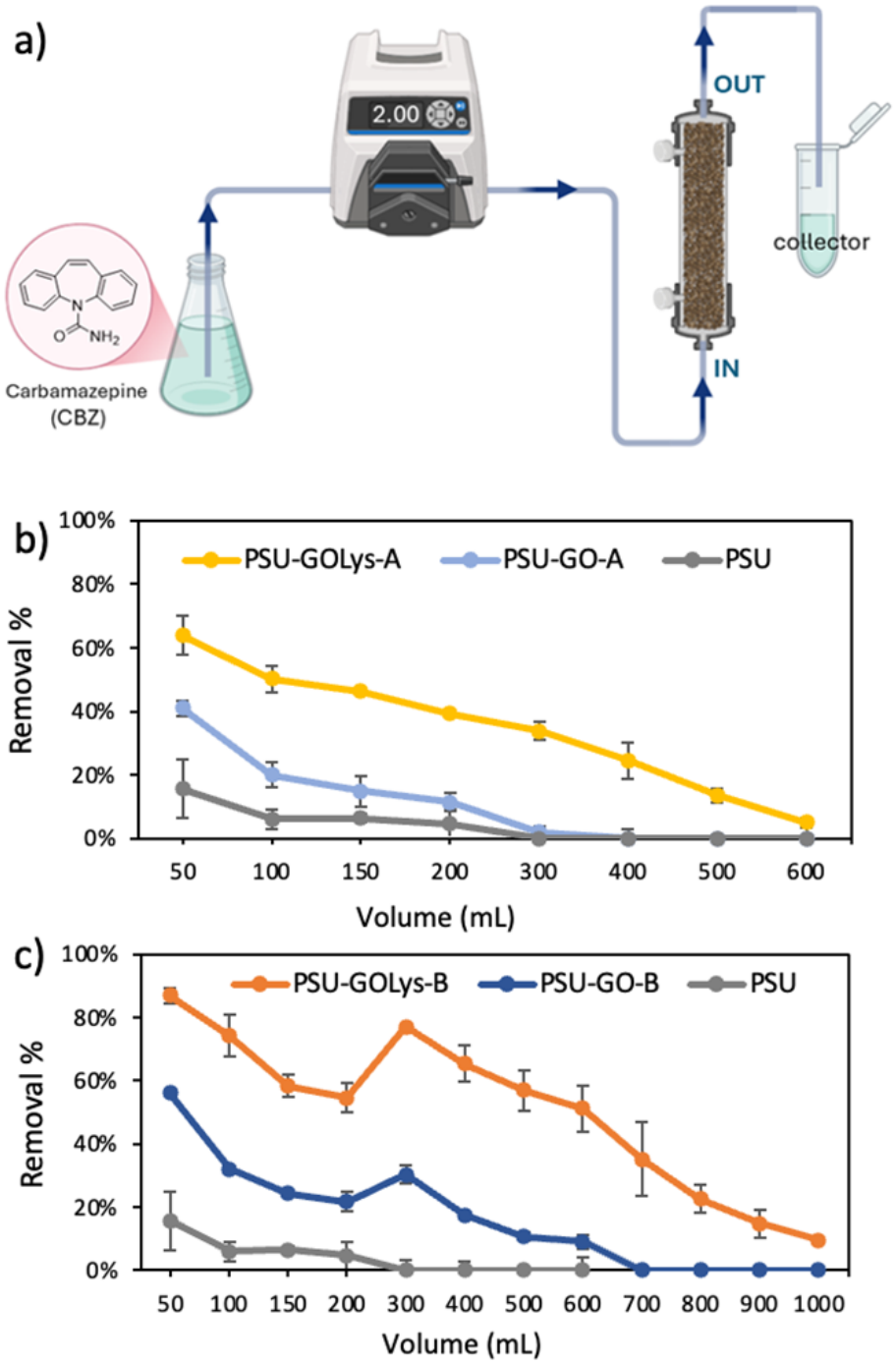

Figure 3.10 *a) Experimental setup used for the adsorption tests of CBZ in flow conditions. Spiked water (C_{IN} CBZ=0.5 mg L^{-1}, total volume=1L) is flowed through the cartridge (flow rate 5 mL $min^{-1)}$ and filtered water is collected and analyzed. Removal performance of b) PSU, PSU-GO-A and PSU-GOLys-A and c) PSU, PSU-GO-B and PSU-GOLys-B in the adsorption of CBZ under flow conditions.*

3.3 Functionalization of graphene oxide-polyethersulfone coated membranes

This section examines GO integrated as a multilayer coating on polyethersulfone hollow fibers, where GO is located at the membrane surface, forming a continuous and water-accessible layer that can be selectively modified after deposition, while the PES substrate provides mechanical stability and permeability. Two post-synthetic approaches were investigated. First, covalent modification with lysine was performed using an in-flow recirculation protocol adapted from the composite system to introduce amino functionalities into the surface-exposed GO layers. Second, chemical reduction with ascorbic acid was applied to partially restore sp^2 conjugation and modulate the electronic properties of the coating.

The resulting membranes were subsequently evaluated in selected application contexts to illustrate the functional versatility enabled by GO chemical tuning: lysine-modified coatings were assessed for their enhanced interaction with organic micropollutants, while reduced GO coatings were explored as electroactive membranes in electro-Fenton systems.

3.3.1 Coating procedure and GO layer modification

PES HF modules were coated with graphene oxide using a pressure-driven, water-based filtration procedure adapted from a previously reported protocol (Fig. 3.11).[28] An aqueous GO dispersion (2.0 mg mL^{-1}, pre-sonicated for 4 h) was filtered through the lumen side in cross-flow configuration, promoting the deposition of a conformal multilayer GO film on the fiber wall. Two dead-end filtration configurations were applied: "in-out," which immobilizes GO on the inner fiber wall, and "out-in," which results in deposition on the external fiber surface After deposition, the coating was thermally fixed by annealing at 80 °C for 16 h.

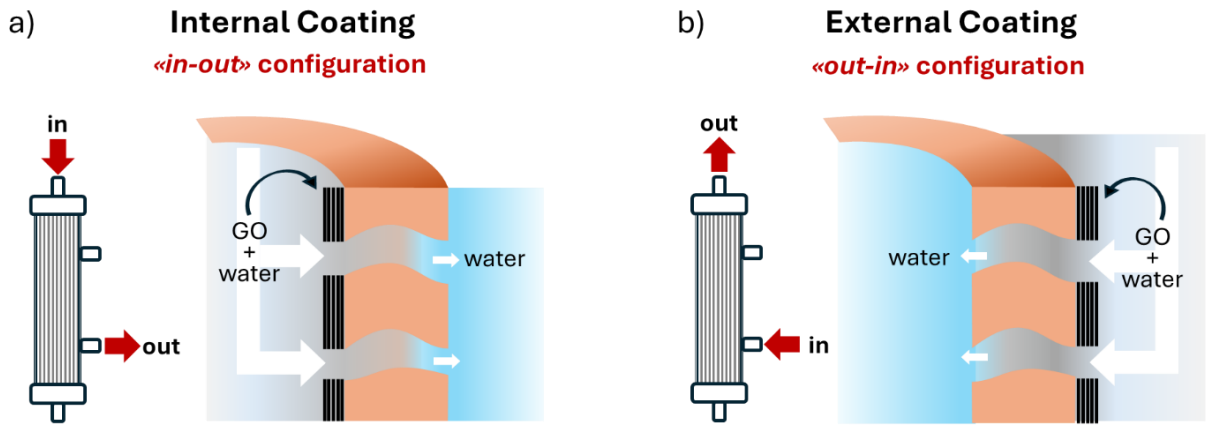

Figure 3.11 *Representation of the coating procedure. a) Filtration "in-out" to immobilize GO on the inner wall of PES HF; b) filtration "out-in" to deposit GO multilayer on the outer fiber wall. (Adapted from ref 28)*

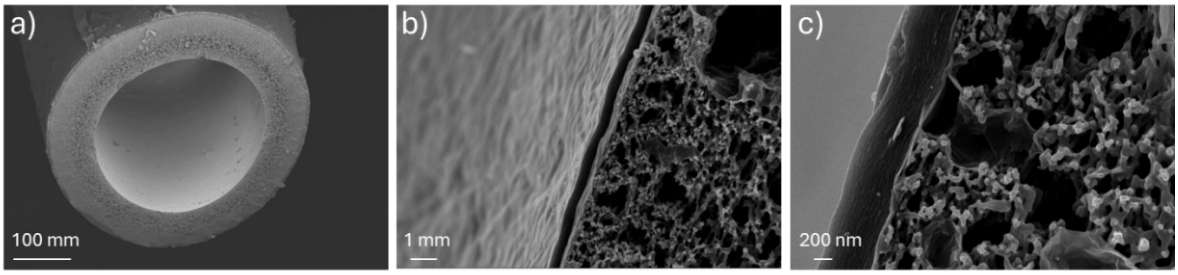

Figure 3.12 *SEM images of PES-GO coated HF membrane cross section (a) and GO coating external layer at different magnification (b-c).*

Reiteration of the filtration/fixation cycle allows control over coating thickness and overall GO loading. In this work, 7.5 mL of a 2 mg mL^{-1} GO dispersion was filtered per cycle and the process was repeated twice, alternating the entry point each time to maximize homogeneity. This procedure yielded PES-GO HF modules with a final GO content of approximately 5 % w/w (GO/PES). SEM micrographs of PES-GO coated HF membrane, reported in Fig. 3.12, show the coating layer and the preserved porosity of PES HF after the coating.

3.3.1.1 Lysine-functionalization and characterization

The synthetic pathways for the functionalization of polyethersulfone hollow fibers with lysine modified GO coatings are shown in Scheme 3.5. PES-GO coated HF were subjected to a recirculation-based treatment analogous to that developed for PSU-GO composites(Section 3.2.2). A basic aqueous solution of L-lysine (pH ≈ 9.7) was continuously recirculated for 2 h through the PES-GO HF modules in "in-out" or "out-in" configuration, to functionalize internally and externally GO-coated fibers, respectively. Following recirculation, the cartridges were sealed and incubated at 80 °C for 16 h to promote covalent bond formation. The modules were then thoroughly washed with ultrapure water to remove any unreacted lysine. These samples are hereafter denoted as PES-GOLys-A (Fig. 3.13).

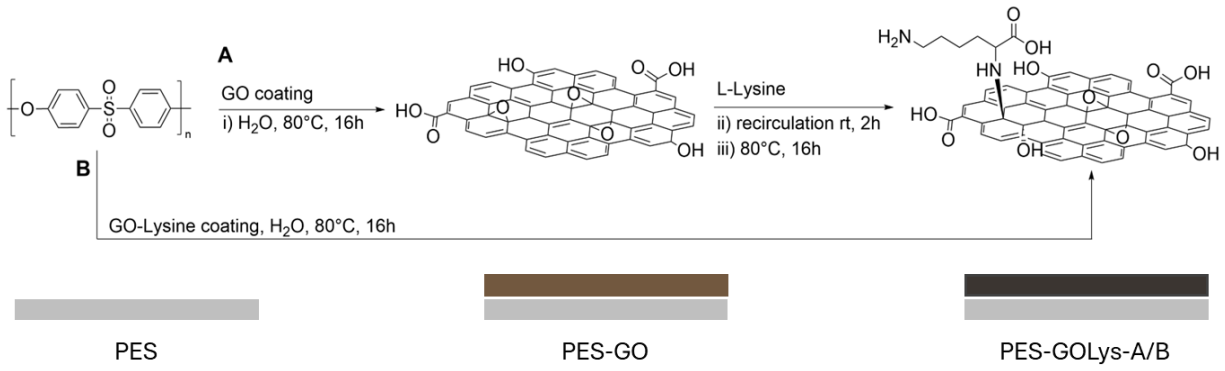

Scheme 3.5 *Functionalization routes for PES HF coated with Lysine-modified graphene oxide through two synthetic pathways: A) post functionalization of GO coated layer through lysine recirculation and fixation; B) functionalization of PES HF through coating with already functionalized GO-Lys.*

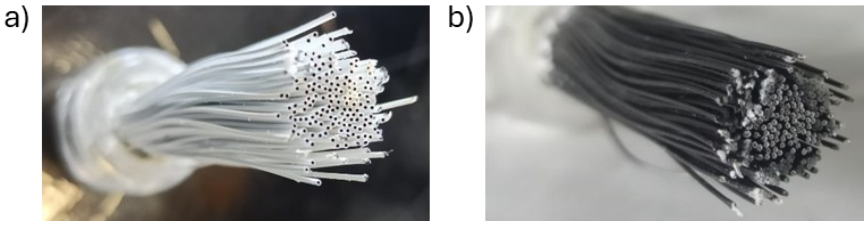

Figure 3.13. *PES HF (a) internally and (b) externally coated with GO functionalized with lysine.*

For comparison, PES HF modules were coated directly with a pre-synthesized GO-Lys dispersion,[128] using the same filtration/fixation protocol as for GO: a GO-Lys dispersion (2 mg mL^{-1}) was prepared by for 4h sonication in ultrapure water, and after annealing at 80 °C for 16 h and extensive washing, the resulting samples were denoted PES-GOLys-B.

The morphology of the lysine-functionalized PES-GO was examined by SEM (Fig. 3.14). Post-functionalized samples (PES-GOLys-A) displayed relatively homogeneous and smooth coatings (Fig 3.14a-c), in some cases allowing the underlying porosity of the PES wall to be discerned. I contrast, fiber coated with pre-synthesized GO-Lys (PES-GOLys-B, Fig. 3.14d-f) exhibited thicker and less uniform films, with visible aggregates disrupting the film morphology. X-ray photoelectron spectroscopy was performed on externally coated fibers to assess surface composition after lysine functionalization (Fig. 3.15). Both PES-GOLys-A and -B displayed a clear N 1s signal, absent in pristine PES-GO, confirming successful lysine incorporation. Atomic compositions (Table 3.5) revealed nitrogen contents of 3.6 at% for PES–GOLys-A and 2.4 at% for PES–GOLys-B. The nitrogen level measured for PES-GOLys-B is consistent with the lysine loading previously determined for free-standing GO-Lys nanosheets (~15%), confirming that the functionalized phase is preserved upon deposition onto the PES surface.

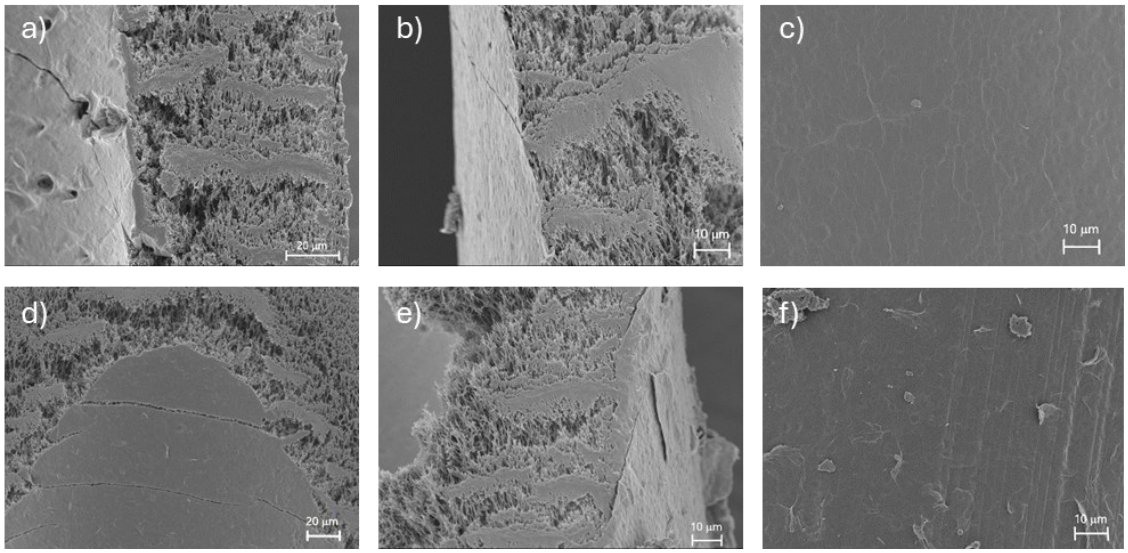

Figure 3.14 *SEM images of PES-GO HF after lysine functionalization. Internal coatings: (a) PES-GOLys-A and (d) PES-GOLys-B. External coatings: PES-GOLys-A(b,c) and PES-GO-B(e,f), shown at different magnifications.*

The slightly higher nitrogen content observed for PES–GOLys-A indicates that the in situ post-functionalization strategy enables efficient lysine grafting directly on the surface-exposed GO layer, without requiring prior nanosheet functionalization. A minor feature observed near 260 eV in the survey spectrum of PES–GOLys-B corresponds to the Na KLL Auger signal (kinetic energy ≈ 994 eV), arising from residual sodium species associated with the NaOH-assisted synthesis of GO-Lys nanosheets. This signal is not detected in PES–GOLys-A, where lysine grafting was performed directly on the coated membrane without NaOH addition. The presence of residual sodium in PES–GOLys-B therefore reflects the synthetic history of the precursor material and does not affect the interpretation of nitrogen incorporation as evidence of covalent functionalization.

Contact angle measurements (CA) further supported the surface modification (Fig. 5.14, Appendix C). Unmodified PES-GO coated HF showed a CA of 72.9°, which increased after lysine functionalization, to 83.8° for PES-GOLys-A and 78.9° for PES-GOLys-B. This shift is consistent with the partial reduction of GO layer after functionalization, as also indicated by the increase in C/O ratio from 2.3 (PES-GO) to 4.0-4.1 (PES-GOLys, Table 3.5).

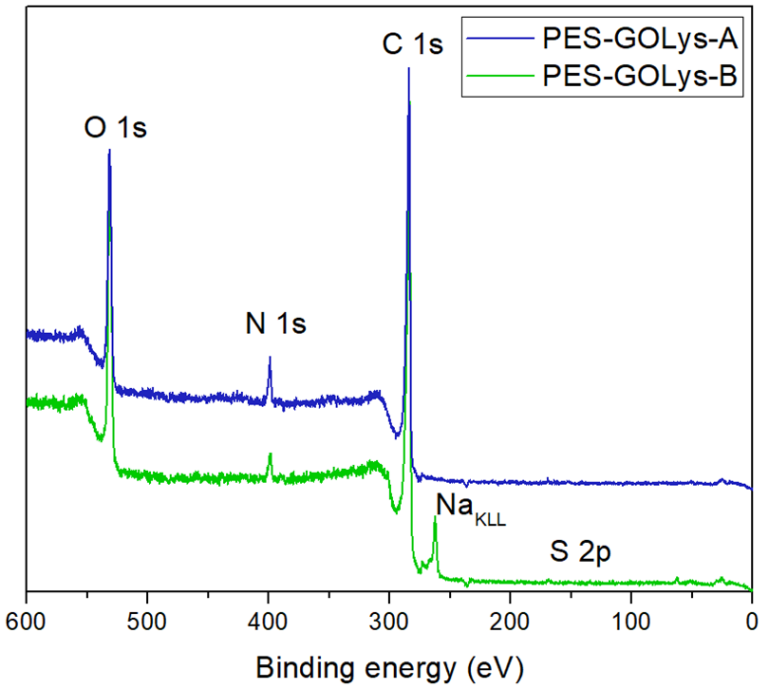

Figure 3.15 *XPS survey spectra for PES-GOLys samples.*

Table 3.5 *Atomic composition of PES-GO and PES-GOLys obtained by XPS.*

Membrane	C%	O%	N%	S%	C/O	Lys Loading
PES-GO	69.5	30.5	-	-	2.3	-
PES-GOLys-A	77.5	18.7	3.6	0.2	4.1	18%
PES-GOLys-B	77.1	19.1	2.4	0.4	4.0	12%

3.3.1.2 Reduction of GO coating layer and characterization

Whereas lysine grafting enriches the GO coating with polar, interactive groups for adsorption, chemical reduction targets a complementary goal: restoring sp^2 conjugation to enhance electrical conductivity and alter interfacial properties needed for electrochemical processes. The complete functionalization pathway is illustrated in Figure 3.16a. Externally coated PES-GO HF modules (Fig. 3.16c) were prepared as in 3.3.1 using the "out-in" filtration configuration. L-ascorbic acid (AsA) was selected as a mild, water compatible and environmentally friendly reducing agent.[188, 189] Reduction was performed by injecting 3 mL of 0.2 M AsA solution into the dead volume of the PES-GO hollow fiber membrane module. The sealed module was incubated at 60 °C for 2 hours to promote uniform in situ reduction.

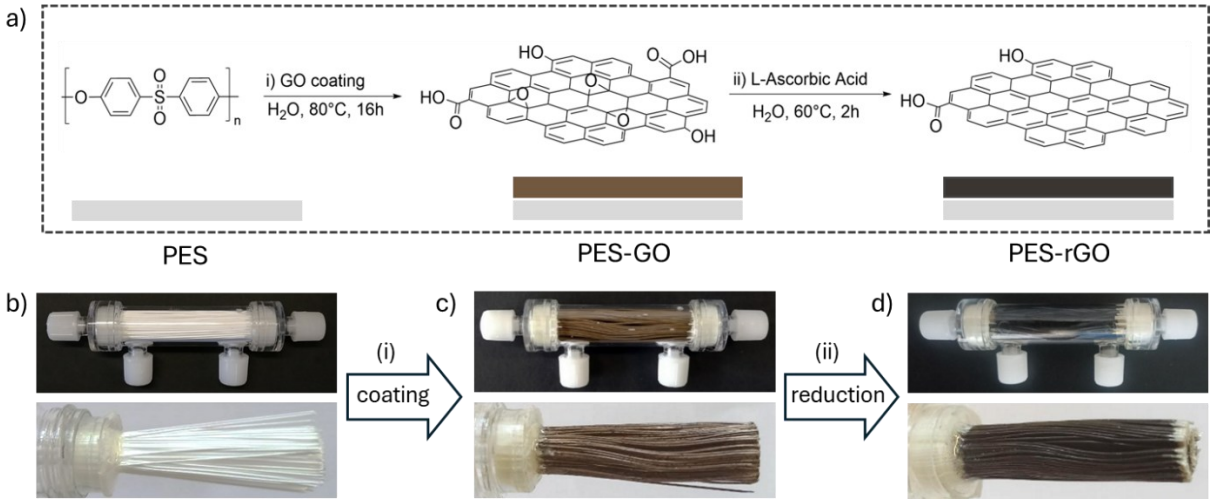

***Figure 3.16**. a) Synthetic pathway for the functionalization of polyethersulfone (PES) HF membranes through graphene oxide external coating (i) and chemical reduction of GO to rGO with L-Ascorbic Acid (ii); cartridge module and free hollow fiber bundles of b) pristine PES-GO and d) PES-rGO.*

Following the reaction, PES-rGO membrane (Fig. 3.16d) was thoroughly rinsed with distilled water to remove any residual byproducts. All membrane cartridges were cut open to extract the HF bundles from the module casing. The membranes were subsequently used in the form of free HF bundles for all characterization and electrochemical experiments, ensuring consistent geometry and proper electrical contact throughout the study. FTIR spectra of pristine PES and PES-GO/rGO HFs (Fig. 5.15, Appendix C) highlight the functionalization changes induced by GO coating and its subsequent reduction. PES showed characteristic bands of the polymer backbone, including aromatic ring stretching (~1580 cm^{-1}), sulfone groups (1320 and 1150 cm^{-1}), and C-O-C stretching vibrations (~1235 cm^{-1}).[190] Upon GO deposition, additional bands associated with oxygenated functional groups appeared, such as C=O (~1725 cm^{-1}), O-H (~3400 cm^{-1}), and C-O (1225 and 1050 cm^{-1}).[191]

Following chemical reduction with L-ascorbic acid, a noticeable attenuation in the intensity of these oxygen-related bands was observed, particularly in the C=O and O-H regions, indicating partial removal

of oxygenated groups. This shift is consistent with the partial restoration of sp^2 carbon domains and the formation of reduced graphene oxide.[192, 193] XPS was employed to investigate the surface elemental composition and chemical states of the GO- and rGO-functionalized PES membranes. XPS survey spectra did not reveal a significant presence of sulfur on the surface, suggesting that PES external wall is uniformly coated by the GO and rGO layers (Fig. 3.17a). The atomic C/O ratio was found to increase from 2.3 in the PES-GO membrane to 3.9 in PES-rGO (Table 3.6), reflecting a notable reduction in surface oxygen functionalities following chemical reaction with L-ascorbic acid. Further insight into the carbon bonding environment was obtained through deconvolution of the high-resolution C 1s spectra (Fig. 3.17b-c and Fig. 5.16, Appendix C).

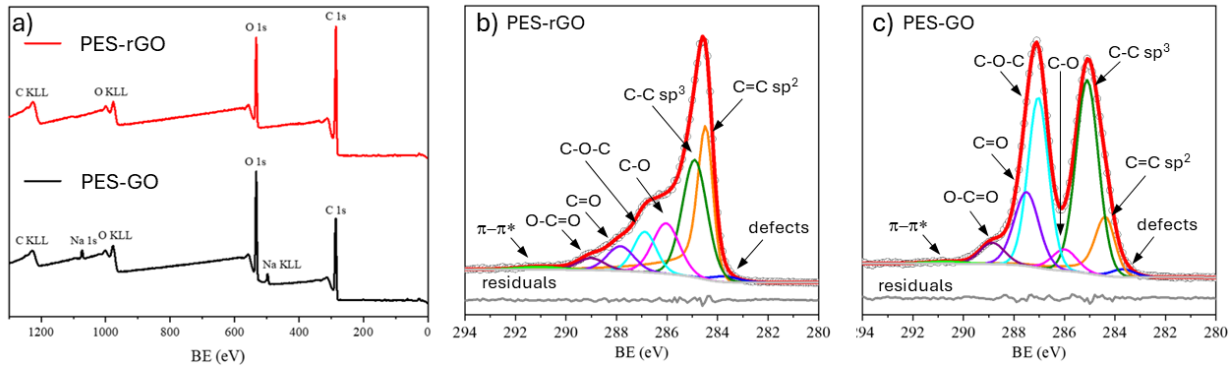

Figure 3.17 *a) XPS Survey spectra of PES-rGO and PES-GO coated hollow fiber membranes; High resolution (PE = 10 eV) spectra for C 1s region and curve-fitting for PES-rGO (b) and PES-GO (c) membranes.*

Table 3.6 *XPS atomic percentage and C/O ratio for PES-GO and PES -rGO membranes.*

Membranes	**C%**	**O%**	**C/O ratio**
PES-GO	69.5	30.5	2.3
PES-rGO	79.4	20.6	3.9

Minor peaks included a low-binding-energy shoulder (<284 eV), indicative of structural defects in the graphitic domains, and a π–π* satellite (~291.0 eV), associated with aromatic conjugation. The evolution of peak intensities and relative atomic percentages (Table 3.6) confirms a significant deoxygenation of the GO coating upon reduction, along with partial restoration of graphitic domains, supporting the spectroscopic evidence obtained by FTIR.

To assess the effect of GO functionalization and subsequent reduction on the electrical properties of the membranes, the effective bulk electrical resistivity of the hollow-fiber bundles was determined using a four-point probe configuration.[194] The measurements yield an averaged resistivity value over the fiber bundle geometry and are used here to compare the relative electrical behavior of PES, PES–GO, and PES–rGO membranes under identical probing conditions. The voltage–current relationships obtained at the three applied potential setpoints are reported in Figure 5.17 (Appendix C).

For all samples, the measured voltage drop increased proportionally with the recorded current, indicating consistent electrical response across the investigated range and supporting the reliability of the resistivity determination. As shown in Table 3.7, the pristine PES membrane exhibited a high resistivity of 4.4×10^7 Ω·m, consistent with its insulating polymeric nature. Upon GO deposition, resistivity decreased to 1.2×10^2 Ω·m, indicating the introduction of localized conductive surface domains despite the intrinsically insulating character of graphene oxide. A significant decreased was observed after chemical reduction, with PES-rGO membrane displaying a resistivity of 4.7 Ω·m, reflecting partial restoration of sp^2-hybridized carbon domains and enhanced electron transport. Although this value confirms successful reduction and functionalization, it remains several orders of magnitude higher than those reported for thin film rGO materials, which typically range from 10^{-5} to 10^{-3} Ω·m.[195, 196] This discrepancy can be attributed to the structural complexity of the hollow fiber system, where incomplete percolation between rGO domains across the three-dimensional membrane surface limits macroscopic conductivity.

Table 3.7 *Electrical resistivity of PES, PES-GO and PES-rGO membranes.*

Membrane	ρ (Ω·m)[a]
PES	4.4×10^7
PES-GO	1.2×10^2
PES-rGO	4.7

[a]Electrical resistivity (ρ) was calculated using the standard relation: $\rho = \left(\frac{V}{I}\right)\left(\frac{A}{L}\right)$ *where V is the measured voltage, I the recorded current, L the distance between the voltage probes (L=4 cm), and A the cross-sectional area of the fibers bundle (A=~311 cm², calculated considering 275 fibers, 60x0.3 mm each). For each membrane type, measurements were performed at three different current intensities, and the reported resistivity values represent the average to ensure reproducibility.*

Cathodic polarization experiments were performed to investigate the electrochemical response of the functionalized membranes under applied voltage.[197, 198] The tests were conducted in a single-compartment glass cell (200 mL), with PES, PES-GO, and PES-rGO used as the working electrode. The polarization curves (Fig. 3.18) show that PES-rGO consistently delivered higher current across the entire voltage range, with a maximum of -87.3 mA at -10 V, exceeding the values obtained for PES (-73.5 mA) and PES-GO (-69.4 mA). Notably, the relatively high current densities observed even for pristine PES, despite its insulating character inferred from resistivity measurements, suggest additional mechanisms involved in the electrochemical response. The modest increase in cathodic current relative to the pronounced decrease in bulk resistivity indicates that the electrochemical behavior is governed not only by electronic conductivity, but also by interfacial charge-transfer kinetics and the limited fraction of electrochemically accessible conductive pathways within the polymer matrix. Accordingly, the enhanced response of PES-rGO can be attributed to improved electronic transport within rGO domains, rather than uniform increase in macroscopic conductivity.

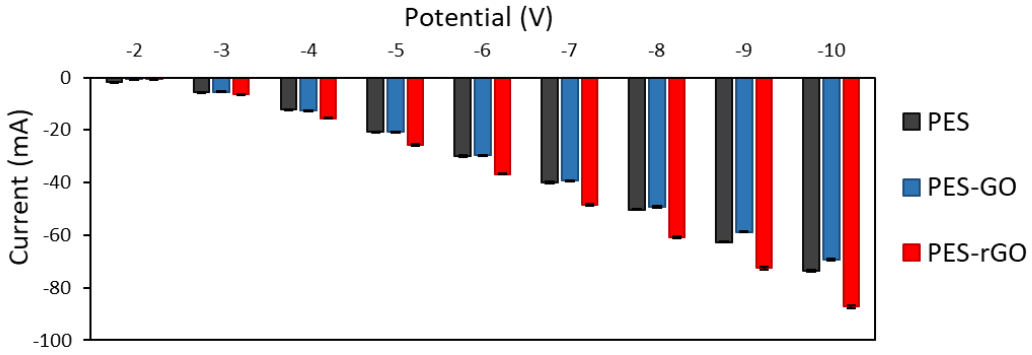

Figure 3.18 *Current response of PES, PES-GO, and PES-rGO membranes measured at increasing cathodic potentials (0 to -10 V) in phosphate buffer solution (5.5 mS cm^{-1}, pH 7).*

3.3.2 Applications

3.3.2.1 Lysine-functionalized coated membranes for carbamazepine adsorption

Lysine-functionalized graphene oxide coatings on polyethersulfone hollow fibers provide a compact adsorptive membrane platform for the removal of contaminants from water. The GO layer on the lumen wall concentrates active sites at the pore-water interface, and *in-out* cross-flow operation promotes convective transport across functional the film. Lysine grafting introduces amine-bearing and polar functionalities that increase hydrogen-bonding and polar–π interaction sites, favoring capture of micropollutants. PES-GOLys-coated hollow fibers were evaluated for their adsorption capability toward carbamazepine in water. CBZ is an was selected as a probe contaminant based on previous studies reporting enhanced CBZ affinity with lysine-functionalized GO, both as free nanosheets and as GO-based composites.[128, 145, 178, 199]

Accordingly, tests used internally coated fibers operated in in–out mode to ensure direct convective contact with the lysine-modified lumen surface, as sketched in Figure 3.19.

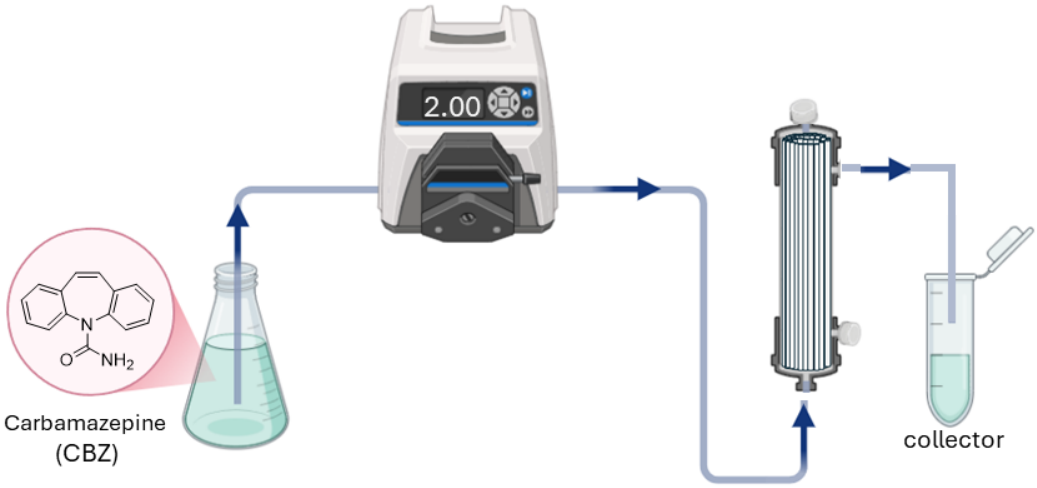

Figure 3.19 *Experimental setup used for the adsorption tests of CBZ in cross-flow conditions with PES, PES-GO and PES-GOLys-A/B membranes. Spiked water (C_{IN}=0.5 mg L^{-1}) is flowed through the cartridge (flow rate 5 mL min^{-1}) and filtered water is collected and analyzed.*

Two functionalization strategies were compared on otherwise identical internally coated fibers: PES-GOLys-A, obtained by post-functionalization of the immobilized GO layer via lysine recirculation, and PES-GOLys-B, prepared by coating with a pre-functionalized GO-Lys dispersion. As detailed in 3.3.1.1 (XPS, SEM), the post-functionalized films exhibit higher lysine incorporation and a more uniform morphology than the pre-functionalized coatings, features expected to influence site density, accessibility, and breakthrough behavior under flow.

Adsorption performance was assessed under standardized hydraulic conditions (CBZ in ultrapure water; C_{IN} = 0.5 mg L^{-1}, 5 mL min^{-1}, treated volume = 1 L) and is reported as removal profiles and cumulative uptake for pristine PES, PES-GO, PES-GOLys-A, and PES-GOLys-B (Fig. 3.20). Pristine PES and PES-GO showed negligible CBZ uptake, saturating within 200 mL (cumulative removals 9.9 µg and 23.6 µg, respectively). Lysine functionalization markedly improved CBZ affinity: PES-GOLys-A maintained >60% removal through the first 300 mL and reached a total uptake of 233.6 µg after 1 L of treated solution, outperforming all other membranes. PES-GOLys-B also exceeded PES and PES-GO, reaching127.5 µg of CBZ removed, although its efficiency decreased more rapidly with treated volume, consistent with the lower lysine loading quantified by XPS (Table 3.5).

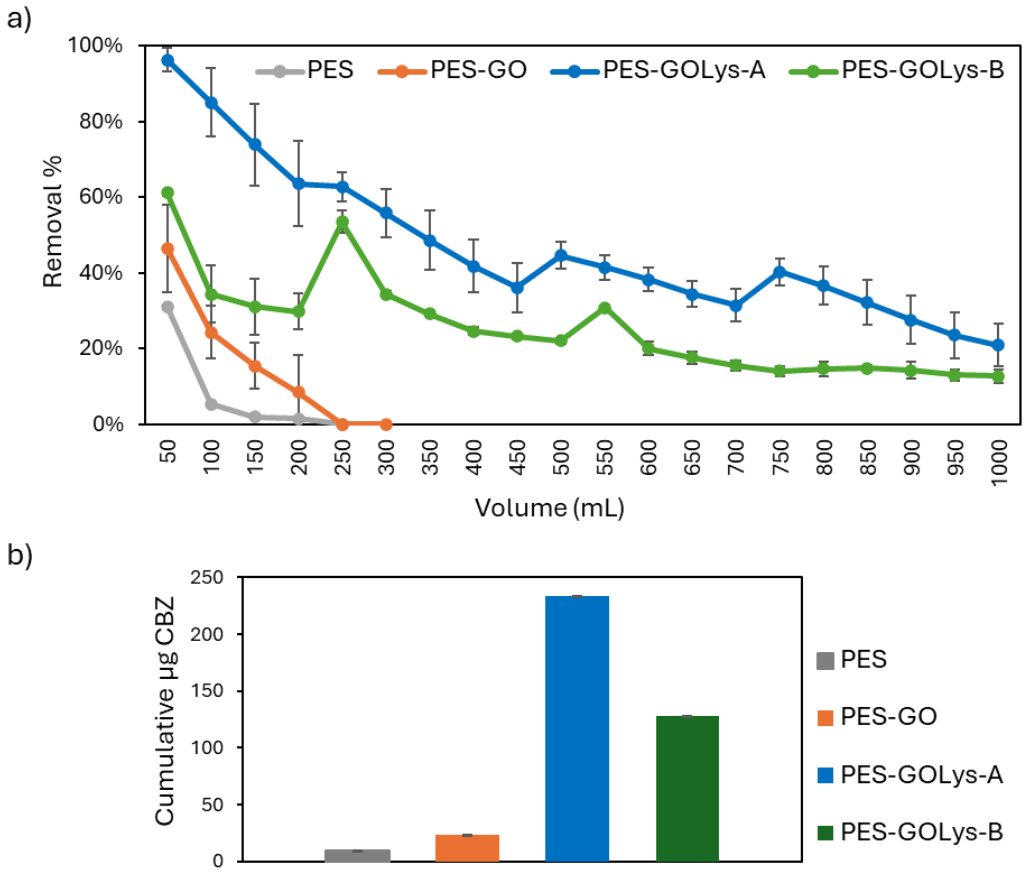

Figure 3.20 *a) Removal performance of PES, PES-GO and PES-GOLys-A/B in the adsorption of CBZ under flow conditions (C_{IN} = 0.5 mg L^{-1}, total volume = 1 L). b) Cumulative µg of CBZ removed by PES, PES-GO and PES-GOLys-A/B (C_{IN} = 0.5 mg L^{-1}, flow rate = 5 mL min^{-1}, treated volume 1 L).*

3.3.2.2 Reduced graphene oxide coated membranes for electrochemical applications

The chemical reduction of the GO coating on PES-GO hollow fibers (presented in 3.3.1.2) increased the conductivity of the membrane surface (Tab. 3.7, Fig. 3.18), opening opportunities for applications beyond traditional filtration supports. Within the framework of collaborative research activities carried out with the Lequia Institute (University of Girona),[79] rGO-coated PES membranes have shown promising behavior as electroactive interfaces, promoting improved interactions with electroactive biological systems under aerobic conditions, enhanced biodegradation kinetics, and improved membrane operational stability, without the need for external electrical circuits or increased system complexity.

Building on this broader context, the present section focuses on a different application scenario explored during my six-month research period at the Lequia Institute, namely the use of PES–rGO membranes as cathodes in electro-Fenton (EF) processes. This work is presented as a feasibility study aimed at evaluating whether rGO-coated hollow fibers can sustain cathodic operation under EF conditions, with specific objectives of (i) generating hydroxyl radicals (•OH), (ii) promoting oxidative pretreatment of polyethylene (PE) waste, and (iii) enhancing its subsequent biodegradability. EF experiments were conducted in aqueous electrolyte under acidic conditions (pH ≈ 3), using iron as a homogeneous catalyst (0.18 mM Fe^{2+}). The membrane module operates as a cathode by supplying electrons to sustain the catalytic cycle through oxygen reduction to H_2O_2 at the cathode surface and electrochemical regeneration of Fe^{2+} from Fe^{3+} in solution. Hydroxyl radicals are then produced in the bulk electrolyte via the homogeneous Fenton reaction between Fe^{2+} and H_2O_2. Full details of the electrolyte composition, applied potentials, and analytical protocols are reported in Appendix C. The electrochemical activity of the membranes was first evaluated through •OH quantification, using terephthalic acid (TA) as a molecular probe. The experimental setup and the EF mechanism are illustrated in Figure 3.21.

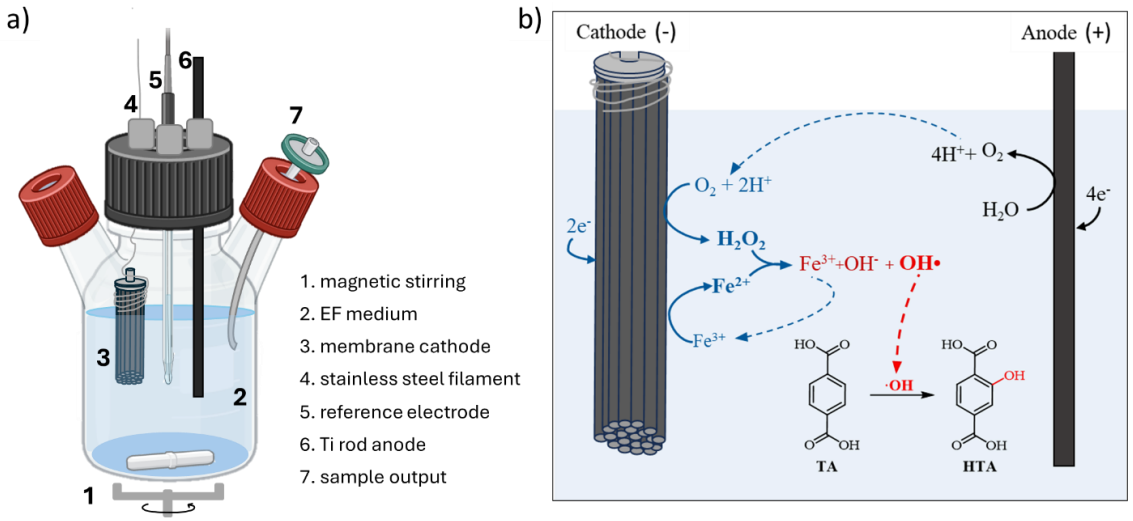

Figure 3.21 *a) Experimental setup for hydroxyl radical quantification under EF conditions using PES, PES-GO, and PES-rGO membranes as cathodes; b) schematic representation of the electro-Fenton reactions responsible for OH generation and their subsequent reaction with terephthalic acid (TA).*

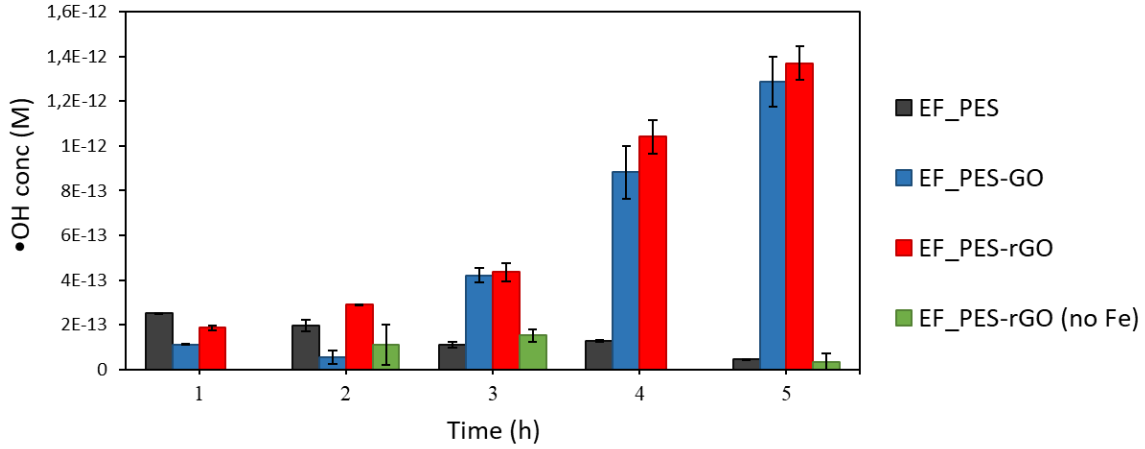

Figure 3.22 *Hydroxyl radical (OH) concentration profiles over 5 hours of electro-Fenton operation using PES, PES-GO, and PES-rGO membranes as cathodes. A control experiment without iron is included.*

In the present context, •OH concentration is not interpreted as a short-time performance metric, but as an indicator of the ability of the membrane cathode to sustain electro-Fenton activity over time (Fig. 3.22). Pristine PES exhibits a transient •OH signal during the initial stages of operation (1–2 h), which rapidly levels off, whereas GO- and rGO-coated membranes showed continuous •OH concentration increasing, reaching 10^{-12} M within 5h. Control experiments carried out in the absence of Fe^{2+} showed negligible radical formation, confirming that •OH generation proceeded via the EF mechanism.

These results indicate that the presence of a GO-based coating is sufficient to activate and sustain the EF process under the investigated conditions. In this regime, the role of rGO is therefore not to increase instantaneous radical concentration, but to support prolonged cathodic operation at the membrane interface, limiting direct electrochemical stress on the polymer substrate and enabling stable EF performance over extended operation times.

To explore the applicability of these membranes as cathodes for plastic oxidation, a 20h EF pretreatment was applied to PE fragments derived from agricultural plastic waste (Fig. 5.18, Appendix C). The extent of PE oxidation after EF pretreatment was investigated using complementary surface-sensitive techniques with different probing depths. CA analysis, probing the outermost molecular layer (~1 nm), revealed negligible differences across samples. A slight increase in hydrophilicity was observed for PE treated with PES-rGO fibers, with contact angles reduced by ~5-10° compared to untreated PE (Fig. 5.19, Appendix C). This suggests either a limited introduction of polar functionalities at the immediate surface, or a partial reorientation of oxidized moieties away from the air interface, potentially masking stronger modifications beneath.

XPS, probing the first few nanometers of the surface, confirmed only a modest increase in oxygen content after EF treatment (Table 3.8 and Fig. 5.20, Appendix C). The composition of pristine PE (100% C) was already altered in the control sample, where the oxygen is about 6 %at., indicative of natural surface weathering.[200]

Table 3.8 *XPS atomic composition of PE and degraded PE. Sample immersed in electrochemical solution presents also some residual from Cl (Cl 2p at 200 eV) and P (P 2p at c.a. 134 eV, POx) lower that 1%.*

	C 1s		***O 1s***	**N 1s**	***Si 2p***
	285.0 eV		***532.5 eV***	**400 eV**	***102 eV***
	C-C	**C-O/C=O**	**O-C/O-Si**		**Si-O**
PE_control	80.8	10.1	6.0	1.5	1.6
PE_PES_EF	80.0	7.8	8.1	1.4	1.5
PE_PES-GO_EF	71.7	9.7	11.8	2.4	4.2
PE_PES-rGO_EF	78.6	8.6	9.3	1.3	1.1

Although oxygen fractions increased following exposure to PES-GO and PES- rGO fibers, much of this signal could be attributed to inorganic contaminants (SiOx, POx, electrolyte residues), rather than to genuine PE oxidation. The C 1s line shape was essentially unchanged across all samples (Fig. 5.21, Appendix C), with small increase of C-O or C=O components.

In contrast, ATR-FTIR spectroscopy (Fig. 3.23), which probes deeper beneath the surface, revealed more evident oxidation features following EF treatment with PES-rGO membrane. New vibrational bands appeared at 1700-1750 cm^{-1} 1000-1240 cm^{-1}, corresponding to carbonyl and C-O stretching modes, characteristics of ketones, acids, and alcohols.[201-203] These changes are compatible with surface oxidation processes initiated by hydroxyl radicals generated at the cathode during EF operation.[204]

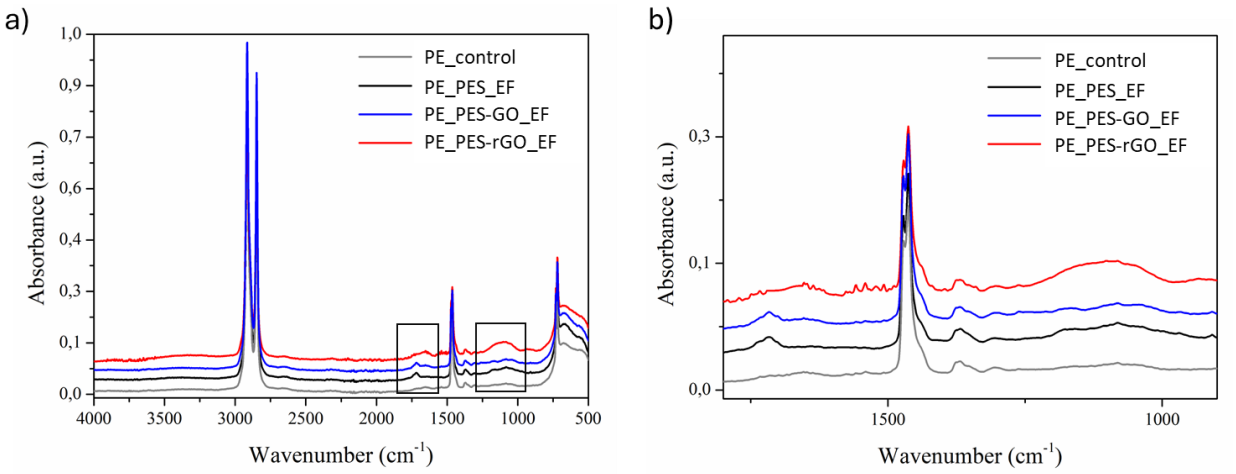

Figure 3.23*. a) ATR-FTIR spectra of polyethylene (PE) before (control) and after electro-Fenton (EF) treatment using PES, PES-GO, and PES-rGO membranes as cathodes, with magnification (b) of the 1800–900 cm⁻¹ region highlighting oxidative modifications.*

To assess the impact of EF pretreatment on polyethylene biodegradability, microbial respiration was monitored over a 21-day period, allowing quantification of microbial oxygen consumption as an indirect measure of the PE biodegradation (set-up described in Fig. 5.22, Appendix C).[205, 206] The results (Fig. 3.24) suggest that the PES-rGO membrane effectively performs as cathode for EF pretreatment,

enhancing microbial accessibility to the polymer surface and promoting subsequent biodegradation, with a BOD value of 25±4 mg O_2/g PE. This is comparable to the value obtained for PE treated with a standard stainless steel (SS) cathode (20±6 mg O_2/g PE), and both are markedly higher than the BOD value measured for the BIO control (10±3 mg O_2/g PE), i.e. PE subjected only to biological treatment without EF pretreatment.

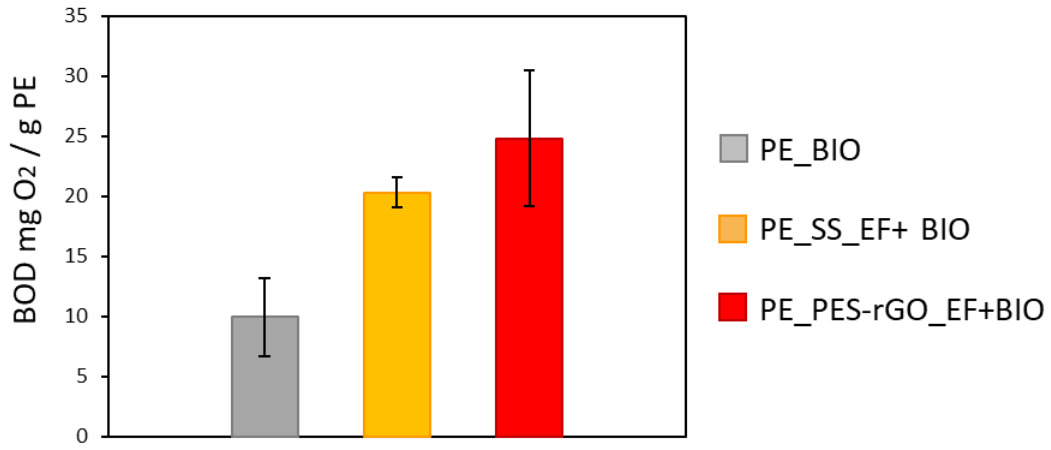

Figure 3.24 *BOD values for EF-treated PE using PES-rGO membranes as cathode (red), compared to untreated PE (BIO control) and EF-treated PE using a standard stainless steel (SS) cathode.*

At this stage, biodegradability tests were intentionally limited to PE pretreated with PES–rGO membranes, as respirometric measurements are time-consuming and were selected to verify whether the oxidative modifications detected after EF treatment translated into a measurable biological response. A more systematic comparison across membrane types, conducted under standardized conditions and examining both the solid PE fraction and any soluble oxidation intermediates, would help clarify the respective contributions of membrane composition, GO loading, and coating stability to the observed biodegradation response, as well as the role of low-molecular-weight species generated during EF treatment in contributing to microbial oxygen demand. Within this context, the behavior of the PES-rGO membrane points to a broader conceptual opportunity: electroactive GO-based coatings may enable polymeric HF into multifunctional filtration platforms, combining microplastics retention at the membrane surface with sustained EF-driven oxidative activation and downstream biological processing, thereby outlining a potential tandem EF–biodegradation strategy for integrated microplastic treatment.

4 Conclusions and future perspectives

The research presented in this thesis has demonstrated that graphene oxide, when embedded in polysulfone and polyethersulfone membrane systems, retains its intrinsic chemical reactivity and can be exploited as a platform for post-synthetic functionalization. This result is particularly relevant in an industrial context, as it confirms that the incorporation of GO into membrane architectures does not simply lead to the stabilization of a passive additive, but instead preserves a set of reactive sites that remain addressable even after integration within a polymer matrix. By validating this concept across different material levels, ranging from model GO nanosheets to industrially upcycled granules and hollow fiber membranes, the work provides a consistent framework for designing functional composites that can be tailored to specific environmental challenges. In particular, post-synthetic chemical modification of GO enables deliberate tuning of membrane functionality after integration, independently of the specific architecture in which GO is embedded. This architectural transferability represents a key outcome of the thesis and provides a unifying principle across the investigated systems.

The functionalization of GO nanosheets with amino acids constituted the first step of this investigation. By targeting epoxide moieties under mild aqueous basic conditions, it was possible to obtain covalent modifications that were both stable and versatile. The choice of different amino acids allowed tuning of surface chemistry and revealed the potential of these materials for enhancing adsorption of pharmaceuticals, enabling selective sensing applications, and promoting CO_2 capture and conversion. While these systems were explored primarily as model platforms, they were fundamental for establishing the chemical methodology and conceptual basis to be transferred into more complex polymer-integrated systems.

The transition to polysulfone-graphene oxide composites represented a critical step in bridging laboratory-scale chemistry with industrial reality. Production scraps generated during the fabrication of Graphisulfone® membranes were successfully repurposed into granular sorbents, embodying the principles of circular economy. Importantly, the post-synthetic functionalization of these granules under scalable flow conditions proved feasible. Lysine modification resulted in a substantial increase in carbamazepine adsorption capacity, demonstrating the direct impact of chemical grafting on sorption performance, and confirming that functionalization strategies not only remain viable within polymer-GO composites but can also deliver targeted improvements in performance, tailored to specific classes of pollutants.

Polyethersulfone hollow fibers coated with GO layers were subsequently investigated to further explore the functional versatility of surface-exposed GO within membrane architectures. In this configuration, lysine functionalization enhanced carbamazepine uptake compared to unmodified GO-coated PES, while chemical reduction of the GO layer altered its electronic characteristics and provided access to electrochemical functionalities, as illustrated through a representative electro-Fenton case study. Together, these results highlight the adaptability of the GO platform, which can be engineered to impart

adsorptive, catalytic, and electroactive behavior to membrane systems, extending their role beyond simple separation toward multifunctional, reactive interfaces.

The findings collected here suggest several directions for future research and development. The demonstration of chemical tunability provides the basis for designing adaptive membrane systems, in which surface functionality can be selectively introduced to address specific treatment needs. The incorporation of photocatalytic or redox-active groups could, for instance, promote *in situ* degradation of retained and adsorbed contaminants, potentially enabling regeneration of active sites and extension of device service life. Such developments would mark a decisive evolution from passive filtration toward dynamic and multifunctional interfaces.

Expanding the chemical scope of functionalization represents a further concrete step. While amino acids were employed here as proof-of-concept modifiers, the broad range of nucleophiles available and compatible with GO chemistry offers significant opportunities. Functional groups such as thiols, phosphonates, or other redox-active moieties could introduce specific affinities for metals, endocrine disruptors, or microplastic degradation products. The possibility of combining different functional groups on the same composite could enable multifunctional systems that balance broad applicability with selective recognition.

An additional perspective concerns validation under realistic operating conditions. Although laboratory-scale experiments have demonstrated promising performance, assessment in natural waters, wastewater effluents, and industrial discharge streams is essential to evaluate competitive adsorption, fouling, and chemical interferences, and long-term robustness. In parallel, scaling up the functionalization protocols remains a key objective. The strategies developed for PSU-GO granules have already proven their compatibility with continuous processing, and their transfer to pilot-scale systems would represent a natural progression toward industrial implementation. Such an evolution would allow functionalization to move from laboratory proof-of-concept to an integrated stage of membrane manufacturing, consolidating the link between chemical innovation and industrial practice.

Overall, this thesis outlines a coherent pathway in which GO-based composites evolve from nanoscale tunability to industrially relevant membrane systems. By aligning molecular-level chemical control with scalable architectures and circular economy principles, the work contributes to the advancement of membrane technologies capable of addressing emerging environmental challenges with enhanced adaptability, functionality, and sustainability.

5 Appendices: methodology and additional data

5.1 Appendix A - Covalent modification of graphene oxide nanosheets in solution phase

Characterization of GO-amino acid derivatives

SEM analyses were performed with a ZEISS LEO 1530 FEG. The samples were deposited on a cleaned silicon wafer by dropping 100 µL of suspension at 0.1 mg mL^{-1} concentration in dimethylformamide. The energy of electrons was 5 keV and the signal was acquired using an inLens detector at a working distance of 3–5 mm.

XPS was performed by using a Phoibos 100 hemispherical energy analyzer (Specs GmbH, Berlin, Germany), using Mg Kα radiation (ħω = 1253.6 eV; X-Ray power = 125W) in constant analyzer energy (CAE) mode, with analyzer pass energies of 40 eV for survey spectra. Base pressure in the analysis chamber during analysis was 5.3x10-8 mbar. Spectra were fitted by using CasaXPS (www.casaxps.com) after Shirley background subtraction and all spectra were calibrated to the C1s binding energy (285.0 eV). XPS samples were obtained by preparing a tablet from the dry powder of each material and fixing it on the sample holder with conductive carbon tape. EA was performed on modified GO powders by using an Elementar Unicube Elemental analyser, method GRAPHITE. ATR-FTIR spectra were recorded with Agilent Cary 630 FTIR Spectrophotometer, and the spectra are expressed by wavenumber (cm^{-1}).

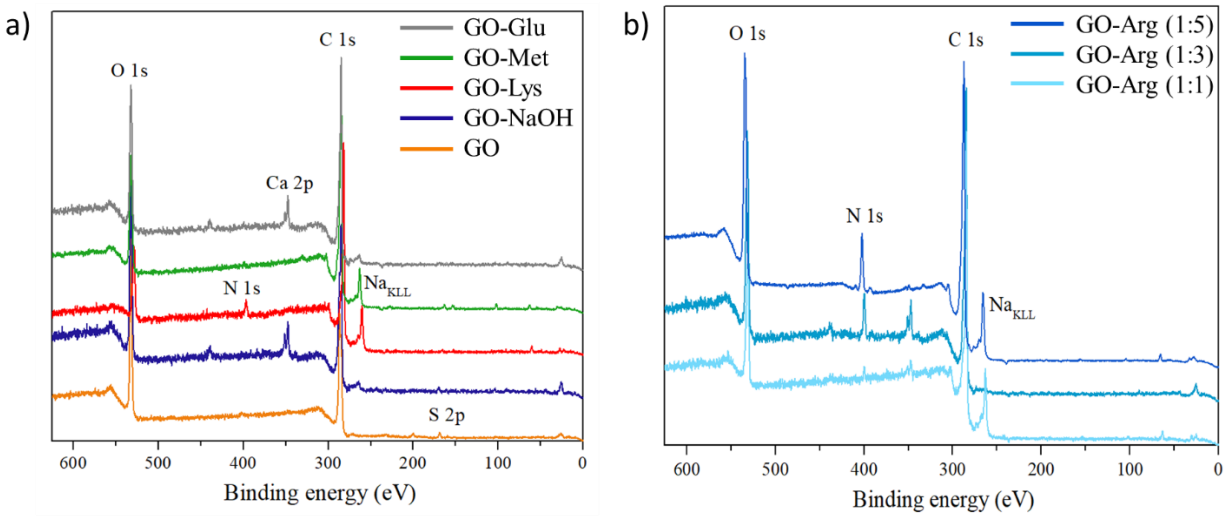

Figure 5.1 *XPS survey spectra of: a) GO (orange), GO-NaOH (blue), GO-Lys (red), GO-Met (green) and GO-Glu (grey); b) GO-Arg prepared at different GO:Arg weight ratios.*

Table 5.1 *EA Atomic composition of amino acid-modified GO materials*

Material	C%	H%	N%	S%	O%
GO	40.1	28.6	0.1	0.46	30.8
GO-NaOH	33.5	35.8	0.0	0.11	30.6
GO-Lys	42.8	34.9	2.6	0.03	19.6
GO-Met	44.2	32.7	0.9	0.53	21.8
GO-Glu	43.5	26.6	0.2	0.10	29.7
GO-Arg	36.6	36.2	5.4	0.01	21.8
GO-Arg_{pH9}	36.3	38.3	4.8	0.01	20.6

Table 5.2 *Atomic ratios of amino acid-modified GO materials obtained by XPS*

Material	N/C	S/C	O/C
GO	0.01	0.014	0.38
GO-NaOH	0.003	-	0.36
GO-Lys	0.04	-	0.14
GO-Met	0.011	0.010	0.19
GO-Glu	0.009	-	0.26
GO-Arg	0.06	-	0.26
GO-Arg_{pH9}	0.06	-	0.27

Table 5.3 *Atomic ratios of amino acid-modified GO materials obtained by EA.*

Material	H/C	N/C	S/C	O/C
GO	0.71	0.002	0.010	0.77
GO-NaOH	1.07	0.001	0.003	0.92
GO-Lys	0.96	0.06	-	0.62
GO-Met	0.74	0.020	0.012	0.49
GO-Glu	0.95	0.008	-	0.67
GO-Arg	0.99	0.14	-	0.59
GO-Arg_{pH9}	1.05	0.13	-	0.58

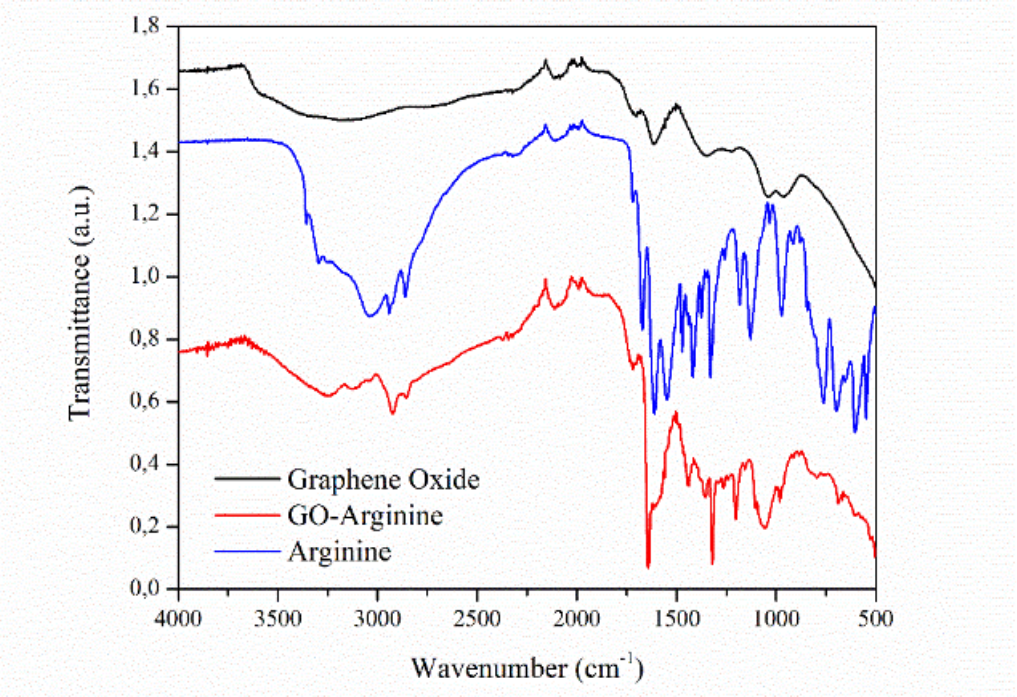

Figure 5.2 *ATR-IR spectra of GO, GO-arginine and L-arginine.*

Adsorption selectivity and kinetic experiments

A stock solution of eight emerging contaminants (CAF, OFLOX, BP4, CBZ, BPA, RhB, DCF, BP3, Fig. 5.3) at 10 mg L^{-1} each was prepared in tap water. In a typical experiment, 25 mg of the tested adsorbent were sonicated for 2 h in 5 mL of ultrapure water. After that time, 5 mL of the stock solution were added, to reach a final concentration of 5 mg L^{-1} for each contaminant. The suspensions were gently stirred in the dark for 1, 4, and 24 h and then centrifuged at 15 000 rpm for 10 min. GO, GO-NaOH, and rGO were tested under the same conditions.[128] Analyses of the treated water samples were performed by HPLC on a Dionex Ultimate 3000 system equipped with a diode array detector. Aliquots of 0.5 mL were used as sources for automated injection. Chromatographic separation was carried out on a reverse-phase analytical column (Agilent Eclipse XDB-C8, 4.6 × 150 mm, 5 μm) at a flow rate of 1.0 mL min^{-1}, using a linear gradient of TFA 0.05% in water/acetonitrile from 80:20 to 0:100, with detection at the λ_max of each analyte. The percentage removal of each compound was calculated by comparison with the initial untreated solution. Results are expressed as the mean of two independent experiments ± SD.

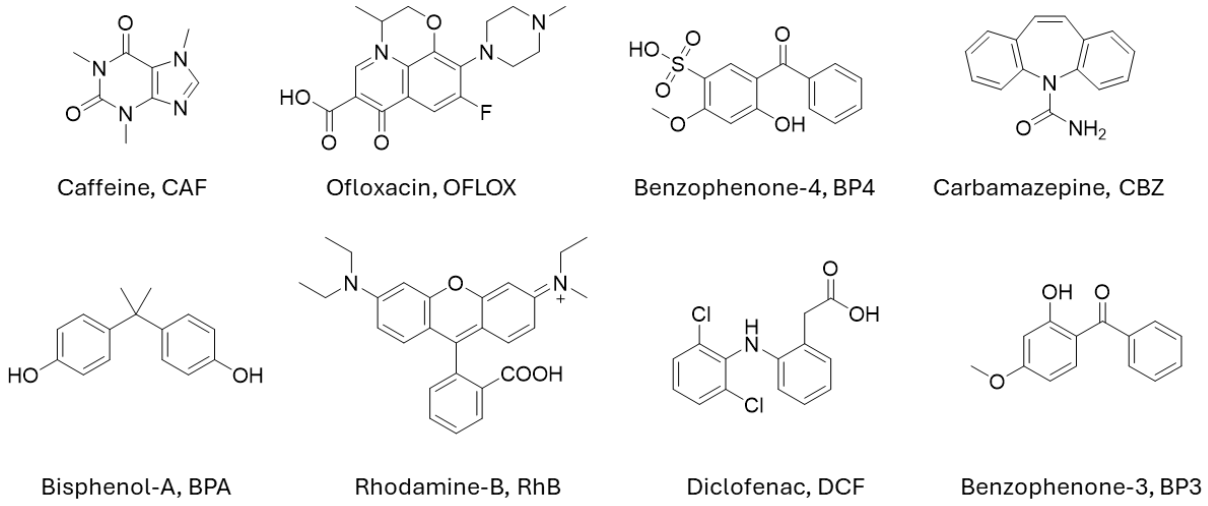

Figure 5.3 *Molecular structure of selected organic contaminants.*

Adsorption isotherms on organic contaminants

The adsorption isotherms of GO-Glu and GO-Met for BP4, BPA, and CBZ were obtained by varying both the concentration of contaminant and the amount of adsorbent. Stock solutions of each contaminant were prepared in ultrapure water, according to the maximum solubility of each molecule: BP4 1.0 mg mL^{-1}, BPA 0.3 mg mL^{-1}, and CBZ 0.1 mg mL^{-1}. For each sorbent, two suspensions were prepared, 2 mg mL^{-1} and 3 mg mL^{-1} in ultrapure water and used after 2 h of sonication. The adsorption experiments were carried out in a total volume of 5 mL, under gentle stirring in the dark for 4 h, followed by centrifugation at 15 000 rpm for 10 min. Supernatants were analyzed by UV–Vis spectroscopy or HPLC. The same procedure was applied to each sorbent–sorbate pair, adjusting the sorbent-to-solute ratio according to the different adsorption capacities. Each experiment was repeated twice on different batches of material. Isotherms for GO, GO-NaOH, and GO-Lys were reported previously.[128] Langmuir and Brunauer–Emmett–Teller (BET) models were used to fit the adsorption data and extract maximum adsorption capacities (Qm). All equations and complete model-fitting parameters (Langmuir and BET) are reported in the corresponding publication.[145]

Molecular dynamics simulations

MD simulations were performed to complement the experimental adsorption measurements by examining the interactions between BP4, BPA, CBZ and the GO-AA surfaces at atomistic resolution. Model structures of GO-Glu and GO-Met were generated by decorating graphene fragments with oxygenated groups and amino acid moieties at loadings consistent with XPS data. All GO-AA systems were parameterized using the GAFF force field, with atomic charges obtained by AM1 calculations. The contaminants (BP4, BPA and CBZ) were parameterized with GAFF as well, with atomic charges derived from HF/6-31G(d) calculations followed by RESP fitting. Each GO–pollutant complex was solvated in a TIP3P water box and neutralized with counterions. Energy minimization was carried out in two steps:

in the first, only water molecules and ions were relaxed while keeping the solute fixed; in the second, all atoms were allowed to move freely. Systems were then equilibrated for 10 ns, gradually heating from 0 to 298 K under periodic boundary conditions. Production trajectories of 100 ns were generated using AMBER16. Binding affinities were estimated by the MM-GBSA method, decomposed into electrostatic, van der Waals and non-polar solvation contributions. The variation of solvent-accessible surface area (ΔSASA) upon binding was also computed to quantify shape complementarity between each contaminant and the sorbent surface. The resulting values are summarized in Table 5.3. Full computational details are reported in the corresponding publication.

Table 5.4 *Computed total binding affinity (E_{TOT}) and its contributions i.e., van der Waals (vdW), electrostatic (E_{El}) and non-polar solvation ($E_{non\text{-}polar\ solvation}$), together with ΔSASA (Å²), for BP4, CBZ and BPA on GO, GO-Glu and GO-Met. All energies are reported in kcal mol^{-1}.*

Contaminant	Material	E_{TOT}	E_{El}	$E_{non\text{-}polar\ solvation}$	ΔSASA [Å²]
BP4	GOa	−11.9	10.1	−1.1	372.7
	GO-Glu	−21.1	12.2	−2.8	686.3
	GO-Met	−22.0	12.1	−2.9	704.8
CBZ	GO	−18.4	4.1	−0.7	298.9
	GO-Glu	−20.8	3.6	−2.4	612.5
	GO-Met	−21.5	3.9	−2.5	657.7
BPA	GO	−15.7	4.4	−0.8	317.3
	GO-Glu	−17.1	4.5	−2.0	538.7
	GO-Met	−18.9	5.7	−2.5	631.0

Glyphosate adsorption and electrochemical sensing

A stock solution of glyphosate (GLY, 0.5 mg L^{-1}) was prepared and stored at 4 °C until use. For each test, 25 mg of sorbent (GO, GO-AA or rGO) were dispersed in 2.5 mL of ultrapure water by sonication for 2 h (GAC samples were used without pre-sonication). Subsequently, 22.5 mL of tap water were added (final volume = 25 mL, pH ≈ 6.9), and the suspensions were spiked with 100 µL of the GLY stock to reach a final concentration of 2 mg L^{-1}. Samples were stirred on a rotary shaker and aliquots were collected after 15 min and 1 h of contact, each condition being tested in triplicate. After centrifugation (10,000 rpm, 10 min), supernatants were analyzed by HPAEC–MS/MS using glyphosate-2-^{13}C,^{15}N as internal standard, following a validated chromatographic protocol.[169] Analyses were performed using a Dionex ICS-5000 HPAEC system (Thermo Scientific) coupled to a TSQ Altis™ Plus Triple Quadrupole MS, equipped with a Dionex IonPac™ AS19 RFIC™ 2×250 mm anion-exchange column and corresponding guard column (AG19 RFIC™ 2×50 mm).

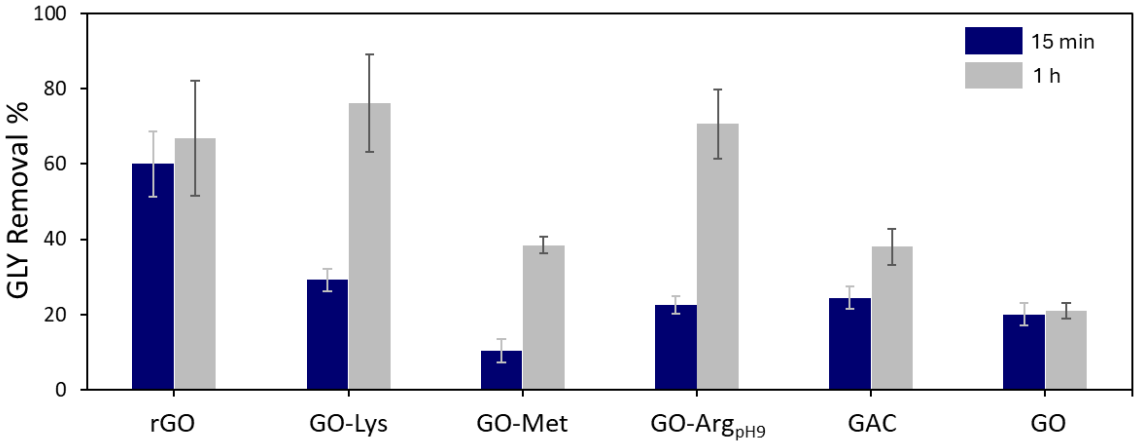

Figure 5.4 *Glyphosate (GLY) removal % at different contact time (15 min, 1h) on the different materials tested: rGO, GO-Lys, GO-Met, GO-Arg, GAC and GO. Total volume = 25 mL, sorbent amount = 25 mg,* $C_{IN,\,GLY}$ *= 2 mg* L^{-1}*. The bars report the standard deviation calculated from triplicate measurements.*

To evaluate their performance as electroactive interfaces for GLY detection, GO-AA materials were deposited onto graphite disk electrodes (GEs, 5 mm diameter). GEs were polished, sonicated in Milli-Q water, rinsed and dried before modification. Homogeneous suspensions were obtained by sonicating 0.5 mg of GO-based powders in 1 mL of deionized water (60 kHz). Drop-casting followed a two-step protocol: a first deposition of 4 µL of GO-Lys/GO-Arg/GO-Met/GO suspension was applied and allowed to dry, followed by deposition of a second 4 µL aliquot. To obtain conductive films, GO-modified electrodes were electrochemically reduced to rGO by polarization at –1.25 V for 300 s in 0.1 M phosphate buffer (pH 7.4). Prior to sensing measurements, electrodes were conditioned by immersion in 0.5 M $LiClO_4$ for 10 min, then rinsed with deionized water.[207] Electrochemical measurements were carried out at 20 °C using a PGSTAT 12 potentiostat (EcoChemie) with NOVA 2.1 software. A standard three-electrode glass cell (V = 10 mL) was employed, using the modified GO-AA electrode as the working electrode, Ag/AgCl (sat. KCl) as reference, and a platinum wire as counter electrode. Conditions for GLY oxidation were screened in Britton–Robinson buffers (pH 5–8). For adsorption/transduction tests, electrodes were incubated in GLY solutions (short exposure to overnight), rinsed, and analyzed by differential pulse voltammetry in BR buffer at pH ≈ 6, using voltametric parameters optimized beforehand for maximum peak intensity and minimal capacitive background.

CO_2 capture and conversion

Tandem CO_2 Fixation and Carbocatalysis with GO-Arg. In a typical experiment, an oven-dried Schlenk tube was loaded with 40 mg of GO-Arg, evacuated, and subjected to three vacuum/CO_2 cycles to replace the nitrogen atmosphere with pure CO_2. The solid was then kept stirring under CO_2 at 100 °C for 2 h, enabling the adsorption and preliminary activation of the gas. After cooling, CO_2 was evacuated and the tube purged with N_2. Subsequently, 1 mL of dry DMF, 0.01 mmol rac-styrene oxide (12.5 µL),

and 37 mg of TBAI (0.01 mmol) were added sequentially. The reaction mixture was stirred at 100 °C for 48 h, after which the insoluble GO–Arg was removed by filtration and washed with EtOAc. Residual DMF was eliminated under high vacuum. The crude mixture was analyzed by ^{1}H NMR, using mesitylene (6 µL) as internal standard to quantify the conversion into the corresponding cyclic carbonate. Purification of product 2 was performed by flash chromatography on silica gel (n-hexane/EtOAc = 2:1). Recycling tests were conducted following the same procedure. After each catalytic cycle, the GO–Arg material was recovered by repeated centrifugation with EtOAc to separate product, solvent, and TBAI. The solid was then washed with deionized water, freeze-dried, and reused in subsequent reactions.

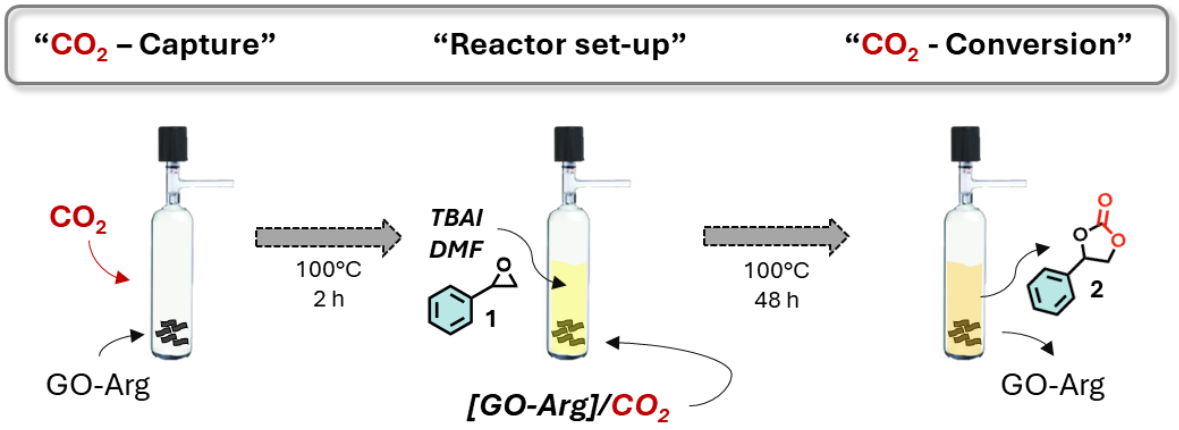

Figure 5.5 *Schematic representation of the integrated "capture-CO_2-conversion" strategy (TBAI: tetrabutylammonium iodide).*

CO_2 Adsorption Measurements. The CO_2 adsorption capacity of GO and GO–Arg samples was evaluated by thermogravimetric analysis (TGA) using a STA 449 F3 Jupiter thermo-microbalance (Netzsch-Gerätebau). Two complementary methods were employed to assess adsorption under flow (method a) and static (method b) CO_2 exposure. Prior to each experiment, samples were weighed into Al_2O_3 crucibles and subjected to a cleaning step at 90 °C for 30 min (10 °C min^{-1}) under high-purity N_2 (99.999%) to remove pre-adsorbed volatiles.

(a) Flow CO_2 adsorption: after cleaning, samples were cooled to 40 °C at 1 °C min^{-1} under N_2 and subjected to a 100-min isothermal adsorption step under a CO_2/N_2 (1:1 v/v) gas mixture. Desorption was then performed by heating the sample to 90 °C (10 °C min^{-1}) under pure N_2.

(b) Static CO_2 adsorption: cleaned samples were transferred to a sealed glass vessel containing pure CO_2 (99.995%) and maintained at 40 °C for 2 h. Afterwards, the crucibles were placed back in the TGA instrument and subjected to a desorption cycle identical to that used in method (a) (heating to 90 °C under N_2). For both methods, CO_2 uptake was calculated from the mass variation measured during the adsorption (method a) or desorption (method b) steps, and expressed as mg CO_2 per g of adsorbent.

5.2 Appendix B - In situ functionalization of graphene oxide-polysulfone composite granules

Materials

GO powder was purchased from Layer One (Norway, previously Abalonyx) and used without further purification (graphene oxide dry powder <35 mesh, product code 1.8). L-Lysine (Lys) and carbamazepine (CBZ) were purchased from Merck and used without further purification. PSU-GO hollow fibers at 3.5% (PSU-GO-A) and 10% (PSU-GO-B) w/w (GO/PSU) were obtained by phase inversion procedure (NMP→water) of a GO:PSU casting solution at room temperature, through an industrial spinning line (Medica S.p.A.). 1 PSU and PSU-GO granules were prepared by mechanical grinding of commercial PSU and PSU-GO hollow fibers scraps with a commercial blade grinder (Ceramic Instruments Srl, IT, sieve cut-off = 2 mm). 2 Small prototype cartridges (14 mm diameter, 65 mm length, dead volume 6 mL, bed volume = 0.01 L) were filled with PSU and PSU-GO granules and the final weight of material in the cartridges was 1.2 g for PSU, 0.8 g for PSU-GO-A, and 1.0 g for PSU-GO-B. All materials were washed with 2 L of ultrapure water and air-dried before use.

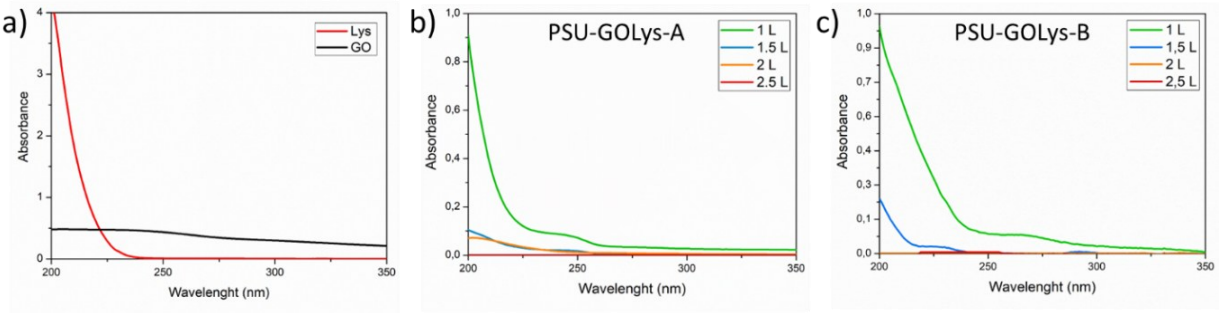

Figure 5.6 *UV-Vis spectra of a) L-Lysine (2 mg mL^{-1}) and GO (10 mg L^{-1}); washing aliquots from the purification of PSU-GOLys-A (b) and PSU-GOLys-B (c).*

Characterization

SEM analyses were performed with a ZEISS LEO 1530 FEG. The energy of electrons was 5 keV and the signal was acquired using an inLens detector at a working distance of 3–5 mm. ATR-FTIR spectra were recorded with Agilent Cary 630 FTIR Spectrophotometer, and the spectra are expressed by wavenumber (cm^{-1}). High-resolution XPS by using a Phoibos 100 hemispherical energy analyzer (Specs GmbH, Berlin, Germany), using Mg Kα radiation (ħω = 1253.6 eV; X-Ray power = 125W) in CAE mode, with analyzer pass energies of 40 eV for survey spectra. Base pressure in the analysis chamber during analysis was 5.3x10-8 mbar. Spectra were fitted by using CasaXPS (www.casaxps.com) after Shirley background subtraction and all spectra were calibrated to the C1s binding energy (285.0 eV).

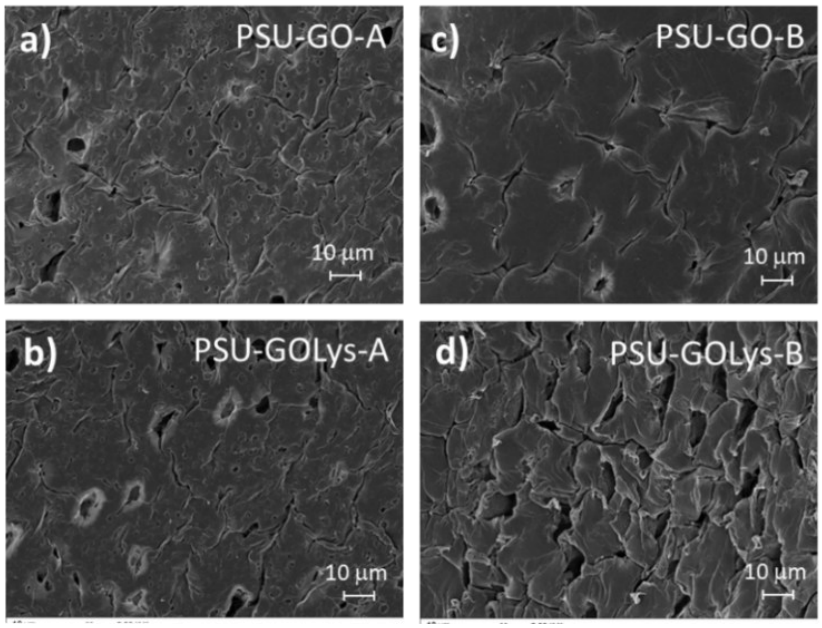

Figure 5.7 *SEM images of a) PSU-GO-A, b) PSU-GO-B, c) PSU-GOLys-A and d) PSU-GOLys-B.*

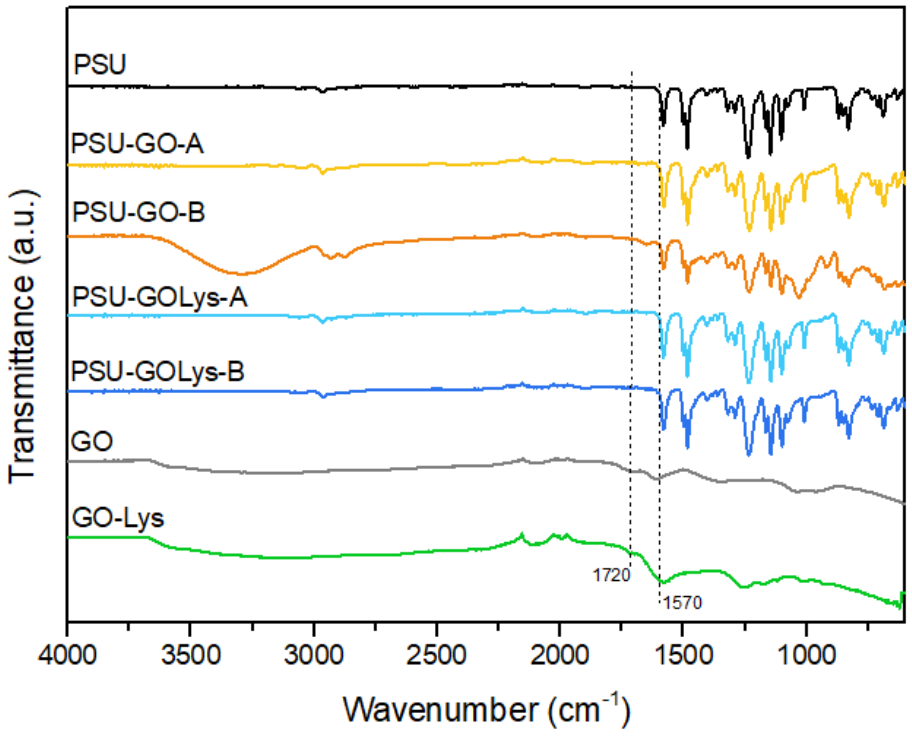

Figure 5.8 *ATR-FTIR spectra of GO, GO-Lys, PSU, PSU-GO-A, PSU-GO-B, PSU-GOLys-A and PSU-GOLys-B.*

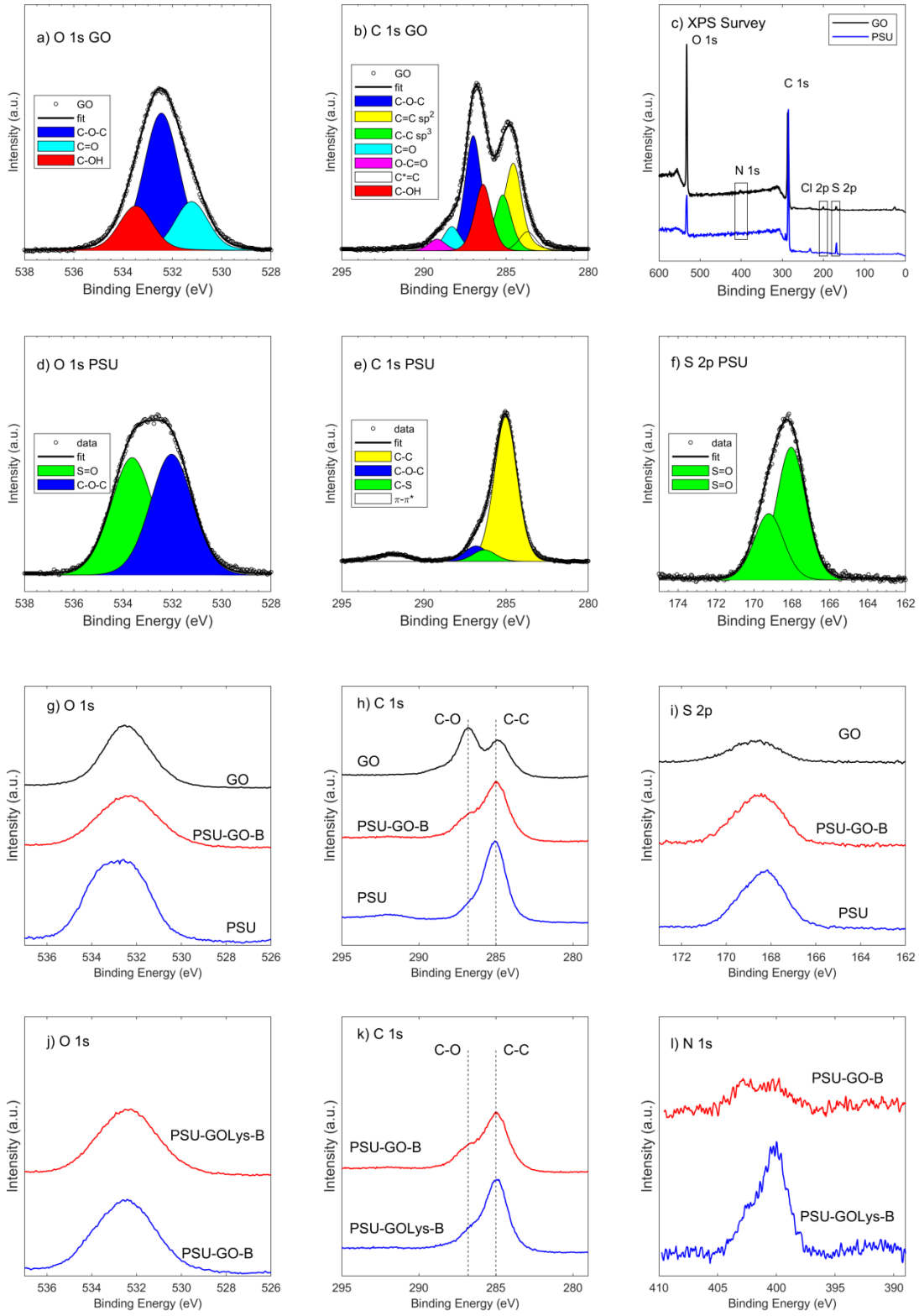

Figure 5.9 *XPS spectra. a) O 1s and b) C 1s of GO; c) survey of GO and PSU; d) O 1s, e) C 1s and f) S 2p of PSU; g) O 1s, h) C 1s and i) S 2p comparison between GO, PSU-GO-B and PSU; j) O 1s, k) C 1s and l) N 1s comparison between PSU-GO-B and PSU-GOLys-B.*

Organic contaminants adsorption tests.

Adsorption batch experiments on the mixture of six selected organic contaminants (Fig. 5.10) were carried out by dispersing GO and GO-Lys nanosheets (after sonication for 2 h) in spiked ultrapure water and analyzing treated water samples after 15 min by HPLC analysis. Flow-through experiments were carried out by filtering a solution of the mixture of the six organic contaminants in ultrapure water (C_{IN}= 0.5 mg L^{-1} each) through PSU, PSU-GO-A/B and PSU-GOLys-A/B cartridges at a constant flow of 5 mL min^{-1}. Samples were collected every 50 mL and analyzed by HPLC-UV. All tests were conducted in duplicate, with results reported as the mean value with standard deviation. HPLC analyses of the selected emerging contaminants and carbamazepine (CBZ) were performed using a Shimadzu HPLC-UV system. The chromatographic separation was performed on a reverse phase Agilent Eclipse XDB column at flow rate of 1.0 mL min^{-1}. The gradient was set as shown in Table 5.4 Each analyte was detected at a specific retention time at λ_{max} (Table 5.5). The results are expressed as the means of two independent experiments ± SD. Detection limit=0.05 mg L^{-1}.

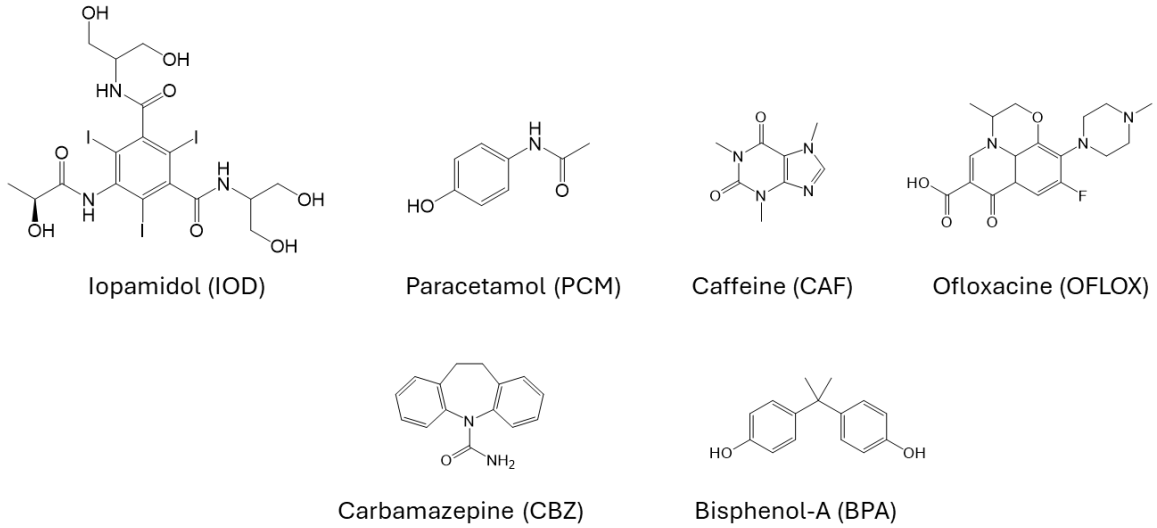

Figure 5.10 *Molecular structure of selected organic contaminants.*

Table 5.4 *Gradient setting for HPLC analyses of Organic contaminants.*

Time (min)	% Water:TFA (0.1% v/v)	% Methanol:TFA (0.1% v/v)
0	90	10
1	90	10
6	40	60
9	40	60
9.5	90	10
12.5	90	10

Table 5.5 *Retention time and wavelength for the detection of organic contaminants by HPLC analyses.*

Compound	Retention time (min)	λ_{max} (nm)
IOD	2.31	242
PCM	4.12	242
CAF	5.75	272
OFLOX	6.27	294
CBZ	8.57	287
BPA	9.29	225

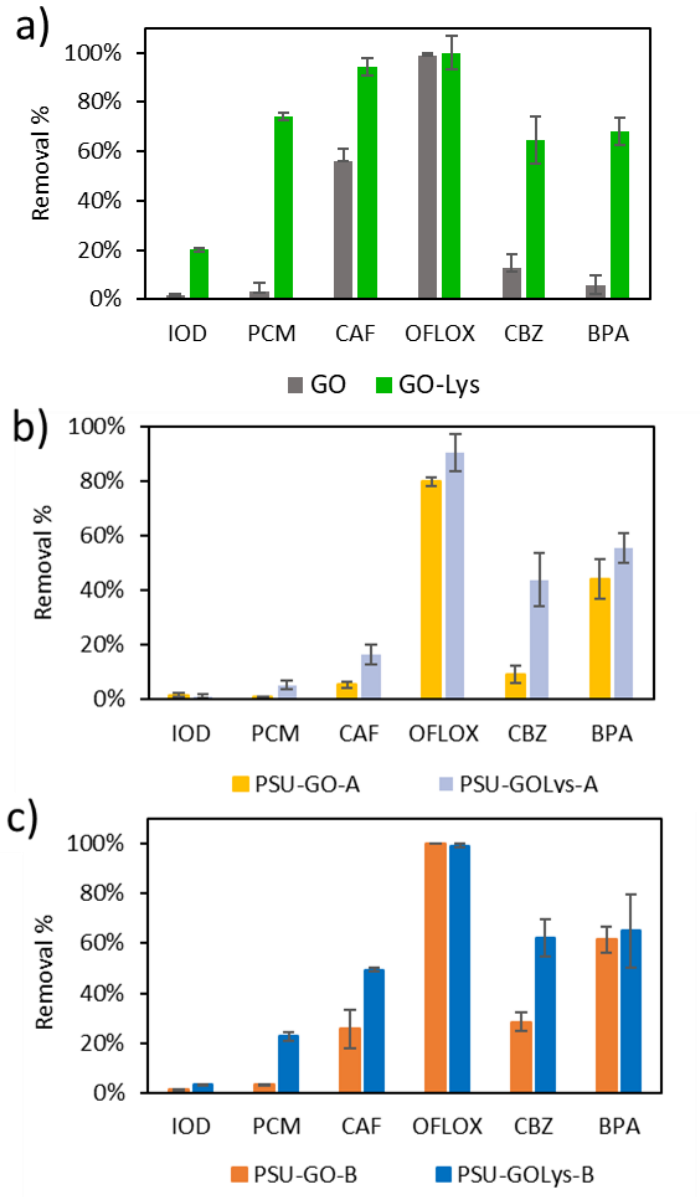

Figure 5.11 *Adsorption selectivity of a) GO and GO-Lys in batch conditions (C_{IN}=0.5 mg L^{-1} each, V_{TOT} = 25 mL, 25 mg of sorbent) in 15 min of contact time; b) PSU-GO-A and PSU-GOLys-A, c) PSU-GO-B and PSU-GOLys-B cartridges in flow conditions (flow rate 5 mL min^{-1}, treated volume 200 mL) on a mixture of six organic contaminants (C_{IN}=0.5 mg L^{-1} each) in ultrapure water.*

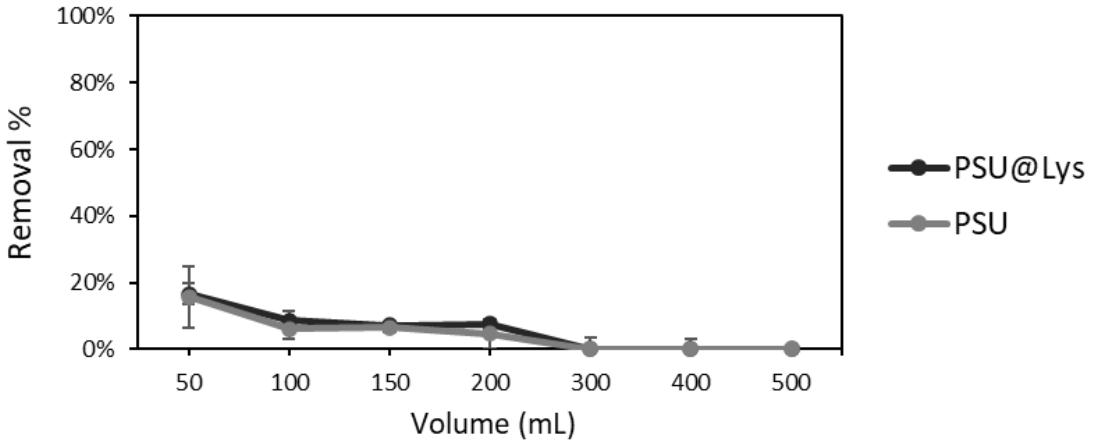

Figure 5.12 *Removal performance of CBZ with PSU and PSU@Lys control (C_{IN} = 0.5 mg L^{-1}, flow rate = 5 mL min^{-1}, treated volume 300 mL).*

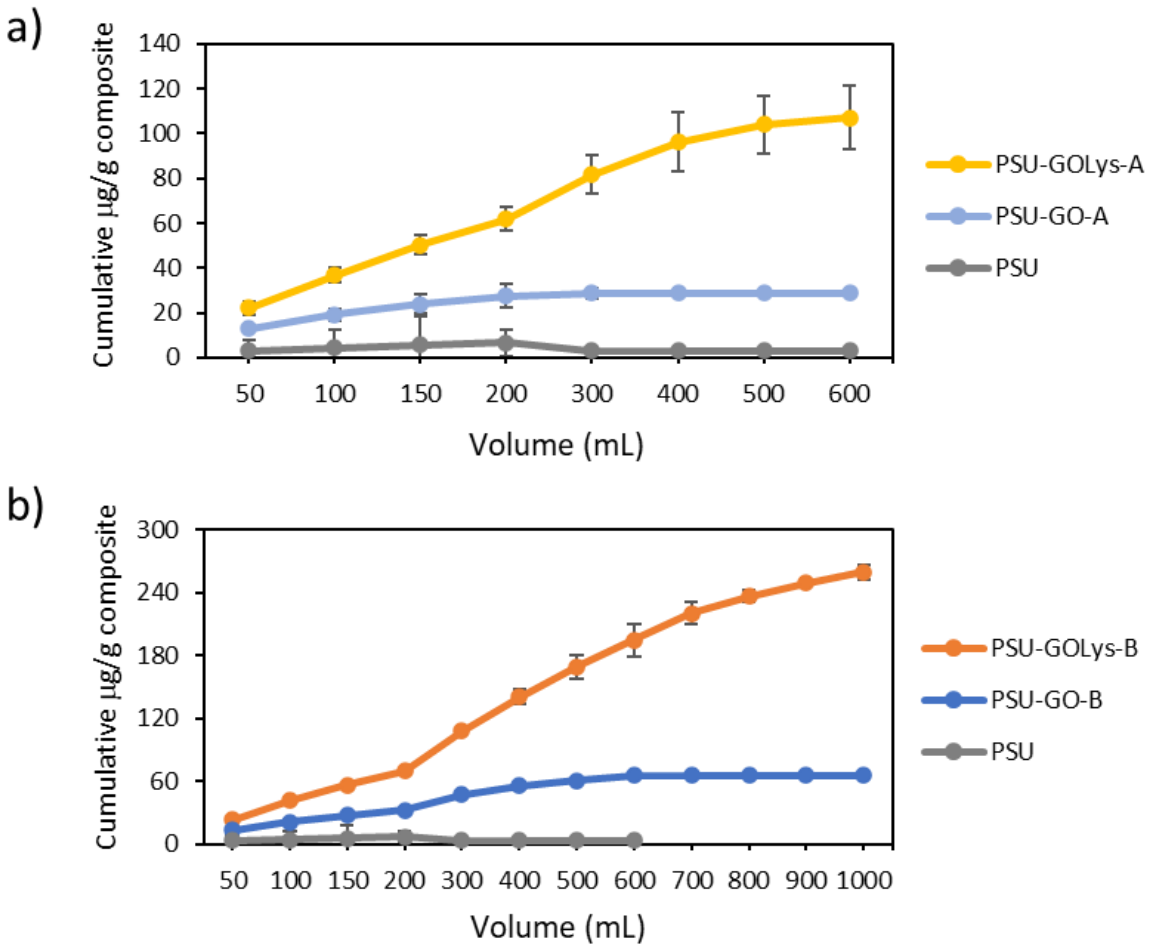

Figure 5.13 *Cumulative µg of CBZ removed/g of a) PSU, PSU-GO-A and PSU-GOLys-A; b) PSU, PSU-GO-B and PSU-GOLys-B (C_{IN} = 0.5 mg L^{-1}, flow rate = 5 mL min^{-1}, treated volume 1 L).*

5.3 Appendix C - Functionalization of graphene oxide-polyethersulfone coated membranes

Materials

Polyethersulfone (Plasmart 25 filled with Versatile PES®, filter surface area of 0.1 m², average pore size 100-200 nm) modules were provided by Medica Spa. GO powder was purchased from Layer One (Norway, previously Abalonyx) and used without further purification (graphene oxide dry powder <35 mesh, product code 1.8). L-Ascorbic Acid was purchased by Sigma Aldrich and used without further purification. Polyethylene (PE) from real agricultural waste consisted of a single-layer film with two visually distinct surfaces: a white side and a black side, typical of agricultural-grade films.

Characterization of PES-GOLys coated HF

SEM analyses were performed with a ZEISS LEO 1530 FEG. The energy of electrons was 5 keV and the signal was acquired using an inLens detector at a working distance of 3–5 mm. ATR-FTIR spectra were recorded with Agilent Cary 630 FTIR Spectrophotometer, and the spectra are expressed by wavenumber (cm^{-1}). XPS was performed by using a Phoibos 100 hemispherical energy analyzer (Specs GmbH, Berlin, Germany), using Mg Kα radiation (ħω = 1253.6 eV; X-Ray power = 125W) in CAE mode, with analyzer pass energies of 40 eV for survey spectra. Base pressure in the analysis chamber during analysis was 5.3x10-8 mbar. Spectra were fitted by using CasaXPS (www.casaxps.com) after Shirley background subtraction and all spectra were calibrated to the C1s binding energy (285.0 eV).

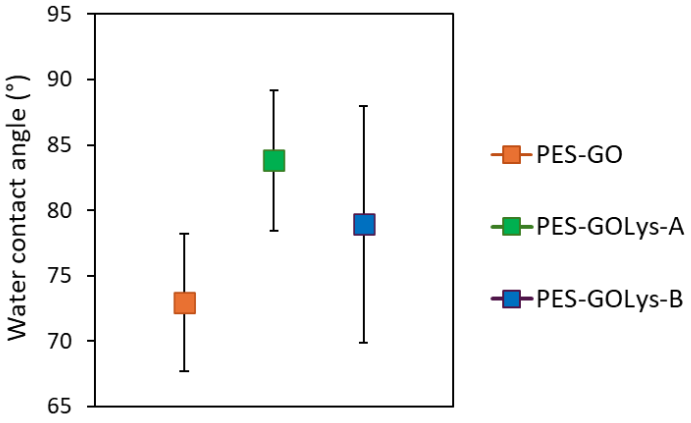

Figure 5.14 *Static water contact angle measurements on polysulfone-graphene oxide coated hollow fiber surfaces before (PES-GO) and after (PES-GOLys-A/B) lysine functionalization.*

Characterization of PES-rGO coated HFs

Structural and Chemical Characterization. SEM analyses were performed with a ZEISS LEO 1530 FEG. The energy of electrons was 5 keV and the signal was acquired using an inLens detector at a working distance of 3–5 mm. XPS measurements were performed with a Thermo Scientific ESCALAB QXi spectrometer employing a monochromatic Al Kα X-ray source (1486.6 eV) with a spot size of 650 µm × 200 µm circa. Survey scans were measured in a binding energy range of 0–1350 eV with a constant pass energy of 200 eV, at 1.0 eV/step, with a dwell time of 50 ms. High resolution spectra were recorded using a constant pass energy (10 eV), at 0.1 eV/step, with a dwell time of 50 ms. Charge compensation was applied as previously detailed. [208] Peak fittings were performed in the framework of the Avantage software after background correction with the smart-background function implemented in the same software using pseudo-Voigt functions for the synthetic peaks. Graphitic sp^2 carbon was modelled with an asymmetric peak. Fitting parameters for C 1s peak are reported in Table 5.6 and 5.7. The spectra were deconvoluted into the following components: graphitic C=C sp^2 carbon (284.4 eV), and aliphatic C–C sp^3 carbon (285 eV), and hydroxyl C–OH (286 eV), epoxy C–O–C (287 eV), carbonyl C=O (287.5 eV) and carboxyl O–C=O (290 eV) groups. Two additional minor contributions were included: one at low binding energy (BE < 284 eV), attributed to defective graphitic carbon, and another around 291 eV, corresponding to the π–π* satellite feature. FWHM of the fitted peak was between 1.0 and 1.2 eV.

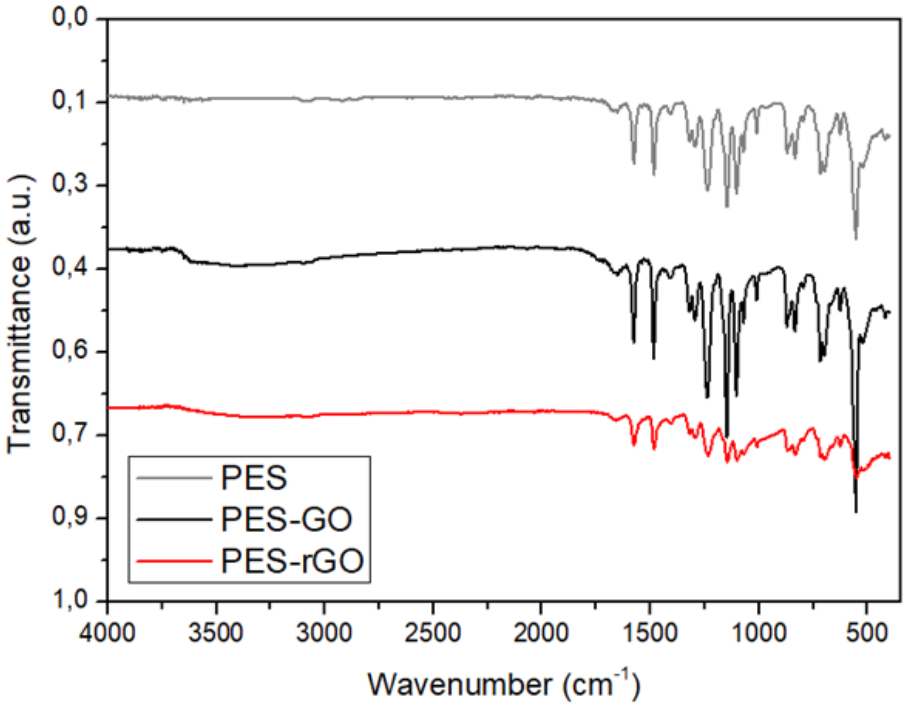

Figure 5.15 *FT-IR spectra of pristine PES, PES-GO and PES-rGO coated hollow fiber membranes.*

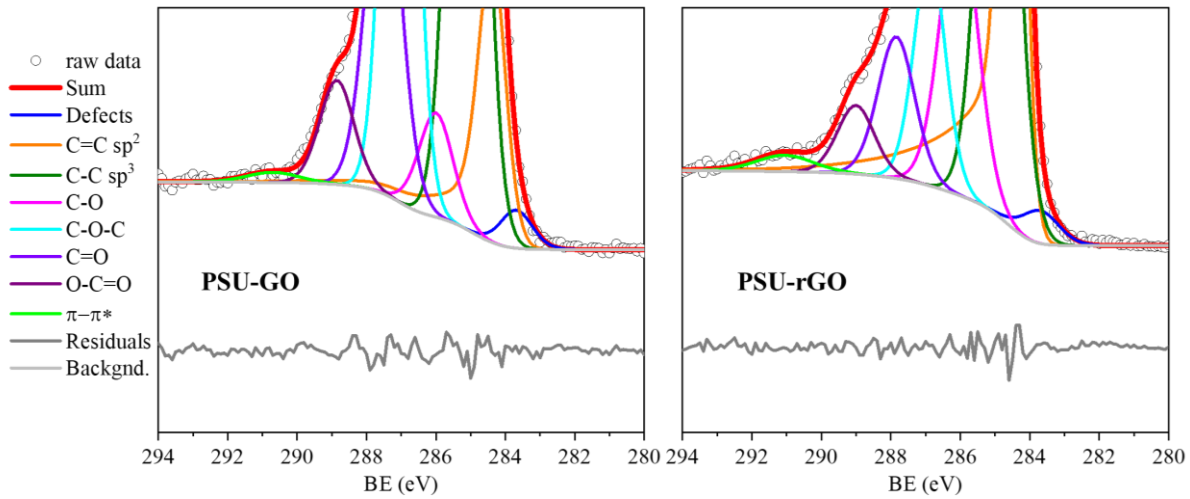

Figure 5.16 *Zoom-in on the low-intensity peaks in the C 1s region curve-fitting for the PSU-GO and PSU-rGO samples.*

Table 5.6 *General fitting parameters for C 1s peak for samples PES-GO and PES-rGO.*

Peak name	Peak BE (eV)	FWHM (eV)	L/G Mix (%) Product	Tail Mix (%)	Tail Height (%)	Tail Exponent
defect	B-0.80 (±0.2)	C*1 (±0.1)	30	100	0	0
C=C	284.3:284.6	0.7 : 1.2	25 : 35	50 : 80	0	0.02 : 0.08
C–C	B+0.50 (±0.2)	0.8 : 1.5	30	100	0	0
C–O	B+1.6 (±0.2)	C*1 (±0.1)	30	100	0	0
C-O-C	B+2.50 (±0.2)	C*1 (±0.1)	30	100	0	0
C=O	B+3.50 (±0.2)	C*1 (±0.1)	30	100	0	0
O–C=O	B+4.50 (±0.3)	C*1 (±0.1)	30	100	0	0
π–π*	B+6.50 (±0.2)	1.0 : 2.0	30	100	0	0

Table 5.7 *C 1s curve-fitting results for samples PES-GO and PES-rGO: binding energy (BE, eV), full width at half maximum (FWHM, eV) and percentage of total C 1s area (%).*

	PES-GO			PES-rGO		
	BE (eV)	FWHM (eV)	%	BE (eV)	FWHM (eV)	%
defect	283.7	1.08	1.4	283.7	1.2	1.6
C=C	284.4	0.95	11.4	284.4	0.73	35.6
C–C	285.1	1.06	33.2	284.9	1.1	32.9
C–O	286.0	1.16	5.2	286.0	1.01	11.2
C-O-C	287.0	0.97	28.2	286.9	1.00	10.3
C=O	287.5	1.16	14.7	287.8	1.01	4.6
O–C=O	288.9	1.16	5.2	288.9	1.01	2.3
π–π*	290.7	1.78	0.6	290.9	1.64	1.5

Electrochemical Characterization. Resistivity measurements on PES, PES-GO and PES-rGO HF were performed using a four-point probe configuration: four stainless-steel filaments were carefully wrapped around the free fiber bundle, two at each end. The outer pair was connected to a potentiostat (BioLogic, EC-Lab® software) operated in voltage-controlled mode, applying three fixed voltage setpoints (1, 2 and 3 V), while the resulting current was recorded (Fig. 5.17). The inner pair was connected to a multimeter to measure the voltage drop within the current path. This configuration enabled direct determination of the electrical resistivity (ρ) was calculated using the standard relation:

$$\left\{\rho = \left(\frac{V}{I}\right) \cdot \left(\frac{A}{L}\right)\right\}$$

where V is the measured voltage, I is the current recorded during the measurement, L the distance between the voltage probes, and A the cross-sectional area of the fiber bundle. For each membrane the reported resistivity values represent the average of the three different measures.

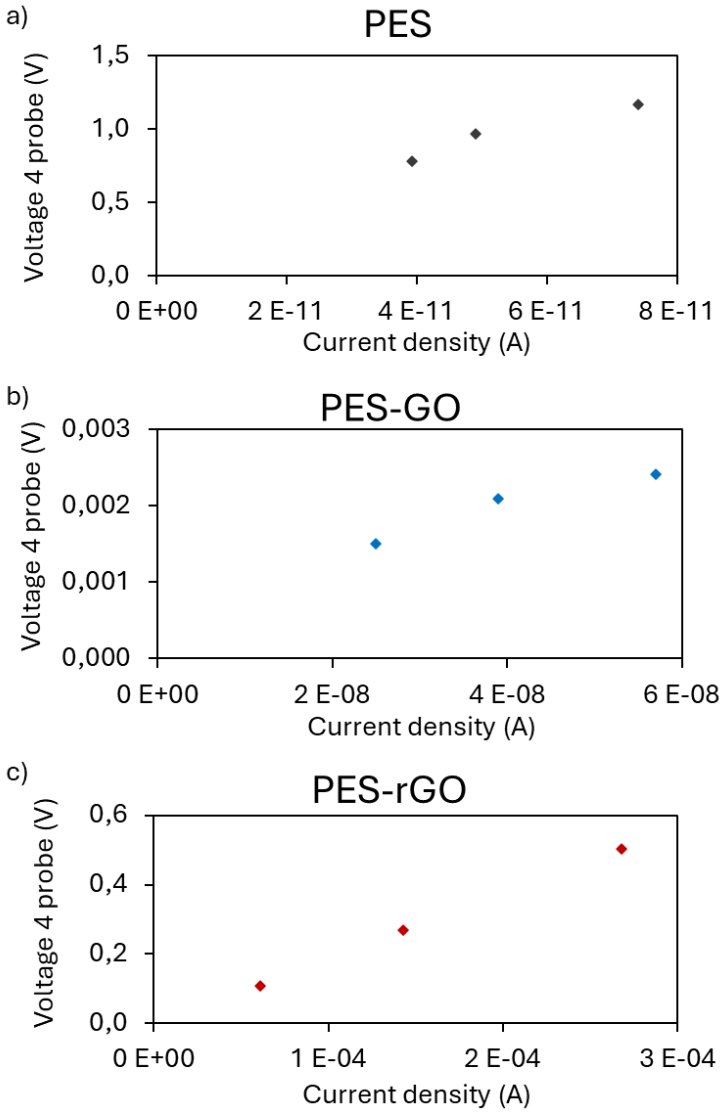

Figure 5.17*. Voltage drop (measured between the inner probes) as a function of the recorded current for (a) PES, (b) PES-GO and (c) PES-rGO hollow fibers, measured using a four-point probe configuration.*

Cathodic polarization experiments were conducted in a single-compartment glass cell (200 mL), where each hollow fiber membrane type - PES, PES-GO, and PES-rGO - was used as the working electrode. A titanium rod functioned as the counter electrode. Electrical connection was made by attaching a stainless-steel filament to the top of the fiber bundle, positioned outside the electrolyte. The remaining submerged portion was immersed in phosphate buffer (pH 7, conductivity 5.5 mS cm^{-1}). The membranes were subjected to a sequence of cathodic potentials from 0 V to –10 V, applied in 1 V increments with 5-minute holds at each step, and the corresponding current response was recorded.

Hydroxyl radicals evaluations

Hydroxyl radicals (•OH) generation under electro-Fenton (EF) conditions was assessed using terephthalic acid (TA, benzene-1,4-dicarboxylic acid) as an indirect chemical probe**.** The experiments were carried out under potentiostatic control at -8 V in a single-chamber batch reactor with a 200 mL total volume. PES, PES-GO, and PES-rGO membranes were used as working electrodes, while a titanium rod and an Ag/AgCl (sat. KCl) electrode served as the anode and reference, respectively. Electrical contact was established by wrapping a stainless-steel filament around the dry portion of each membrane module, ensuring current flow while keeping the active surface area fully submerged in the EF electrolyte. The electrolyte composition is detailed in Table 5.8. The solution was acidified to pH 3 using concentrated H_2SO_4 and TA (20 mg L^{-1}) was added. Radical generation was monitored by tracking the decline in TA absorbance at 240 nm.

Samples (1 mL) were collected hourly, diluted 1:10, and immediately analyzed via UV-Vis spectrophotometry. The concentration of hydroxyl radicals over time was calculated from the depletion of TA absorbance at 240 nm,

Table 5.8 *Electro-Fenton medium composition used for hydroxyl radical quantification experiments.*

Compound	**Concentration (g L^{-1})**
NaH_2PO_4	2.44
KH_2PO_4	1.52
Mg SO_4 x $7H_2O$	0.20
$CaCl_2$ x $2H_2O$	0.05
$(NH_4)_2Fe(SO_4)_2$ x $6H_2O$	0.07

Electro-Fenton experiments

PE fragments were manually cut into ~1 cm^2 pieces (Fig. 5.17) and introduced into the EF electrolyte (composition as in Table 5.8 with pH adjusted to 3 with concentrated H_2SO_4) at a concentration of 0.5 g L^{-1}. Experiments were carried out for 20 h under potentiostatic control at -8 V using a single-chamber batch reactor (200 mL total volume), with PES, PES-GO, and PES-rGO membranes used as

working electrodes. A titanium rod and an Ag/AgCl (sat. KCl) electrode as the anode and reference, respectively, and electrical contact established by wrapping a stainless-steel filament around the dry portion of each membrane. After EF treatment, PE samples were recovered, filtered and thoroughly rinsed with deionized water and dried at 45°C overnight.

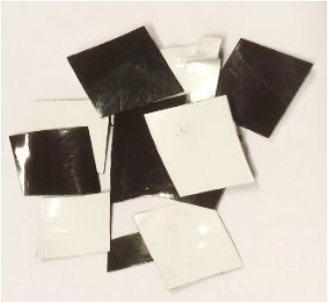

Figure 5.18. *Polyethylene fragments (1 cm²) used for electro-Fenton treatment.*

Polyethylene characterization

PE fragments (both white and black sides) were analyzed independently prior and after electro-Fenton treatments, through Static CA measurements, XPS and ATR-FTIR. CA were performed with a Contact Angle Meter (GBX Scientific LTD, Ireland): prior to analysis, the droplet relaxation behavior was assessed on untreated PE (black side) to define a reliable acquisition protocol. Measurements were then performed under static conditions, averaging values from four droplets per membrane-treated sample, for both sides of the PE fragments.

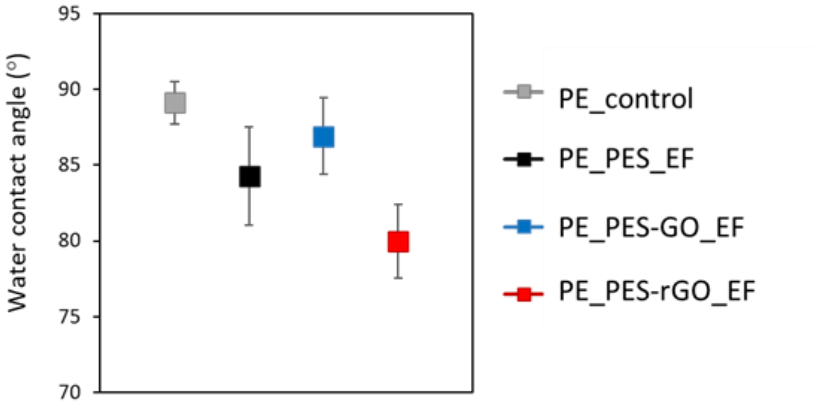

Figure 5.19 *Static water contact angle measurements on polyethylene (PE) surfaces after electro-Fenton (EF) treatment using PES, PES-GO, and PES-rGO membranes as cathodes.*

XPS was performed by using a Phoibos 100 hemispherical energy analyzer (Specs GmbH, Berlin, Germany), using Mg Kα radiation (ħω = 1253.6 eV; X-Ray power = 125W) in CAE mode, with analyzer pass energies of 40 eV for survey spectra. Base pressure in the analysis chamber during analysis was 5.3x10-8 mbar. Spectra were fitted by using CasaXPS (www.casaxps.com) after Shirley background subtraction. C 1s signal was fitted according to literature,[209 210] with C-C at 285.0 eV, C-O at 286.6 eV, C=O at 288.2 eV and O-C=O at 289.2 eV. All spectra were calibrated to C 1s at 285 eV.

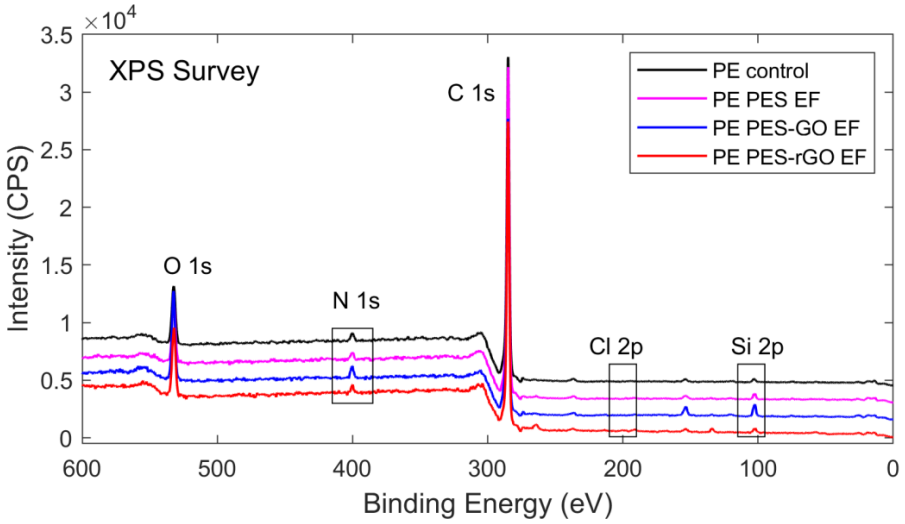

Figure 5.20 *XPS survey spectra of untreated polyethylene (PE control) and PE after electro-Fenton treatment with PES, PES-GO and PES-rGO membranes as cathodes.*

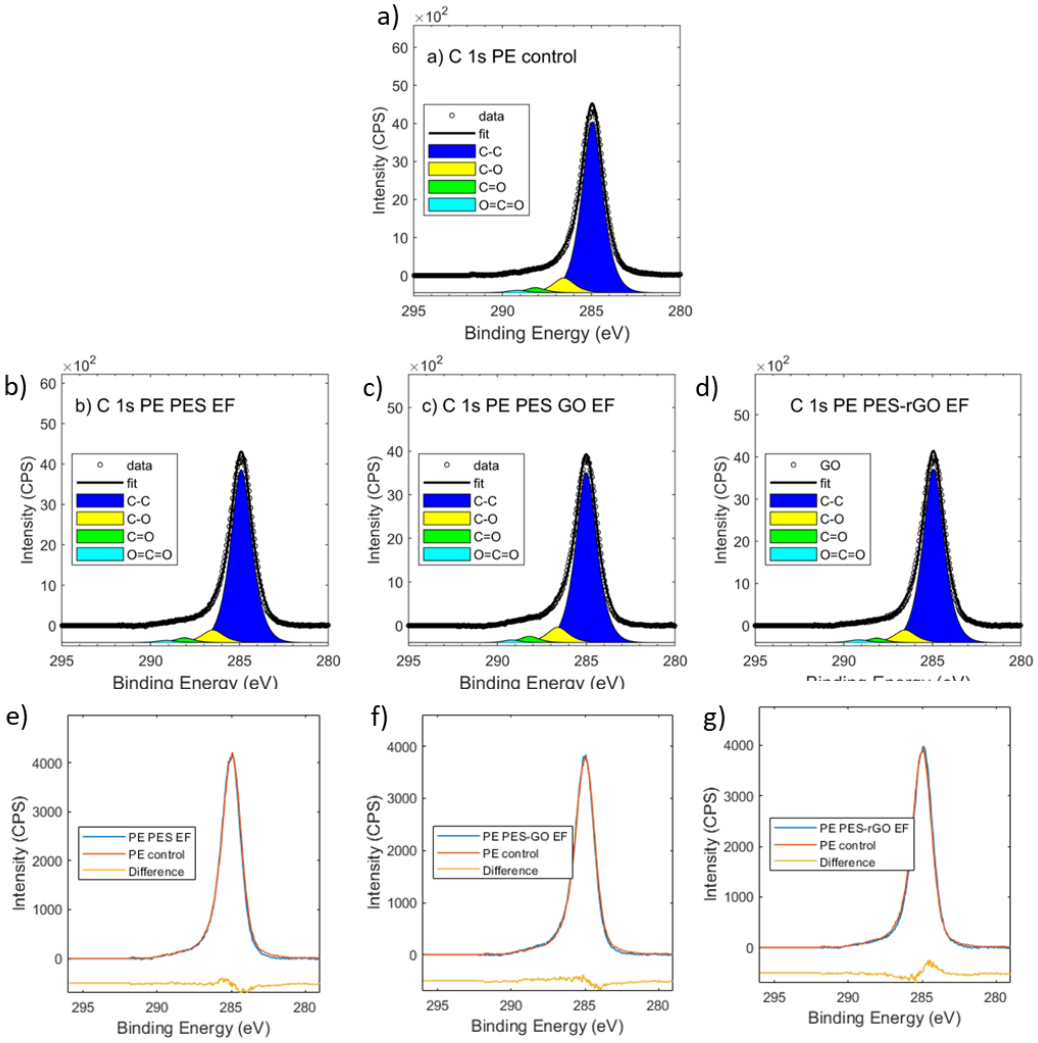

Figure 5.21 *XPS C 1s signals of untreated PE (a) and PE after electro-Fenton treatment with PES, PES–GO, and PES–rGO cathodes: (b–d) deconvoluted peaks; (e–g) comparison with untreated PE (control) highlighting differences.*

Biodegradation Assessment

Microbial respiration was monitored over 21 days through experiments conducted in 200 mL airtight glass bottles, sealed with OxiTop® pressure sensors (Fig. 5.20). All tests were carried out in EF electrolyte medium without the addition of iron and without pH adjustments. Samples were incubated at 26°C and included duplicates of: (i) blank (medium + bacteria); (ii) untreated PE (control); and (iii) EF-treated PE using PES-rGO membranes. Each bottle received four drops of a nitrification inhibitor to suppress ammonia oxidation, ensuring aerobic biological oxygen demand (BOD) measurements. After incubation, headspace gas composition was analyzed by gas chromatography (GC, Agilent 490MicroGC Gas Chromatograph) A reference GC measurement of ambient air was used as the time-zero baseline, enabling correlation between residual oxygen content and pressure variation over time.

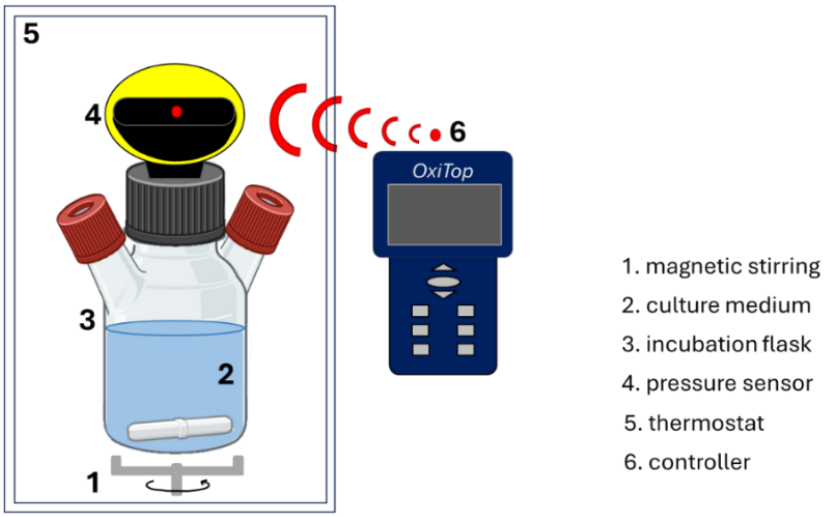

Figure 5.22 *Experimental setup for respirometric measurements using the OxiTop® system.*

6 Bibliography

1. Sholl, D. S.; Lively, R. P., Seven Chemical Separations to Change the World. *Nature* **2016,** *532* (7600), 435-437.
2. Baker, R. W., *Membrane Technology and Applications*. John Wiley & Sons: **2023**.
3. Huang, Y.; Xiao, C.; Huang, Q.; Liu, H.; Zhao, J., Progress on Polymeric Hollow Fiber Membrane Preparation Technique from the Perspective of Green and Sustainable Development. *Chemical Engineering Journal* **2021,** *403*, 126295.
4. Shimizu, Y.; Okuno, Y.-I.; Uryu, K.; Ohtsubo, S.; Watanabe, A., Filtration Characteristics of Hollow Fiber Microfiltration Membranes Used in Membrane Bioreactor for Domestic Wastewater Treatment. *Water Research* **1996,** *30* (10), 2385-2392.
5. Sewerin, T.; Elshof, M. G.; Matencio, S.; Boerrigter, M.; Yu, J.; de Grooth, J., Advances and Applications of Hollow Fiber Nanofiltration Membranes: A Review. *Membranes* **2021,** *11* (11), 890.
6. Lau, H. S.; Lau, S. K.; Soh, L. S.; Hong, S. U.; Gok, X. Y.; Yi, S.; Yong, W. F., State-of-the-Art Organic- and Inorganic-Based Hollow Fiber Membranes in Liquid and Gas Applications: Looking Back and Beyond. *Membranes* **2022,** *12* (5), 539.
7. Scholz, M.; Wessling, M.; Balster, J., Design of Membrane Modules for Gas Separations. In *Membrane Engineering for the Treatment of Gases: Gas-Separation Problems with Membranes*, Drioli, E.; Barbieri, G.; Drioli, E.; Barbieri, G., Eds. The Royal Society of Chemistry: **2011**; Vol. 1.
8. Giwa, A.; Ahmed, M.; Hasan, S. W., Polymers for Membrane Filtration in Water Purification. In *Polymeric Materials for Clean Water*, Das, R., Ed. Springer International Publishing: Cham, **2019**; pp 167-190.
9. Chong, H. Y.; Muhammad, S. A. H.; Norazmi, S. N.; Chang, Z. H.; Teow, Y. H., A Review on Membrane Fabrication: Structure, Properties and Performance Relationship. *Journal of Applied Membrane Science & Technology* **2025,** *29* (1), 73-97.
10. Akram, S.; Naddeo, V.; Rehan, Z.; Zahid, M.; Rashid, A.; Razzaq, W., A Comprehensive Review on Polymeric Nano-Composite Membranes for Water Treatment. *Journal of Membrane Science & Technology* **2018,** *08*, 1000179.
11. Khulbe, K. C.; Matsuura, T., Thin Film Composite and/or Thin Film Nanocomposite Hollow Fiber Membrane for Water Treatment, Pervaporation, and Gas/Vapor Separation. *Polymers* **2018,** *10* (10), 1051.
12. Dibrov, G.; Kagramanov, G.; Sudin, V.; Molchanov, S.; Grushevenko, E.; Yushkin, A.; Volkov, V., Influence of Draw Ratio and Take-up Velocity on Properties of Ultrafiltration Hollow Fiber Membranes from Polyethersulfone. *Fibers* **2022**.
13. Carruthers, S. B.; Ramos, G. L.; Koros, W. J., Morphology of Integral-Skin Layers in Hollow-Fiber Gas-Separation Membranes. *Journal of Applied Polymer Science* **2003,** *90* (2), 399-411.
14. Anis, S.; Hashaikeh, R.; Hilal, N., Microfiltration Membrane Processes: A Review of Research Trends over the Past Decade. *Journal of Water Process Engineering* **2019,** *32* (100941).

15. Dietz, P.; Hansma, P. K.; Inacker, O.; Lehmann, H.-D.; Herrmann, K.-H., Surface Pore Structures of Micro- and Ultrafiltration Membranes Imaged with the Atomic Force Microscope. *Journal of Membrane Science* **1992,** *65* (1), 101-111.
16. Ismail, A. F.; Matsuura, T., 5 - Ultrafiltration and Microfiltration. In *Membrane Separation Processes*, Ismail, A. F.; Matsuura, T., Eds. Elsevier: **2022**; pp 69-75.
17. Zhao, C.; Zhou, X.; Yue, Y., Determination of Pore Size and Pore Size Distribution on the Surface of Hollow-Fiber Filtration Membranes : A Review of Methods. *Desalination* **2000,** *129*, 107-123.
18. Zhang, R.-X.; Liu, T.; Braeken, L.; Liu, Z.; Wang, X.-L.; Van der Bruggen, B., A Design of Composite Hollow Fiber Membranes with Tunable Performance and Reinforced Mechanical Strength. *Journal of Applied Polymer Science* **2015,** *132* (2).
19. Alsalhy, Q., Influence of Spinning Conditions on the Morphology, Pore Size, Pore Size Distribution, Mechanical Properties, and Performance of Pvc Hollow Fiber Membranes. *Separation Science and Technology* **2012,** *48*, 234-245.
20. Sun, S. P.; Wang, K.; Rajarathnam, D.; Hatton, T.; Chung, T., Polyamide-Imide Nanofiltration Hollow Fiber Membranes with Elongation-Induced Nano-Pore Evolution. *Aiche Journal* **2010,** *56*, 1481-1494.
21. Akhondi, E.; Zamani, F.; Law, A. W. K.; Krantz, W.; Fane, A.; Chew, J., Influence of Backwashing on the Pore Size of Hollow Fiber Ultrafiltration Membranes. *Journal of Membrane Science* **2017,** *521*, 33-42.
22. Tan, X.; Rodrigue, D., A Review on Porous Polymeric Membrane Preparation. Part Ii: Production Techniques with Polyethylene, Polydimethylsiloxane, Polypropylene, Polyimide, and Polytetrafluoroethylene. *Polymers* **2019,** *11* (8), 1310.
23. Kheirieh, S.; Asghari, M.; Afsari, M., Application and Modification of Polysulfone Membranes. *Reviews in Chemical Engineering* **2018,** *34*, 657-693.
24. Beek, O.; Pavlenko, D.; Stamatialis, D., Hollow Fiber Membranes for Long-Term Hemodialysis Based on Polyethersulfone-Slipskin™ Polymer Blends. *Journal of Membrane Science* **2020,** *604*, 118068.
25. Wojciechowski, C.; Wasyłeczko, M.; Lewińska, D.; Chwojnowski, A., A Comprehensive Review of Hollow-Fiber Membrane Fabrication Methods across Biomedical, Biotechnological, and Environmental Domains. *Molecules* **2024,** *29*, 11, 2637.
26. Wang, D.; Li, K.; Teo, W., Polyethersulfone Hollow Fiber Gas Separation Membranes Prepared from Nmp/Alcohol Solvent Systems. *Journal of Membrane Science* **1996,** *115*, 85-108.
27. https://www.medica-spa.com/it/azienda/estrusione-membrane-capillari.
28. Kovtun, A.; Bianchi, A.; Zambianchi, M.; Bettini, C.; Corticelli, F.; Ruani, G.; Bocchi, L.; Stante, F.; Gazzano, M.; Marforio, T. D.; Calvaresi, M.; Minelli, M.; Navacchia, M. L.; Palermo, V.; Melucci, M., Core–Shell Graphene Oxide–Polymer Hollow Fibers as Water Filters with Enhanced Performance and Selectivity. *Faraday Discussions* **2021,** *227*, 274-290.
29. Mofijur, M.; Hasan, M. M.; Ahmed, S. F.; Djavanroodi, F.; Fattah, I. M. R.; Silitonga, A. S.; Kalam, M. A.; Zhou, J. L.; Khan, T. M. Y., Advances in Identifying and Managing Emerging Contaminants in Aquatic Ecosystems: Analytical Approaches, Toxicity

Assessment, Transformation Pathways, Environmental Fate, and Remediation Strategies. *Environmental Pollution* **2024,** *341*, 122889.
30. Noguera-Oviedo, K.; Aga, D. S., Lessons Learned from More Than Two Decades of Research on Emerging Contaminants in the Environment. *Journal of Hazardous Materials* **2016,** *316*, 242-251.
31. Wan Ismail, W. N.; Mohktar, S. U., Various Methods for Removal, Treatment, and Detection of Emerging Water Contaminants. In *Emerging Contaminants*, Nuro, A., Ed. IntechOpen: Rijeka, 2021; pp 27-54.
32. Focazio, M. J.; Kolpin, D. W.; Barnes, K. K.; Furlong, E. T.; Meyer, M. T.; Zaugg, S. D.; Barber, L. B.; Thurman, M. E., A National Reconnaissance for Pharmaceuticals and Other Organic Wastewater Contaminants in the United States — Ii) Untreated Drinking Water Sources. *Science of The Total Environment* **2008,** *402* (2), 201-216.
33. Kleywegt, S.; Pileggi, V.; Yang, P.; Hao, C.; Zhao, X.; Rocks, C.; Thach, S.; Cheung, P.; Whitehead, B., Pharmaceuticals, Hormones and Bisphenol a in Untreated Source and Finished Drinking Water in Ontario, Canada — Occurrence and Treatment Efficiency. *Science of The Total Environment* **2011,** *409* (8), 1481-1488.
34. Jiang, T.; Wu, W.; Ma, M.; Hu, Y.; Li, R., Occurrence and Distribution of Emerging Contaminants in Wastewater Treatment Plants: A Globally Review over the Past Two Decades. *Science of The Total Environment* **2024,** *951*, 175664.
35. Valbonesi, P.; Profita, M.; Vasumini, I.; Fabbri, E., Contaminants of Emerging Concern in Drinking Water: Quality Assessment by Combining Chemical and Biological Analysis. *Science of The Total Environment* **2021,** *758*, 143624.
36. Morin-Crini, N.; Lichtfouse, E.; Fourmentin, M.; Ribeiro, A. R. L.; Noutsopoulos, C.; Mapelli, F.; Fenyvesi, É.; Vieira, M. G. A.; Picos-Corrales, L. A.; Moreno-Piraján, J. C.; Giraldo, L.; Sohajda, T.; Huq, M. M.; Soltan, J.; Torri, G.; Magureanu, M.; Bradu, C.; Crini, G., Removal of Emerging Contaminants from Wastewater Using Advanced Treatments. A Review. *Environmental Chemistry Letters* **2022,** *20* (2), 1333-1375.
37. Riva, F.; Zuccato, E.; Davoli, E.; Fattore, E.; Castiglioni, S., Risk Assessment of a Mixture of Emerging Contaminants in Surface Water in a Highly Urbanized Area in Italy. *Journal of hazardous materials* **2019,** *361*, 103-110.
38. Baken, K.; Sjerps, R.; Schriks, M.; Van Wezel, A., Toxicological Risk Assessment and Prioritization of Drinking Water Relevant Contaminants of Emerging Concern. *Environment international* **2018,** *118*, 293-303.
39. Shanmuganathan, R.; Kadri, M. S.; Mathimani, T.; Le, Q. H.; Pugazhendhi, A., Recent Innovations and Challenges in the Eradication of Emerging Contaminants from Aquatic Systems. *Chemosphere* **2023**, 138812.
40. Rout, P. R.; Zhang, T. C.; Bhunia, P.; Surampalli, R. Y., Treatment Technologies for Emerging Contaminants in Wastewater Treatment Plants: A Review. *Science of The Total Environment* **2021,** *753*, 141990.
41. Sengupta, A.; Jebur, M.; Kamaz, M.; Wickramasinghe, S. R., Removal of Emerging Contaminants from Wastewater Streams Using Membrane Bioreactors: A Review. *Membranes* **2022,** *12* (1), 60.

42. Adam, M.; Othman, M.; Kurniawan, T. A.; Puteh, M.; Ismail, A.; Khongnakorn, W.; Rahman, M.; Jaafar, J., Advances in Adsorptive Membrane Technology for Water Treatment and Resource Recovery Applications: A Critical Review. *Journal of Environmental Chemical Engineering* **2022,** *10* (3), 107633.
43. Zambianchi, M.; Khaliha, S.; Bianchi, A.; Tunioli, F.; Kovtun, A.; Navacchia, M. L.; Salatino, A.; Xia, Z.; Briñas, E.; Vázquez, E.; Paci, D.; Palermo, V.; Bocchi, L.; Casentini, B.; Melucci, M., Graphene Oxide-Polysulfone Hollow Fibers Membranes with Synergic Ultrafiltration and Adsorption for Enhanced Drinking Water Treatment. *Journal of Membrane Science* **2022,** *658*, 120707.
44. Sophia A, C.; Lima, E. C., Removal of Emerging Contaminants from the Environment by Adsorption. *Ecotoxicology and Environmental Safety* **2018,** *150*, 1-17.
45. Ellis, A.; Boyer, T.; Fang, Y.; Liu, C.; Strathmann, T., Life Cycle Assessment and Life Cycle Cost Analysis of Anion Exchange and Granular Activated Carbon Systems for Remediation of Groundwater Contaminated by Per- and Polyfluoroalkyl Substances (Pfass). *Water research* **2023,** *243*, 120324.
46. Siriwardena, D.; James, R.; Dasu, K.; Thorn, J.; Iery, R.; Pala, F.; Schumitz, D.; Eastwood, S.; Burkitt, N., Regeneration of Per- and Polyfluoroalkyl Substance-Laden Granular Activated Carbon Using a Solvent Based Technology. *Journal of environmental management* **2021,** *289*, 112439.
47. Norra, G.-F.; Radjenovic, J., Removal of Persistent Organic Contaminants from Wastewater Using a Hybrid Electrochemical-Granular Activated Carbon (Gac) System. *Journal of hazardous materials* **2021,** *415*, 125557.
48. Altmann, J.; Rehfeld, D.; Träder, K.; Sperlich, A.; Jekel, M., Combination of Granular Activated Carbon Adsorption and Deep-Bed Filtration as a Single Advanced Wastewater Treatment Step for Organic Micropollutant and Phosphorus Removal. *Water Research* **2016,** *92*, 131-139.
49. Modi, A.; Bellare, J., Zeolitic Imidazolate Framework-67/Carboxylated Graphene Oxide Nanosheets Incorporated Polyethersulfone Hollow Fiber Membranes for Removal of Toxic Heavy Metals from Contaminated Water. *Separation and Purification Technology* **2020,** *249*, 117160.
50. Wu, S.; Shi, W.; Li, K.; Cai, J.; Xu, C.; Gao, L.; Lu, J.; Ding, F., Chitosan-Based Hollow Nanofiber Membranes with Polyvinylpyrrolidone and Polyvinyl Alcohol for Efficient Removal and Filtration of Organic Dyes and Heavy Metals. *International journal of biological macromolecules* **2023**, 124264.
51. Mondal, R.; De, S., Removal of Copper(Ii) from Aqueous Solution Using Zinc Oxide Nanoparticle Impregnated Mixed Matrix Hollow Fiber Membrane. *Environmental Technology & Innovation* **2022,** *26*, 102300.
52. Liu, Y.; Zhu, J.; Zheng, J.; Gao, X.; Tian, M.; Wang, X.; Xie, Y.; Zhang, Y.; Volodin, A.; Bruggen, B., Porous Organic Polymer Embedded Thin-Film Nanocomposite Membranes for Enhanced Nanofiltration Performance. *Journal of Membrane Science* **2020,** *602*, 117982.

53. Sahu, A.; Dosi, R.; Kwiatkowski, C.; Schmal, S.; Poler, J. C., Advanced Polymeric Nanocomposite Membranes for Water and Wastewater Treatment: A Comprehensive Review. *Polymers* **2023,** *15* (3), 540.
54. Smith, A.; LaChance, A.; Zeng, S.; Liu, B.; Sun, L., Synthesis, Properties, and Applications of Graphene Oxide/Reduced Graphene Oxide and Their Nanocomposites. *Nano Materials Science* **2019,** *1* (1), 31-47.
55. Huang, X.; Liu, L.; Zhou, S.; Zhao, J., Physical Properties and Device Applications of Graphene Oxide. *Frontiers of Physics* **2019,** *15*, 1-70.
56. Wu, J.; Lin, H.; Moss, D.; Loh, K.; Jia, B., Graphene Oxide for Photonics, Electronics and Optoelectronics. *Nature Reviews Chemistry* **2023,** *7*, 162-183.
57. Konkena, B.; Vasudevan, S., Understanding Aqueous Dispersibility of Graphene Oxide and Reduced Graphene Oxide through Pka Measurements. *The Journal of Physical Chemistry Letters* **2012,** *3* (7), 867-872.
58. Yan, H.; Wu, H.; Li, K.; Wang, Y.; Tao, X.; Yang, H.; Li, A.; Cheng, R., Influence of the Surface Structure of Graphene Oxide on the Adsorption of Aromatic Organic Compounds from Water. *ACS applied materials & interfaces* **2015,** *7 12*, 6690-6697.
59. Ersan, G.; Apul, O.; Perreault, F.; Karanfil, T., Adsorption of Organic Contaminants by Graphene Nanosheets: A Review. *Water research* **2017,** *126*, 385-398.
60. Cao, K.; Tian, Z.; Zhang, X.; Wang, Y.-B.; Zhu, Q., Green Preparation of Graphene Oxide Nanosheets as Adsorbent. *Scientific Reports* **2023,** *13*, 9314.
61. Chenab, K. K.; Sohrabi, B.; Jafari, A.; Ramakrishna, S., Water Treatment: Functional Nanomaterials and Applications from Adsorption to Photodegradation. *Materials Today Chemistry* **2020**, 100262.
62. Khaliha, S.; Bianchi, A.; Kovtun, A.; Tunioli, F.; Boschi, A.; Zambianchi, M.; Paci, D.; Bocchi, L.; Valsecchi, S.; Polesello, S.; Liscio, A.; Bergamini, M.; Brunetti, M.; Luisa Navacchia, M.; Palermo, V.; Melucci, M., Graphene Oxide Nanosheets for Drinking Water Purification by Tandem Adsorption and Microfiltration. *Separation and Purification Technology* **2022,** *300*, 121826.
63. Zhao, Q.; Zhao, Z.-Z.; Rao, R.; Yang, Y.; Ling, S.; Bi, F.; Shi, X.; Xu, J.; Lu, G.; Zhang, X., Universitetet I Oslo-67 (Uio-67)/Graphite Oxide Composites with High Capacities of Toluene: Synthesis Strategy and Adsorption Mechanism Insight. *Journal of colloid and interface science* **2022,** *627*, 385-397.
64. Catherine, H.; Ou, M.-H.; Manu, B.; Shih, Y.-H., Adsorption Mechanism of Emerging and Conventional Phenolic Compounds on Graphene Oxide Nanoflakes in Water. *The Science of the total environment* **2018,** *635*, 629-638.
65. Alkhouzaam, A.; Qiblawey, H., Functional Go-Based Membranes for Water Treatment and Desalination: Fabrication Methods, Performance and Advantages. A Review. *Chemosphere* **2021,** *274*, 129853.
66. Jiříčková, A.; Jankovský, O.; Sofer, Z.; Sedmidubský, D., Synthesis and Applications of Graphene Oxide. *Materials* **2022,** *15*, 920.
67. Guo, S.; Garaj, S.; Bianco, A.; Ménard-Moyon, C., Controlling Covalent Chemistry on Graphene Oxide. *Nature Reviews Physics* **2022,** *4*, 1-16.

68. Palomba, M.; Carotenuto, G.; Longo, A., A Brief Review: The Use of L-Ascorbic Acid as a Green Reducing Agent of Graphene Oxide. *Materials* **2022,** *15* (18), 6456.
69. https://graphene-flagship.eu/.
70. https://graphene-flagship.eu/innovation/spearheads/c3-sh01-graphil/.
71. https://www.medica-spa.com/storage/app/media/Brochure/Filtri%20Graphil_ENG_REV00.pdf.
72. Melucci, M.; Bocchi, L.; Zambianchi, M.; Palermo, V., Graphene-Based Filters for Customized Drinking Water Purification. *Nature Water* **2025,** *3* (4), 369-371.
73. https://liferemembrance.eu/#project.
74. Zambianchi, M.; Aluigi, A.; Capobianco, M. L.; Corticelli, F.; Elmi, I.; Zampolli, S.; Stante, F.; Bocchi, L.; Belosi, F.; Navacchia, M. L.; Melucci, M., Polysulfone Hollow Porous Granules Prepared from Wastes of Ultrafiltration Membranes as Sustainable Adsorbent for Water and Air Remediation. *Advanced Sustainable Systems* **2017,** *1* (7), 1700019.
75. Zambianchi, M.; Durso, M.; Liscio, A.; Treossi, E.; Bettini, C.; Capobianco, M. L.; Aluigi, A.; Kovtun, A.; Ruani, G.; Corticelli, F.; Brucale, M.; Palermo, V.; Navacchia, M. L.; Melucci, M., Graphene Oxide Doped Polysulfone Membrane Adsorbers for the Removal of Organic Contaminants from Water. *Chemical Engineering Journal* **2017,** *326*, 130-140.
76. Posati, T.; Nocchetti, M.; Kovtun, A.; Donnadio, A.; Zambianchi, M.; Aluigi, A.; Capobianco, M. L.; Corticelli, F.; Palermo, V.; Ruani, G.; Zamboni, R.; Navacchia, M. L.; Melucci, M., Polydopamine Nanoparticle-Coated Polysulfone Porous Granules as Adsorbents for Water Remediation. *ACS Omega* **2019,** *4* (3), 4839-4847.
77. Khaliha, S.; Tunioli, F.; Foti, L.; Bianchi, A.; Kovtun, A.; Marforio, T. D.; Zambianchi, M.; Bettini, C.; Briñas, E.; Vázquez, E.; Bocchi, L.; Palermo, V.; Calvaresi, M.; Navacchia, M. L.; Melucci, M., Upcycling of Plastic Membrane Industrial Scraps and Reuse as Sorbent for Emerging Contaminants in Water. *Environmental Science: Water Research & Technology* **2024,** *10* (5), 1097-1107.
78. Tawalbeh, M.; Aljaghoub, H.; Qasim, M.; Al-Othman, A., Surface Modification Techniques of Membranes to Improve Their Antifouling Characteristics: Recent Advancements and Developments. *Frontiers of Chemical Science and Engineering* **2023,** *17* (12), 1837-1865.
79. Kim, H.; Shim, I.; Zhan, M., Chemical Enhanced Backwashing for Controlling Organic Fouling in Drinking Water Treatment Using a Novel Hollow-Fiber Polyacrylonitrile Nanofiltration Membrane. *Applied Sciences* **2021**, 6764.
80. Le, T.; Jamshidi, E.; Beidaghi, M.; Esfahani, M., Functionalized-Mxene Thin-Film Nanocomposite Hollow Fiber Membranes for Enhanced Pfas Removal from Water. *ACS applied materials & interfaces* **2022,** *14* (22), 25397-25408.
81. Gao, Z. F.; Liu, J.; Chung, T., Rapid in-Situ Growth of Covalent Organic Frameworks on Hollow Fiber Substrates with Janus-Like Characteristics for Efficient Organic Solvent Nanofiltration. *Separation and Purification Technology* **2022,** *294*, 121166.
82. Shengjie, X.; Li, S.; Tian, L.; Su, B., Fabrication of Polyimide-Based Hollow Fiber Membrane by Synergetic Covalent-Crosslinking Strategy for Organic Solvent

Nanofiltration (Osn) Application. *Separation and Purification Technology* **2020,** *241*, 116751.
83. Wang, W.; Huang, X.; Wu, M.; Wu, Q.; Yang, J.; Liu, J.; Zhang, J., A Novel Hydrophilic Modification Method for Polytetrafluoroethylene (Ptfe) Hollow Fiber Membrane Using Sacrificial Template. *Journal of Membrane Science* **2024,** *699*, 122667.
84. Sun, Q.; Chai, Z.; An, Z.; Dong, J.; Zhang, R., Construction of a High-Performance Hollow Fiber Composite Nf Membrane Via the Simultaneous Modification of Substrate and Selective Layer. *Separation and Purification Technology* **2024,** *341*, 126908.
85. Setiawan, O.; Hu, C.-H.; Hung, W.-S.; Lai, J.-Y.; Chung, T.-S., Enhancing Thin-Film Composite Polyethersulfone Hollow Fiber Membranes through Alkali-Induced Interfacial Polymerization Modification for Effective Separation of Monovalent/Divalent Salts. *Desalination* **2024,** *585*, 117778.
86. Raje, A.; Koll, J.; Schneider, E.; Georgopanos, P., A Novel Organic Solvent-Free Method for Manufacturing Polyethersulfone Hollow Fiber Membranes Using Melt Extrusion. *Journal of Membrane Science* **2023,** *683*, 121837.
87. Roslan, R. A.; Lau, W.; Ismail, A. F.; Kartohardjono, S., Recent 10-Year Development on Surface Modification of Polymeric Hollow Fiber Membranes Via Surface Coating Approach for Gas Separation: A Review. *Journal of Materials Science* **2024,** *59*, 10083-10118.
88. Zhang, S.; Lu, D.; Chen, W.; Xiang, X.; Zheng, D.; Wang, J.; Yao, Z.; Bi, F.; Zhang, L., Fabrication of High-Flux Ptfe Hollow Fiber Membranes through Nonionic Surfactant Infiltration Coupled with Mussel-Inspired Chemistry Coating. *Journal of Membrane Science* **2024,** *702*, 122812.
89. Yang, J.; Sun, W.; Zhu, B.; Wang, H.; Yan, F.; Li, J.; Cui, Z., Construction of Zwitterionic Surface of Pvdf Hollow Fiber Membrane and the Study on the Mechanism of "Autonomy-Response" Synergistic Enhancement Anti-Fouling. *Separation and Purification Technology* **2024,** *354*, 129257.
90. Lin, Y.-T.; Li, J.-Y.; Wey, M.; Tseng, H., Engineered Pinhole-Stitching Process of Pei-Based Hollow Fiber Membrane Enables Preferred Performance toward Light Gas Separation. *International Journal of Hydrogen Energy* **2023,** *50*, 400-408.
91. Haase, M.; Jeon, H.; Hough, N.; Kim, J. H.; Stebe, K.; Lee, D., Multifunctional Nanocomposite Hollow Fiber Membranes by Solvent Transfer Induced Phase Separation. *Nature Communications* **2017,** *8*, 1234.
92. Choi, O.; Karki, S.; Karki, S.; Pawar, R.; Hazarika, S.; Hazarika, S.; Ingole, P.; Ingole, P., A New Perspective of Functionalized Mwcnt Incorporated Thin Film Nanocomposite Hollow Fiber Membranes for the Separation of Various Gases. *Journal of environmental chemical engineering* **2021,** *9*, 104774.
93. Tham, H. M.; Chung, T., One-Step Cross-Linking and Tannic Acid Modification of Polyacrylonitrile Hollow Fibers for Organic Solvent Nanofiltration. *Journal of Membrane Science* **2020,** *610*, 118294.
94. Cabasso, I.; Klein, E.; Smith, J. K., Polysulfone Hollow Fibers. Ii. Morphology. *Journal of Applied Polymer Science* **1977,** *21* (1), 165-180.

95. Peng, J.; Su, Y.; Chen, W.; Shi, Q.; Jiang, Z., Effects of Coagulation Bath Temperature on the Separation Performance and Antifouling Property of Poly(Ether Sulfone) Ultrafiltration Membranes. *Industrial & Engineering Chemistry Research* **2010,** *49* (10), 4858-4864.
96. Widjojo, N.; Chung, T.-S., Thickness and Air Gap Dependence of Macrovoid Evolution in Phase-Inversion Asymmetric Hollow Fiber Membranes. *Industrial & Engineering Chemistry Research* **2006,** *45* (22), 7618-7626.
97. Abdelrasoul, A.; Doan, H.; Lohi, A.; Cheng, C.-H., Morphology Control of Polysulfone Membranes in Filtration Processes: A Critical Review. *ChemBioEng Reviews* **2015,** *2* (1), 22-43.
98. Jiang, J.; Zhang, P.; Zhu, L.; Zhu, B.; Xu, Y., Improving Antifouling Ability and Hemocompatibility of Poly(Vinylidene Fluoride) Membranes by Polydopamine-Mediated Atrp. *Journal of Materials Chemistry B* **2015,** *3* (39), 7698-7706.
99. Mistry, P.; Murthy, C. N., Positively Charged Polysulfone and Polyether Sulfone Mixed Matrix Membranes Modified with Polyethylenimine: Enhancing Heavy Metal Rejection and Antifouling Properties. *ACS ES&T Water* **2023,** *3* (12), 4168-4182.
100. Arundhathi, B.; Pabba, M.; Raj, S. S.; Sahu, N.; Sridhar, S., Advancements in Mixed-Matrix Membranes for Various Separation Applications: State of the Art and Future Prospects. **2024,** *14* (11), 224.
101. Souza, V. C. Q., M. G. N., Organic-Inorganic Hybrid Membranes in Separation Processes: A 10-Year Review. *Brazilian Journal of Chemical Engineering* **2013,** *30* (4), 683-700.
102. Baghbanzadeh, M.; Rana, D.; Lan, C. Q.; Matsuura, T., Effects of Inorganic Nano-Additives on Properties and Performance of Polymeric Membranes in Water Treatment. *Separation & Purification Reviews* **2016,** *45* (2), 141-167.
103. Nasir, R.; Mukhtar, H.; Man, Z.; Mohshim, D. F., Material Advancements in Fabrication of Mixed-Matrix Membranes. *Chemical Engineering &Technology* **2013,** *36* (5), 717-727.
104. Kosobrodova, E.; Kondyurin, A.; Solod'ko, V.; Weiss, A.; McKenzie, D.; Bilek, M., Covalent Biofunctionalisation of the Inner Surfaces of a Hollow Fibre Capillary Bundle Using Packed Bed Plasma Ion Implantation. *ACS applied materials & interfaces* **2020,** *12* (28), 32163-32174.
105. Zheng, Z.; Wang, W.; Huang, X.; Fan, W.; Li, L., Surface Modification of Polysulfone Hollow Fiber Membrane for Extracorporeal Membrane Oxygenator Using Low-Temperature Plasma Treatment. *Plasma Processes and Polymers* **2018,** *15*, 1700122.
106. Ulbricht, M.; Riedel, M.; Marx, U., Novel Photochemical Surface Functionalization of Polysulfone Ultrafiltration Membranes for Covalent Immobilization of Biomolecules. *Journal of Membrane Science* **1996,** *120* (2), 239-259.
107. Shahkaramipour, N.; Tran, T. N.; Ramanan, S.; Lin, H., Membranes with Surface-Enhanced Antifouling Properties for Water Purification. *Membranes* **2017,** *7* (1), 13.
108. Khulbe, K. C.; Matsuura, T., Membrane Modification. In *Nanotechnology in Membrane Processes*, Khulbe, K. C.; Matsuura, T., Eds. Springer International Publishing: Cham, 2021; pp 135-170.

109. Ge, P.; Lin, Z.; Yang, J.; Hu, C.; Liu, Q.; Zhang, Q., Polyethylenimine Grafted Hollow Fiber Membranes for Fast Dye Separation. *Journal of Membrane Science* **2023,** *672*, 121428.
110. Hu, L.; Cheng, J.; Li, Y.; Liu, J.; Zhou, J.; Cen, K., In-Situ Grafting to Improve Polarity of Polyacrylonitrile Hollow Fiber-Supported Polydimethylsiloxane Membranes for Co2 Separation. *Journal of colloid and interface science* **2018,** *510*, 12-19.
111. Ishihara, R.; Asai, S.; Saito, K., Recent Progress in Charged Polymer Chains Grafted by Radiation-Induced Graft Polymerization; Adsorption of Proteins and Immobilization of Inorganic Precipitates. *Quantum Beam Science* **2020,** *4* (2), 20.
112. Ren, X.; Li, H.; Liu, K.; Lu, H.; Yang, J.; He, R., Preparation and Investigation of Reinforced Pvp Blend Membranes for High Temperature Polymer Electrolyte Membranes. *Fibers and Polymers* **2018,** *19*, 2449-2457.
113. Vinodh, R.; Atchudan, R.; Kim, H.-J.; Yi, M., Recent Advancements in Polysulfone Based Membranes for Fuel Cell (Pemfcs, Dmfcs and Amfcs) Applications: A Critical Review. *Polymers* **2022,** *14*.
114. Oulad, F.; Zinadini, S.; Zinatizadeh, A.; Derakhshan, A., Preparation and Characterization of Loose Antifouling Nanofiltration Membrane Using Branched Aniline Oligomers Grafted onto Polyether Sulfone and Application for Real Algal Dye Removal. *Chemical Engineering Journal* **2020,** *401*, 125861.
115. Xiang, T.; Yue, W.; Wang, R.; Liang, S.; Sun, S.; Zhao, C., Surface Hydrophilic Modification of Polyethersulfone Membranes by Surface-Initiated Atrp with Enhanced Blood Compatibility. *Colloids and surfaces. B, Biointerfaces* **2013,** *110*, 15-21.
116. Su, Y.; Yan, X.; Chen, Y.; Guo, X.; Chen, X.; Lang, W. Z., Facile Fabrication of Cof-Lzu1/Pes Composite Membrane Via Interfacial Polymerization on Microfiltration Substrate for Dye/Salt Separation. *Journal of Membrane Science* **2021,** *618*, 118706.
117. Makvandi, P.; Iftekhar, S.; Pizzetti, F.; Zarepour, A.; Zare, E. N.; Ashrafizadeh, M.; Agarwal, T.; Padil, V. V. T.; Mohammadinejad, R.; Sillanpaa, M.; Maiti, T. K.; Perale, G.; Zarrabi, A.; Rossi, F., Functionalization of Polymers and Nanomaterials for Water Treatment, Food Packaging, Textile and Biomedical Applications: A Review. *Environmental Chemistry Letters* **2021,** *19* (1), 583-611.
118. Hoffman, J. R.; Phillip, W. A., 100th Anniversary of Macromolecular Science Viewpoint: Integrated Membrane Systems. *ACS Macro Letters* **2020,** *9* (9), 1267-1279.
119. Noah, N. M., Current Status and Advancement of Nanomaterials within Polymeric Membranes for Water Purification. *ACS Applied Nano Materials* **2024,** *7* (16), 18610-18625.
120. Khraisheh, M.; Elhenawy, S.; AlMomani, F.; Al-Ghouti, M.; Hassan, M. K.; Hameed, B. H., Recent Progress on Nanomaterial-Based Membranes for Water Treatment. *Membranes* **2021,** *11* (12), 995.
121. Zhang, H.; He, Q.; Luo, J.; Wan, Y.; Darling, S. B., Sharpening Nanofiltration: Strategies for Enhanced Membrane Selectivity. *ACS Applied Materials & Interfaces* **2020,** *12* (36), 39948-39966.
122. Iqbal, A.; Cevik, E.; Mustafa, A.; Qahtan, T. F.; Zeeshan, M.; Bozkurt, A., Emerging Developments in Polymeric Nanocomposite Membrane-Based Filtration for Water

Purification: A Concise Overview of Toxic Metal Removal. *Chemical Engineering Journal* **2024,** *481*, 148760.

123. Chabalala, M. B.; Gumbi, N. N.; Mamba, B. B.; Al-Abri, M. Z.; Nxumalo, E. N. Photocatalytic Nanofiber Membranes for the Degradation of Micropollutants and Their Antimicrobial Activity: Recent Advances and Future Prospects *Membranes*, **2021**, 11, 9 678.
124. Salim, S. H.; Al-Anbari, R. H.; Haider, A. J., Polymeric Membrane with Nanomaterial's for Water Purification: A Review. *IOP Conference Series: Earth and Environmental Science* **2021,** *779* (1), 012103.
125. Goh, P. S.; Ng, B. C.; Lau, W. J.; Ismail, A. F., Inorganic Nanomaterials in Polymeric Ultrafiltration Membranes for Water Treatment. *Separation & Purification Reviews* **2015,** *44* (3), 216-249.
126. Tofighy, M. A.; Khanlari, S.; Mohammadi, T., Chapter 6 - Development of Advanced Nanocomposite Membranes by Carbon-Based Nanomaterials (Cnts and Go). In *Nanocomposite Membranes for Water and Gas Separation*, Sadrzadeh, M.; Mohammadi, T., Eds. Elsevier: **2020**; pp 145-162.
127. Wang, C.; Park, M. J.; Yu, H.; Matsuyama, H.; Drioli, E.; Shon, H. K., Recent Advances of Nanocomposite Membranes Using Layer-by-Layer Assembly. *Journal of Membrane Science* **2022,** *661*, 120926.
128. Mantovani, S.; Khaliha, S.; Marforio, T. D.; Kovtun, A.; Favaretto, L.; Tunioli, F.; Bianchi, A.; Petrone, G.; Liscio, A.; Palermo, V.; Calvaresi, M.; Navacchia, M. L.; Melucci, M., Facile High-Yield Synthesis and Purification of Lysine-Modified Graphene Oxide for Enhanced Drinking Water Purification. *Chemical Communications* **2022,** *58* (70), 9766-9769.
129. Melucci, M.; Treossi, E.; Ortolani, L.; Giambastiani, G.; Morandi, V.; Klar, P.; Casiraghi, C.; Samorì, P.; Palermo, V., Facile Covalent Functionalization of Graphene Oxide Using Microwaves: Bottom-up Development of Functional Graphitic Materials. *Journal of Materials Chemistry* **2010,** *20* (41), 9052-9060.
130. Vacchi, I.; Spinato, C.; Raya, J.; Bianco, A.; Ménard-Moyon, C., Chemical Reactivity of Graphene Oxide Towards Amines Elucidated by Solid-State Nmr. *Nanoscale* **2016,** *8 28*, 13714-13721.
131. Vacchi, I.; Raya, J.; Bianco, A.; Ménard-Moyon, C., Controlled Derivatization of Hydroxyl Groups of Graphene Oxide in Mild Conditions. *2D Materials* **2018,** *5*, 035037.
132. Gonçalves, M. G.; Costa, V. O.; Martinez, A. H. G.; Régnier, B. M.; Gomes, G. C. B.; Zarbin, A. J. G.; Orth, E. S., Functionalization of Graphene Oxide Via Epoxide Groups: A Comprehensive Review of Synthetic Routes and Challenges. *Frontiers in Carbon* **2024,** *3*, 1393077.
133. Guo, S.-M.; Garaj, S.; Bianco, A.; Ménard-Moyon, C., Controlling Covalent Chemistry on Graphene Oxide. *Nature Reviews Physics* **2022,** *4*, 247-262.
134. Yu, W.; Sisi, L.; Haiyan, Y.; Jie, L., Progress in the Functional Modification of Graphene/Graphene Oxide: A Review. *RSC Advances* **2020,** *10* (26), 15328-15345.

135. Liu, J.; Chen, S.; Liu, Y.; Zhao, B., Progress in Preparation, Characterization, Surface Functional Modification of Graphene Oxide: A Review. *Journal of Saudi Chemical Society* **2022,** *26* (6), 101560.
136. Trifoglio, A.; Mantovani, S.; Khaliha, S.; Kovtun, A.; Marforio, T. D.; Calvaresi, M.; Melucci, M., Tailoring Graphene Oxide Nanosheets by Alkyl Amine Grafting for Enhanced Adsorption of Pfass in Drinking Water: A Combined Theoretical and Experimental Study. *Nanoscale* **2025,** *17* (19), 12124-12133.
137. Mantovani, S.; Khaliha, S.; Favaretto, L.; Bettini, C.; Bianchi, A.; Kovtun, A.; Zambianchi, M.; Gazzano, M.; Casentini, B.; Palermo, V.; Melucci, M., Scalable Synthesis and Purification of Functionalized Graphene Nanosheets for Water Remediation. *Chemical Communications* **2021,** *57* (31), 3765-3768.
138. Tunioli, F.; Marforio, T. D.; Favaretto, L.; Mantovani, S.; Pintus, A.; Bianchi, A.; Kovtun, A.; Agnes, M.; Palermo, V.; Calvaresi, M.; Navacchia, M. L.; Melucci, M., Chemical Tailoring of B-Cyclodextrin-Graphene Oxide for Enhanced Per- and Polyfluoroalkyl Substances (Pfas) Adsorption from Drinking Water. *Chemistry - A European Journal* **2023,** *29* (60), e202301854.
139. Lombardi, L.; Kovtun, A.; Mantovani, S.; Bertuzzi, G.; Favaretto, L.; Bettini, C.; Palermo, V.; Melucci, M.; Bandini, M., Visible-Light Assisted Covalent Surface Functionalization of Reduced Graphene Oxide Nanosheets with Arylazo Sulfones. *Chemistry - A European Journal* **2022,** *28* (26), e202200333.
140. Vulcano, F.; Kovtun, A.; Bettini, C.; Xia, Z.; Liscio, A.; Terzi, F.; Heras, A.; Colina, A.; Zanfrognini, B.; Melucci, M.; Palermo, V.; Zanardi, C., Dopamine-Functionalized Graphene Oxide as a High-Performance Material for Biosensing. *2D Materials* **2020,** *7* (2), 024007.
141. Melucci, M., Navacchia, M. L. Porous Granules of Polysulphone or Derivatives Thereof for the Removal of Organic Molecules from a Fluid 2016.
142. Melucci M.; Zambianchi M.; Benfenati V.; Bocchi, L. Modified Membrane. **2017**.
143. Melucci, M.; Palermo, V.; Zambianchi, M.; Liscio, A.; Kovtun, A.; Treossi, E.; Navacchia, M. L.; Bocchi, L. Method for the Treatment of a Porous Substrate. **2018**.
144. Melucci, M.; Palermo, V.; Zambianchi, M.; Kovtun, A.; Navacchia, M. L.; Bocchi, L. Method for the Treatment of a Liquid. **2020**.
145. Mantovani, S.; Marforio, T. D.; Khaliha, S.; Pintus, A.; Kovtun, A.; Tunioli, F.; Favaretto, L.; Bianchi, A.; Navacchia, M. L.; Palermo, V.; Calvaresi, M.; Melucci, M., Amino Acid-Driven Adsorption of Emerging Contaminants in Water by Modified Graphene Oxide Nanosheets. *Environmental Science: Water Research & Technology* **2023,** *9* (4), 1030-1040.
146. Moro, G.; Khaliha, S.; Pintus, A.; Mantovani, S.; Feltracco, M.; Gambaro, A.; Marforio, T. D.; Calvaresi, M.; Palermo, V.; Melucci, M.; Zanardi, C., Amino Acid Modified Graphene Oxide for the Simultaneous Capture and Electrochemical Detection of Glyphosate. *Materials Today Chemistry* **2024,** *36*, 101936.
147. Pintus, A.; Mantovani, S.; Kovtun, A.; Bertuzzi, G.; Melucci, M.; Bandini, M., Recyclable Go-Arginine Hybrids for Co2 Fixation into Cyclic Carbonates. *Chemistry - A European Journal* **2023,** *29* (4), e202202440.

148. Mantovani, S.; Pintus, A.; Kovtun, A.; Gondolini, A.; Casadio, S.; Sanson, A.; Marforio, T. D.; Calvaresi, M.; Rancan, M.; Armelao, L.; Bertuzzi, G.; Melucci, M.; Bandini, M., Graphene Oxide-Arginine Composites: Efficient Dual Function Materials for Integrated Co2 Capture and Conversion. *ChemSusChem* **2024,** *17* (5), e202301673.
149. Sturm, V., Dynamics in the Bioeconomy: Markets for Amino Acids and Insect Biomass. *EuroChoices* **2023,** *22* (3), 37-43.
150. Yan, Y.; Li, J.; Kong, F.; Jia, K.; He, S.; Wang, B., L-Lysine-Grafted Graphene Oxide as an Effective Adsorbent for the Removal of Methylene Blue and Metal Ions. *Beilstein Journal of Nanotechnology* **2017,** *8*, 2680-2688.
151. Abdelhalim, A. O. E.; Sharoyko, V. V.; Meshcheriakov, A. A.; Luttsev, M. D.; Potanin, A. A.; Iamalova, N. R.; Zakharov, E. E.; Ageev, S. V.; Petrov, A. V.; Vasina, L. V.; Solovtsova, I. L.; Nashchekin, A. V.; Murin, I. V.; Semenov, K. N., Synthesis, Characterisation and Biocompatibility of Graphene–L-Methionine Nanomaterial. *Journal of Molecular Liquids* **2020,** *314*, 113605.
152. Yadav, S.; Asthana, A.; Singh, A. K.; Chakraborty, R.; Vidya, S. S.; Singh, A.; Carabineiro, S. A. C., Methionine-Functionalized Graphene Oxide/Sodium Alginate Bio-Polymer Nanocomposite Hydrogel Beads: Synthesis, Isotherm and Kinetic Studies for an Adsorptive Removal of Fluoroquinolone Antibiotics. *Nanomaterials* **2021,** *11* (3), 568.
153. Collis, A. B.; Tulip, P. R.; Bates, S. P., Structure and Bonding of Aqueous Glutamic Acid from Classical Molecular Dynamics Simulations. *Physical Chemistry Chemical Physics* **2010,** *12* (20), 5341-5352.
154. Ge, H.; Zou, W., Preparation and Characterization of L-Glutamic Acid-Functionalized Graphene Oxide for Adsorption of Pb(Ii). *Journal of Dispersion Science and Technology* **2017,** *38* (2), 241-247.
155. Khabnadideh, S.; Mirzaei, E.; Amiri-Zirtol, L., L-Arginine Modified Graphene Oxide: A Novel Heterogeneous Catalyst for Synthesis of Benzo[B]Pyrans and Pyrano[3,2-C]Chromenes. *Journal of Molecular Structure* **2022,** *1261*, 132934.
156. Lee, H. M.; Youn, I. S.; Saleh, M.; Lee, J. W.; Kim, K. S., Interactions of Co2 with Various Functional Molecules. *Physical Chemistry Chemical Physics* **2015,** *17* (16), 10925-10933.
157. P, S.; Mandal, S. K., From Co2 Activation to Catalytic Reduction: A Metal-Free Approach. *Chemical Science* **2020,** *11* (39), 10571-10593.
158. Wang, Y.; Hao, Z.; Pan, L., Evaluation of Multiple Hydrophilic Interaction Chromatography Columns and Surrogate Matrix for Arginine Quantification in Saliva by High-Resolution Mass Spectrometry. *Journal of Separation Science* **2021,** *44*, 3580-3593.
159. Perreault, F.; Fonseca de Faria, A.; Elimelech, M., Environmental Applications of Graphene-Based Nanomaterials. *Chemical Society Reviews* **2015,** *44* (16), 5861-5896.
160. Khan, A.; Wang, J.; Li, J.; Wang, X.; Chen, Z.; Alsaedi, A.; Hayat, T.; Chen, Y.; Wang, X., The Role of Graphene Oxide and Graphene Oxide-Based Nanomaterials in the Removal of Pharmaceuticals from Aqueous Media: A Review. *Environmental Science and Pollution Research* **2017,** *24* (9), 7938-7958.
161. Khaliha, S.; Marforio, T. D.; Kovtun, A.; Mantovani, S.; Bianchi, A.; Luisa Navacchia, M.; Zambianchi, M.; Bocchi, L.; Boulanger, N.; Iakunkov, A.; Calvaresi, M.; Talyzin,

A. V.; Palermo, V.; Melucci, M., Defective Graphene Nanosheets for Drinking Water Purification: Adsorption Mechanism, Performance, and Recovery. *FlatChem* **2021,** *29*, 100283.
162. Li, C.; Xu, Q.; Xu, S.; Zhang, X.; Hou, X.; Wu, P., Synergy of Adsorption and Photosensitization of Graphene Oxide for Improved Removal of Organic Pollutants. *RSC Advances* **2017,** *7* (26), 16204-16209.
163. Thakur, K.; Kandasubramanian, B., Graphene and Graphene Oxide-Based Composites for Removal of Organic Pollutants: A Review. *Journal of Chemical & Engineering Data* **2019,** *64* (3), 833-867.
164. Adeleye, A. S.; Xue, J.; Zhao, Y.; Taylor, A. A.; Zenobio, J. E.; Sun, Y.; Han, Z.; Salawu, O. A.; Zhu, Y., Abundance, Fate, and Effects of Pharmaceuticals and Personal Care Products in Aquatic Environments. *Journal of Hazardous Materials* **2022,** *424*, 127284.
165. da Silva, A. C.; Alves de Oliveira, L. V.; Amaral Alexandre, L.; Rocha Ribas, M.; Lemos Dal Pizzol, J.; Rocha, G.; Kasuko Palmeiro, J.; Perin, M.; Hoff, R.; Verruck, S., Suspect Screening and Quantitative Analysis of 165 Contaminants of Emerging Concern in Water, Sediments, and Biota Using Lc-Ms/Ms: Ecotoxicological and Human Health Risk Assessment. *Science of The Total Environment* **2025,** *963*, 178434.
166. Chaves, M. d. J. S.; Barbosa, S. C.; Malinowski, M. d. M.; Volpato, D.; Castro, Í. B.; Franco, T. C. R. d. S.; Primel, E. G., Pharmaceuticals and Personal Care Products in a Brazilian Wetland of International Importance: Occurrence and Environmental Risk Assessment. *Science of The Total Environment* **2020,** *734*, 139374.
167. Benbrook, C. M., Trends in Glyphosate Herbicide Use in the United States and Globally. *Environmental sciences Europe* **2016,** *28* (1), 3.
168. Silva, V.; Montanarella, L.; Jones, A.; Fernández-Ugalde, O.; Mol, H. G. J.; Ritsema, C. J.; Geissen, V., Distribution of Glyphosate and Aminomethylphosphonic Acid (Ampa) in Agricultural Topsoils of the European Union. *Sci Total Environ* **2018,** *621*, 1352-1359.
169. Feltracco, M.; Barbaro, E.; Morabito, E.; Zangrando, R.; Piazza, R.; Barbante, C.; Gambaro, A., Assessing Glyphosate in Water, Marine Particulate Matter, and Sediments in the Lagoon of Venice. *Environmental Science and Pollution Research* **2022,** *29* (11), 16383-16391.
170. Ighalo, J. O.; Ajala, O. J.; Adeniyi, A. G.; Babatunde, E. O.; Ajala, M. A., Ecotoxicology of Glyphosate and Recent Advances in Its Mitigation by Adsorption. *Environmental science and pollution research international* **2021,** *28* (3), 2655-2668.
171. Bai, S. H.; Ogbourne, S. M., Glyphosate: Environmental Contamination, Toxicity and Potential Risks to Human Health Via Food Contamination. *Environmental Science and Pollution Research* **2016,** *23* (19), 18988-19001.
172. Castrejón-Godínez, M. L.; Tovar-Sánchez, E.; Valencia-Cuevas, L.; Rosas-Ramírez, M. E.; Rodríguez, A.; Mussali-Galante, P., Glyphosate Pollution Treatment and Microbial Degradation Alternatives, a Review. *Microorganisms* **2021,** *9* (11).
173. Maccaferri, G.; Zanardi, C.; Xia, Z. Y.; Kovtun, A.; Liscio, A.; Terzi, F.; Palermo, V.; Seeber, R., Systematic Study of the Correlation between Surface Chemistry, Conductivity

and Electrocatalytic Properties of Graphene Oxide Nanosheets. *Carbon* **2017,** *120*, 165-175.
174. Ambrosi, A.; Chua, C. K.; Bonanni, A.; Pumera, M., Electrochemistry of Graphene and Related Materials. *Chemical Reviews* **2014,** *114* (14), 7150-7188.
175. Brunetti, A.; Pintus, A.; Lombardi, L.; Kovtun, A.; Mascietti, F.; Bruno, F.; Ravera, E.; Melucci, M.; Bertuzzi, G.; Bandini, M., Graphene-Oxide Mediated Chemodivergent Ring-Opening of Cyclobutanols. *Chinese Journal of Chemistry* **2023,** *41* (11), 1333-1340.
176. Mantovani, S.; Pintus, A.; Kovtun, A.; Bertuzzi, G.; Melucci, M.; Bandini, M., Synthesis of Indenes Via Graphene Oxide Mediated Manipulation of Morita-Baylis-Hillman Alcohols. *European Journal of Orgnic Chemistry* **2023,** *26* (37), e202300641.
177. Hai, F. I.; Yang, S.; Asif, M. B.; Sencadas, V.; Shawkat, S.; Sanderson-Smith, M.; Gorman, J.; Xu, Z.-Q.; Yamamoto, K., Carbamazepine as a Possible Anthropogenic Marker in Water: Occurrences, Toxicological Effects, Regulations and Removal by Wastewater Treatment Technologies. *Water* **2018,** *10* (2), 107.
178. Tunioli, F.; Khaliha, S.; Mantovani, S.; Bianchi, A.; Kovtun, A.; Xia, Z.; Bafqi, M. S. S.; Okan, B. S.; Marforio, T. D.; Calvaresi, M.; Palermo, V.; Navacchia, M. L.; Melucci, M., Adsorption of Emerging Contaminants by Graphene Related Materials and Their Alginate Composite Hydrogels. *Journal of Environmental Chemical Engineering* **2023,** *11* (2), 109566.
179. Avram, E.; Elena, B.; Cornelia, L.; and Druta, I., Polymers with Pendant Functional Group. Iii. Polysulfones Containing Viologen Group. *Journal of Macromolecular Science, Part A* **1997,** *34* (9), 1701-1714.
180. Temnikova, N. E.; Stoyanov, O. V., Aromatic Polysulfones: Synthesis, Properties, and Their Application. A Review. *Polymer Science, Series D* **2024,** *17* (1), 140-148.
181. Serbanescu, O. S.; Voicu, S. I.; Thakur, V. K., Polysulfone Functionalized Membranes: Properties and Challenges. *Materials Today Chemistry* **2020,** *17*, 100302.
182. Dumbrava, O.; Filimon, A.; Marin, L., Tailoring Properties and Applications of Polysulfone Membranes by Chemical Modification: Structure-Properties-Applications Relationship. *European Polymer Journal* **2023,** *196*, 112316.
183. de León, A. S.; de la Mata, M.; Delgado, F. J.; Molina, S. I., Printable Graphene Oxide Nanocomposites as Versatile Platforms for Immobilization of Functional Biomolecules. *Macromolecular Materials and Engineering* **2022,** *307* (3), 2100784.
184. Rosen, C. B.; Francis, M. B., Targeting the N Terminus for Site-Selective Protein Modification. *Nature Chemical Biology* **2017,** *13* (7), 697-705.
185. Guiver, M. D.; Robertson, G. P.; Foley, S., Chemical Modification of Polysulfones Ii: An Efficient Method for Introducing Primary Amine Groups onto the Aromatic Chain. *Macromolecules* **1995,** *28* (23), 7612-7621.
186. de Barros, N. G.; Gonzaga Neto, A. C.; Vaccioli, K. B.; Angulo, H. R. V.; de Andrade e Silva, L. G.; Toffoli, S. M.; Valera, T. S., Graphene Oxide: A Comparison of Reduction Methods. *C — Journal of Carbon Research* **2023,** *9* (3), 73.
187. Rezapour, M. R.; Myung, C. W.; Yun, J.; Ghassami, A.; Li, N.; Yu, S. U.; Hajibabaei, A.; Park, Y.; Kim, K. S., Graphene and Graphene Analogs toward Optical, Electronic,

Spintronic, Green-Chemical, Energy-Material, Sensing, and Medical Applications. *ACS Applied Materials & Interfaces* **2017,** *9* (29), 24393-24406.
188. Guex, L. G.; Sacchi, B.; Peuvot, K. F.; Andersson, R. L.; Pourrahimi, A. M.; Ström, V.; Farris, S.; Olsson, R. T., Experimental Review: Chemical Reduction of Graphene Oxide (Go) to Reduced Graphene Oxide (Rgo) by Aqueous Chemistry. *Nanoscale* **2017,** *9* (27), 9562-9571.
189. Palomba, M.; Longo, A.; Carotenuto, G., Gel-Phase Reduction of Graphene Oxide Coatings by L-Ascorbic Acid. *Materials Proceedings* **2021,** *4* (1), 33.
190. Huang, J.; Yang, H.; Chen, M.; Ji, T.; Hou, Z.; Wu, M., An Infrared Spectroscopy Study of Pes Pvp Blend and Pes-G-Pvp Copolymer. *Polymer Testing* **2017,** *59*, 212-219.
191. Salim, A.; Abbas, M. A.; Khan, I. A.; Khan, M. Z.; Javaid, F.; Mushtaq, S.; Batool, M.; Yasir, M.; Khan, A. L.; Khan, A. U.; Deen, K. M.; Ahmad, N. M., Graphene Oxide Incorporated Polyether Sulfone Nanocomposite Antifouling Ultrafiltration Membranes with Enhanced Hydrophilicity. *Materials Research Express* **2022,** *9* (7), 075503.
192. Dreyer, D. R.; Park, S.; Bielawski, C. W.; Ruoff, R. S., The Chemistry of Graphene Oxide. *Chemical Society Reviews* **2010,** *39* (1), 228-240.
193. Chen, C.-M.; Zhang, Q.; Yang, M.-G.; Huang, C.-H.; Yang, Y.-G.; Wang, M.-Z., Structural Evolution During Annealing of Thermally Reduced Graphene Nanosheets for Application in Supercapacitors. *Carbon* **2012,** *50* (10), 3572-3584.
194. Miccoli, I.; Edler, F.; Pfnür, H.; Tegenkamp, C., The 100th Anniversary of the Four-Point Probe Technique: The Role of Probe Geometries in Isotropic and Anisotropic Systems. *Journal of Physics: Condensed Matter* **2015,** *27* (22), 223201.
195. Rao, S.; Upadhyay, J.; Polychronopoulou, K.; Umer, R.; Das, R., Reduced Graphene Oxide: Effect of Reduction on Electrical Conductivity. *Journal of Composites Science* **2018,** *2* (2), 25.
196. Giménez-Pérez, A.; Bikkarolla, S. K.; Benson, J.; Bengoa, C.; Stüber, F.; Fortuny, A.; Fabregat, A.; Font, J.; Papakonstantinou, P., Synthesis of N-Doped and Non-Doped Partially Oxidised Graphene Membranes Supported over Ceramic Materials. *Journal of Materials Science* **2016,** *51* (18), 8346-8360.
197. Williams, M. V.; Kunz, H. R.; Fenton, J. M., Analysis of Polarization Curves to Evaluate Polarization Sources in Hydrogen/Air Pem Fuel Cells. *Journal of The Electrochemical Society* **2005,** *152* (3), A635.
198. Okonkwo, P. C.; Belgacem, I. B.; Ige, O. O.; Emori, W.; Uzoma, P. C.; Eqbal, M. O.; Bhowmik, H., Potentiodynamic Polarization Test as a Versatile Tool for Bipolar Plates Materials at Start-up and Shut-Down Environments: A Review. *International Journal of Green Energy* **2021,** *18* (11), 1193-1202.
199. Pintus, A.; Trifoglio, A.; Khaliha, S.; Mantovani, S.; Paci, D.; Kovtun, A.; Bocchi, L.; Melucci, M., Functionalizing Graphene Oxide in Polysulfone Composite Adsorption Cartridges through in-Flow, in Situ Treatment. *RSC Applied Interfaces* **2025**, 2, 917-921.
200. Liang, J.; Chen, X.; Duan, X.; Gu, X.; Zhao, X.; Zha, S.; Chen, X., Natural Aging and Adsorption/Desorption Behaviors of Polyethylene Mulch Films: Roles of Film Types and Exposure Patterns. *Journal of Hazardous Materials* **2024,** *466*, 133588.

201. Goldman, M.; Lee, M.; Gronsky, R.; Pruitt, L., Oxidation of Ultrahigh Molecular Weight Polyethylene Characterized by Fourier Transform Infrared Spectrometry. *Journal of Biomedical Materials Research* **1997,** *37* (1), 43-50.
202. Rocha, M. F.; Mansur, A. A. P.; Mansur, H. S., Ftir Investigation of Uhmwpe Oxidation Submitted to Accelerated Aging Procedure. **2010,** *296* (1), 487-492.
203. Meldrum, B. J.; Rochester, C. H., In Situ Infrared Study of the Surface Oxidation of Activated Carbon in Oxygen and Carbon Dioxide. *Journal of the Chemical Society, Faraday Transactions* **1990,** *86* (5), 861-865.
204. Salustiano, R.; Nogueira, T. A.; Queiroz, A. A. A. d.; Neto, E. T. W.; Salles, C. d.; Tavares, Í. C., Artificial Rain Accelerated Aging Test of Hdpe Pin Insulators for Medium Voltage Distribution in Brazil. *IEEE Transactions on Dielectrics and Electrical Insulation* **2017,** *24* (4), 2483-2492.
205. Reuschenbach, P.; Pagga, U.; Strotmann, U., A Critical Comparison of Respirometric Biodegradation Tests Based on Oecd 301 and Related Test Methods. *Water Research* **2003,** *37* (7), 1571-1582.
206. Krupp, L. R.; Jewell, W. J., Biodegradability of Modified Plastic Films in Controlled Biological Environments. *Environmental Science & Technology* **1992,** *26* (1), 193-198.
207. Zambrano-Intriago, L. A.; Amorim, C. G.; Rodríguez-Díaz, J. M.; Araújo, A. N.; Montenegro, M. C. B. S. M., Challenges in the Design of Electrochemical Sensor for Glyphosate-Based on New Materials and Biological Recognition. *Science of The Total Environment* **2021,** *793*, 148496.
208. Armelao, L.; Rando, M.; Carlotto, S.; Motta, I.; Bottaro, G.; Rancan, M., Bridging Two Worlds: (Dabco-H)Cuki3 a Hybrid Copper Iodide Phosphor with a Perovskite Structure. *Pure and Applied Chemistry* **2024,** *96* (1), 69-80.
209. Beamson, G.; Briggs, D. R. In *The Xps of Polymers Database*, **2000**.
210. Massey, S.; Adnot, A.; Rjeb, A.; Roy, D., Study of Natural Aging of Industrial Low Density Polyethylene by X-Ray Photoelectron Spectroscopy. *Plastics, Rubber and Composites* **2008,** *37* (1), 7-12.